16

FINAL REPORT
SYSTEM DESIGN OF THE PIONEER VENUS SPACECRAFT

VOLUME 6
POWER SUBSYSTEM STUDIES

By
H. F. PROCHASKA
ET AL.

July 1973

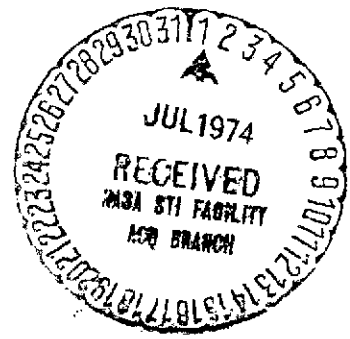

Prepared Under
Contract No. [redacted] NAS 2-7250

By
HUGHES AIRCRAFT COMPANY
EL SEGUNDO, CALIFORNIA

For
AMES RESEARCH CENTER
NATIONAL AERONAUTICS AND
SPACE ADMINISTRATION

PREFACE

The Hughes Aircraft Company Pioneer Venus final report is based on study task reports prepared during performance of the "System Design Study of the Pioneer Spacecraft." These task reports were forwarded to Ames Research Center as they were completed during the nine months study phase. The significant results from these task reports, along with study results developed after task report publication dates, are reviewed in this final report to provide complete study documentation. Wherever appropriate, the task reports are cited by referencing a task number and Hughes report reference number. The task reports can be made available to the reader specifically interested in the details omitted in the final report for the sake of brevity.

This Pioneer Venus Study final report describes the following baseline configurations:

- "Thor/Delta Spacecraft Baseline" is the baseline presented at the midterm review on 26 February 1973.
- "Atlas/Centaur Spacecraft Baseline" is the baseline resulting from studies conducted since the midterm, but prior to receipt of the NASA execution phase RFP, and subsequent to decisions to launch both the multiprobe and orbiter missions in 1978 and use the Atlas/Centaur launch vehicle.
- "Atlas/Centaur Spacecraft Midterm Baseline" is the baseline presented at the 26 February 1973 review and is only used in the launch vehicle utilization trade study.

The use of the International System of Units (SI) followed by other units in parentheses implies that the principal measurements or calculations were made in units other than SI. The use of SI units alone implies that the principal measurements or calculations were made in SI units. All conversion factors were obtained or derived from NASA SP-7012 (1969).

The Hughes Aircraft Company final report consists of the following documents:

Volume 1 - Executive Summary - provides a summary of the major issues and decisions reached during the course of the study. A brief description of the Pioneer Venus Atlas/Centaur baseline spacecraft and probes is also presented.

Volume 2 - Science - reviews science requirements, documents the science peculiar trade studies and describes the Hughes approach for science implementation.

Volume 3 - Systems Analysis - documents the mission, systems, operations, ground systems, and reliability analysis conducted on the Thor/Delta baseline design.

Volume 4 - Probe Bus and Orbiter Spacecraft Vehicle Studies - presents the configuration, structure, thermal control and cabling studies for the probe bus and orbiter. Thor/Delta and Atlas/Centaur baseline descriptions are also presented.

Volume 5 - Probe Vehicle Studies - presents configuration, aerodynamic and structure studies for the large and small probes pressure vessel modules and deceleration modules. Pressure vessel module thermal control and science integration are discussed. Deceleration module heat shield, parachute and separation/despin are presented. Thor/Delta and Atlas/Centaur baseline descriptions are provided.

Volume 6 - Power Subsystem Studies

Volume 7 - Communication Subsystem Studies

Volume 8 - Command/Data Handling Subsystems Studies

Volume 9 - Altitude Control/Mechanisms Subsystem Studies

Volume 10 - Propulsion/Orbit Insertion Subsystem Studies

Volumes 6 through 10 - discuss the respective subsystems for the probe bus, probes, and orbiter. Each volume presents the subsystem requirements, trade and design studies, Thor/Delta baseline descriptions, and Atlas/Centaur baseline descriptions.

Volume 11 - Launch Vehicle Utilization - provides the comparison between the Pioneer Venus spacecraft system for the two launch vehicles, Thor/Delta and Atlas/Centaur. Cost analysis data is presented also.

Volume 12 - International Cooperation - documents Hughes suggested alternatives to implement a cooperative effort with ESRO for the orbiter mission. Recommendations were formulated prior to the deletion of international cooperation.

Volume 13 - Preliminary Development Plans - provides the development and program management plans.

Volume 14 - Test Planning Trades - documents studies conducted to determine the desirable testing approach for the Thor/Delta spacecraft system. Final Atlas/Centaur test plans are presented in Volume 13.

Volume 15 - Hughes IR&D Documentation - provides Hughes internal documents generated on independent research and development money which relates to some aspects of the Pioneer Venus program. These documents are referenced within the final report and are provided for ready access by the reader.

Data Book - presents the latest Atlas/Centaur Baseline design in an informal tabular and sketch format. The informal approach is used to provide the customer with the most current design with the final report.

CONTENTS

1. SUMMARY

Selection of a baseline power subsystem for the probe bus, orbiter, and large and small probes has been performed as a part of the Pioneer Venus Mission Systems Design Study. In each case the selection process has involved trades and incorporated the results of previous related studies. Factors considered primary in the selection of each subsystem approach were cost, and the ability of each of the proposed subsystems to perform reliably under the rigors of the space environment, temperature extremes, and high g loads.

As a result of the Ames Research Center (ARC) RFP statement of work, a trade was made to consider the advantages of an unregulated primary bus versus a regulated bus. The decision to use an unregulated bus was based on cost, weight, and the increase in load isolation achievable through the use of individual load regulators.

Primary power is supplied by N/P, 2 ohm-cm, 0.20 mm (8 mil) thick silicon solar cells with 0.15 mm (6 mil) covers mounted on the cylindrical spacecraft outer surface. The design parameters for both orbiter and probe bus are similar, with the exception of output power required and the operating temperature. Secondary power on the Atlas/Centaur orbiter and probe bus is supplied by two 21 cell, 7 A-hr, nickel-cadmium batteries, with a 14 A-hr combined capacity. The Thor/Delta power configuration uses a single 10 A-hr nickel-cadmium battery on the orbiter, and a single 13.5 silver-zinc battery on the probe bus.

Battery charging and discharging is controlled by individual charge/discharge controllers for each battery. Battery discharging occurs through redundant isolation diodes in the Atlas/Centaur configuration and through a boost add-on discharge controller in the Thor/Delta configuration. Each battery discharges to supplement the panel power when the load demand exceeds the available panel power. Each battery charge controller has two charge modes: 1) an uncontrolled mode where the battery is charged at whatever current rate the solar panel can supply and 2) a constant voltage mode with selectable temperature compensated voltage limits. In the uncontrolled mode, the battery is allowed to charge until the battery voltage rises to some predetermined level. At this time, charging is changed to a constant voltage mode, and the charge current tapers off to a trickle charge rate. In the constant voltage mode, temperature compensated voltage levels are selectable by ground command. Thermal switches are utilized to preclude battery overheating. Each charger can be commanded on/off by ground command.

The power subsystem utilizes five and six bus voltage limiters on the probe and orbiter bus, respectively. These limiters bound the maximum voltage on the unregulated bus during transient periods such as emergence from solar eclipse or when the spacecraft load is less than the available panel power. The limiters will be grouped, and setpoints of each group selected within the range of 32.6 and 33.0 V dc. Each limiter has the capability of dissipating 66 W. The power resistors of each limiter can be appropriately located to minimize the impact to the thermal design. Each limiter has the capability of being commanded on/off by the command subsystem.

On the probe bus a charger has been included to charge the four silver-zinc batteries on the large and small probes. These units also include provisions for supplying checkout power to each probe upon command via the probe bus. The charger proposed for the silver-zinc cells will utilize a current limit at 0.4 ± 0.1 A up to a voltage of 1.93 ± 0.01 V/cell and then clamp at this voltage. This will slowly reduce charging current to a very low trickle rate. To ensure adequate charging voltage at all times, a boost circuit will be employed in the probe battery charger.

An undervoltage switch has been included in the Atlas/Centaur design to provide isolation between the essential bus and the nonessential bus in the event of a bus voltage failure. The switch functions automatically to open the autorestore and nonessential buses when the battery voltage drops to approximately 23.7 ± 0.2 V dc and automatically to restore power on the auto restore bus only when the battery common output voltage rises to 26.0 ± 1.0 V dc. Command circuitry is provided to reset or override the automatic switch functions. Telemetry signals are provided for essential bus voltage, override status and reset status. This feature is incorporated on both buses.

The control of power to orbiter bus experiments is performed by overload control units. Each unit has six outputs that are capable of being individually commanded on/off. The overload control unit operates in a saturated mode for any input voltage between 23 to 33 V dc as long as the output current is less than the limit current. The unit is designed to limit the total current at some predetermined level and to trip or interrupt power when the output falls due to the limiting action. After a trip has occurred, an "on" command must be issued to reapply power. Relays within the unit can be opened to prevent the application of power to all loads simultaneously. Power to heaters will be controlled by a heater switch unit comprised of magnetically latched relays with protective fuses. Each switch unit contains two channels with each being commandable on or off.

The probe bus utilizes a power interface unit to perform the experiment power switching function. Each experiment is individually commandable. All relays in this unit are magnetically latching with redundant protective fuses. In each case, the relays have been appropriately sized for current handling capability of that particular experiment.

The source of power on the large and small probe is a silver-zinc battery, appropriately sized for the energy needs of the mission. The battery on each probe is capable of being charged from the probe bus upon command. The battery is disconnected from the loads by means of relays to minimize battery discharge. This unit is redundant and controlled from the probe bus.

Current sensors are appropriately located throughout the buses and one is in each probe to assess performance of the power subsystem. The current sensor employs a transductor excited by a small two transistor, square-wave inverter. The sensitivity of the transducer is a function of the number of turns looped through two saturable reactors. Therefore, each sensor can be individually adjusted for the appropriate current range.

A checkout bus is provided on each probe to facilitate checkout of all units within the probe. Checkout power is derived from the probe bus.

Power switching is performed by a power interface unit within each probe. The noncritical elements of the system are redundantly fused. The critical elements, i.e., rf, G-switch, and command data and handling are not fused.

2. INTRODUCTION

The power subsystem designs for the Pioneer Venus program vehicles are the result of several studies and tradeoffs directed toward achieving a low cost, highly reliable design with a maximum amount of common hardware between vehicles. The power subsystem designs provide the generation, power management, and control of the power to the using subsystems and experiments by means of an unregulated bus. Studies performed include those tasks specified in the Ames Research Center contract statement of work on power requirements definition, power budgets as a function of missile profile, alternatives of a regulated versus unregulated primary bus, and definition of the losses and margins in the subsystem designs. In addition to these studies, several others were performed to evaluate significant design decisions and tradeoffs.

The trade studies were oriented toward the Thor/Delta designs, but in all cases the results are either common to the Atlas/Centaur or the differences are documented and explained in the sections of this report. Subsystem requirements are discussed and established in Section 3 of the report for the probe bus, large and small probes, and orbiter. Power profiles defining the electrical loads for the power units have been prepared. Section 4 presents the trade studies conducted and establishes conclusions of each study. The Thor/Delta and Atlas/Centaur baseline designs are summarized in Sections 5 and 6, respectively.

3. SUBSYSTEM REQUIREMENTS

The mission and system design requirements which constrain the power subsystem design effort are discussed in this section. This discussion will only describe the requirements for the Thor/Delta spacecraft. Although the mission and system technical requirements are basically the same for Atlas/Centaur, the priorities assigned to weight and cost are different such that the Atlas/Centaur design requirements shall be addressed in Section 6. The following three sections will then describe the mission requirements, the system functional requirements and the power budget.

3.1 MISSION REQUIREMENTS

The mission requirements peculiar to all four vehicles shall be described herein. The two Thor/Delta spacecraft, probe bus and orbiter were scheduled for launch in 1977 and 1978 for a Type I and Type II trajectory, respectively. The large and small probes would be carried aboard the probe bus for nominally 118 days in a dormant state and upon separation from the probe bus they would undergo a 20-day mission on their own power which terminates with impact. The following subsections will describe the various mission constraints as they apply to the four power subsystems.

Probe Bus Mission

The probe bus launch date was 11 January 1977 on a Type I trajectory for a Venus encounter at nominally launch + 128 days (L+128^{d}). Table 3-1 lists the various pertinent parameters applicable to the power subsystem as a function of the mission subphase.

Large and Small Probe Mission

The large and small probe power subsystems must be capable of enduring the dormant mode while in transit to Venus on the probe bus and be capable of providing all the required energy during the specified 20-day mission from separation to entry and through the descent phase to impact. Table 3-2 lists the pertinent parameters applicable to the large and small probe power subsystem mission constraints.

TABLE 3-1. POWER SUBSYSTEM PARAMETERS

Operational Mode	Mission Time* (Start)	Mode Duration	Distance From Sun, km x 10^6	Spin Axis Orientation** deg	Solar Panel Temperature °C	Spin Rate, rpm	Power Source
Launch to spacecraft sun acquisition	L+0^h	1.27^h	147	NA	23.5	0 to 100	Battery
Cruise 1	L+0^d	5^d	147	90	23.5	60	S/P***
TCM 1	L+5^d	0.95^h	147	10	23.5	60	Battery
Cruise 2	L+5^d	15^d	147	90	23.5	60	S/P
TCM 2	L+20^d	0.58^h	146	45	25.0	60	Both
Cruise 3	L+20^d	30^d	146	90	23.5	60	S/P
TCM 3	L+50^d	0.23^h	140	90	30.6	60	S/P
Cruise 4	L+50^d	46^d	140	90	30.6	60	S/P
TCM 4	L+96^d	0.33^h	121	90	52.7	60	S/P
Cruise 5A/5B	L+96^d	11^d	121	90	52.7	30	S/P
Probe C/O	L+107^d	1^d	117	90	58.9	30	Both
Cruise 5C	L+107^d	1^d	117	90	58.9	30	S/P
Probe separation	L+108^d	8^h	116	37 to 57	59.4	15/71	Both
Bus tracking	L+108^d	2^d	116	90	59.4	60	S/P
TCM 6 (bus retarget)	L+110^d	0.85^h	115	35	61.1	60	Both
Cruise 6A	L+110^d	8^d	115	50	61.1	60	S/P
TCM 7 (reorientation)	L+118^d	0.25^h	113	50	64.4	60	
Cruise 6B	L+118^d	10^d	113	58	64.4	60	
Entry 1	L+128^d	2.2^h	110	66	67.7	60	S/P
Entry 2	E-$.25^h$	0.25^h	110	NA	67.7	60	Both

*h = hours, d = days
**Spin axis orientation is with respect to the ecliptic
***S/P = solar panel

TABLE 3-2. PROBE MISSION REQUIREMENTS

Operational Mode	Mission Start Time*	Duration	Dormant or Active	Environment		Remarks
				Temperature °C	Acceleration g	
Transit	L+0^h	106	Dormant	-39 to -18	-	
Battery charge	L+106^d	24^h	Active	-22	-	Top OFF battery from probe bus
Preseparation C/O	L+107^d	0.25^h	Dormant	+37	-	OFF probe bus power subsystem
Post separation operations	L+108^d	0.17^h	Active	+37	-	
Idle (cruise)	L+108^d	20^d	Active	+37 to +5	-	
Preentry	E-15^m	15^m	Active	+5	-	
Entry	E = 0	0.5^m	Active	+5	L = 500** S = 540	
Descent	E + .5^m	L=53.7^m S=74.5^m	Active	+5 to +125	-	

*h = hours; d = days; m = minutes; L = large probe; S = small probe

**For detailed information regarding the acceleration environment during entry for large and small probes, refer to subsection 4.5 of this volume.

TABLE 3-3. ORBITER TRANSIT

Operational Mode	Start Time*	Duration	Distance from Sun km x 10^6	Spin Axis Orientation** deg	Solar Panel Temperature °C	Spin Rate, rpm	Power Source
Launch to spacecraft separation	L+0^h	1.7^h		NA	19.4	0 to 100	Battery
Spacecraft separation to sun acquisition	L+1.7^h	2.4^h		64	19.4	50 to 70	
Cruise 1	L+4.1^h	5^d	152.3	90	19.4	60	
TCM 1	L+5^d	0.87^h	153.3	10	17.8	60	Battery
Cruise 2	L+5^d	15^d	153.3	90	17.8	30	
TCM 2	L+20^d	0.68^h	157.2	45	13.3	30	SP/battery
Cruise 3	L+20^d	30^d	157.2	90	13.3	30	S/P
TCM 3	L+50^d	0.26^h	160.1	90	11.1	30	S/P
Cruise 4A/B	L+50^d	41^d	160.1	90	11.1	30	S/P
Cruise 4C	L+91^d	1^d	152.9	90	18.3	30	S/P
Cruise 4D/E/F	L+92^d	71^d	152.9	90	18.3	30	S/P
TCM 4	L+166^d	0.29^h	116.5	90	59.4	30	S/P
Cruise 5	L+166^d	20^d	116.5	90	59.4	30	S/P
Preinsertion reorientation	L+186^d	0.18^h	108.9	10	71.1	30	Battery
Coast	L+186^d	1^d	108.9	90	71.1	30	S/P
Orbit insertion	L+187^d	1/8^h	108.7	77	71.2	30	S/P

*d = days; h = hours; S/P = solar panel
**Spin axis orientation is with respect to elliptic

Orbiter Spacecraft Mission

The orbiter spacecraft was to be launched on 31 May 1978 on a Type II trajectory for an insertion into an elliptical polar orbit of Venus on 2 December 1978. The spacecraft would have remained in this 200 by 66,000 km orbit for a minimum of 225 days. Tables 3-3 and 3-4 describe the significant mission characteristics for the transit and orbital phases of the mission.

3.2 SUBSYSTEM FUNCTIONAL REQUIREMENTS

The spacecraft systems requirements for all four vehicles are defined in Table 3-5.

3.3 POWER REQUIREMENTS

The purpose of the power requirements study was to develop a detailed power budget for each of the four Pioneer Venus vehicles and in so doing to establish the inputs for "sizing" the power subsystem solar panel and/or battery. Additionally, the power budget was intended to develop an operational technique and rationale, in consonance with the mission sequence and experiment requirements, for each distinct phase of the mission such that the power subsystem, in conjunction with the spacecraft operations, could sufficiently support the load at all times.

Those operational power modes which drive the design or sizing of the solar array and battery are as follows:

1) Probe Bus:

   a.) The solar panel is sized by the battery charge requirements in Cruise 5B in addition to those subsequent modes whereby the solar power output is diminished by the "off" sun angle.

   b.) The battery is sized by the energy required during the 8-h probe release sequence wherein the solar panel cannot completely support the load. A maximum depth of discharge (DOD) of 40 percent is used throughout the mission, including probe release.

2) Orbiter Spacecraft:

   a.) For a Type II trajectory, the solar panel is sized by the "near" earth conditions (at ≈ L + 55 days) and by the battery charge requirements during the apoapsis eclipse season (at ≈ I + 187 days) where the battery is required for both the long eclipse and during periapsis when the planet heat load (at this geometric condition) drives the solar panel output to 0 W at 28 V (see Section 5 for details).

TABLE 3-4. ORBITER MISSION CHARACTERISTICS

Event	Orbit Mission Time	Duration of Event	Solar Panel Temperature °C	Spin Rate, rpm	Power Source
Short eclipse season	I + 26^{d} to I + 116^{d}	0 to 24m	-	5	Battery
			-	5	
Long eclipse season	I + 183^{d} to I + 191^{d}	0 to 310m	-	5	Battery
Periapsis pass					
Panel temperatures*					
BOL orbit	I + 1^{d}	25m	95	5	Both
Long eclipse orbit	I + 187^{d}	40m	132	5	
Normal orbit conditions	Days other than above excluding periapsis	24^{h}	73.9	5	Solar panel

*For detailed information regarding periapsis solar panel temperature response, refer to Section of this volume.

**d = days; h = hours; m = minutes

TABLE 3-5. POWER FUNCTIONAL REQUIREMENTS

Vehicle	Parameter	Requirement
Probe bus	Regulation	Unregulated at nominal 28 ±5 Vdc.
	Primary power source	Provide a spinning cylindrical solar panel capable of supplying all steady state loads for the entire mission while solar illumination is existent and the panel is at a sun angle near 90 deg (perpendicular to sun).
	Secondary power source	Provide a single lightweight battery capable of supplying energy to the spacecraft when the solar panel is not illuminated or at an angle such that it cannot fully supply the required power; i.e., a share mode operation. The maximum number of discharge cycles is estimated at 10.
	Power distribution	Provide a direct coupling to all housekeeping subsystems and a separate fused ON/OFF switch for each probe bus experiment.
	Battery charge	Provide a positive means of recharging the probe bus and probe batteries from the probe bus solar panel.
	Polarity	The power supplied to all users shall be a positive supply, negative return.
	Probe power	Provide a means of supplying each probe with power for probe C/O while on the probe bus.
	Pyrotechnic transients	The pyrotechnic control unit shall be tied directly to the probe bus battery and the battery shall be capable of handling a maximum current pulse of 30 A for 50 ms.
	Other transients	Propulsion valve transients can be accommodated from the solar panel if sufficient margin exists; however, for most cases the operation of these valves depends upon battery energy.
Orbiter spacecraft	Regulation	Same as probe bus.
	Primary power source	Same as probe bus.
	Secondary power source	Provide a single battery capable of supplying energy to the spacecraft when the solar panel is not capable of doing so for various reasons; i.e., off sun angle, eclipse or power degradation due to planet heating loads at periapsis. Minimum number discharge cycles is 214.
	Battery charge	Provide a positive means of recharging the orbiter battery from the solar panel.
	Power distribution	Provide for direct coupling of the power sources and individual ON/OFF subsystems and individual ON/OFF switching, with overload protection, for each science experiment.
	Polarity	Same as probe bus
	Probe power	Not applicable.
	Pyrotechnic transients	Same as probe bus.
	Other transients	The orbiter spacecraft shall experience the same transients as the probe bus plus those presented by the radar altimeter which is defined in detail in Footnote (*).
Large and small probes	Regulation	1) Regulated bus at 28 Vdc ±2 percent. 2) Unregulated bus for pyrotechnic, heaters, and stepper motors.
	Primary power source	A single lightweight battery capable of high depth of discharge for one cycle.
	Battery charge	Battery charge will be accomplished from the probe bus.
	Power distribution	1) Provide ON/OFF switching for all housekeeping subsystems by functional groups. 2) Provide ON/OFF switching for the equipment subsystems by functional groups. ** 3) Provide individual fusing for each science experiment.
	Pyrotechnic transients	Provide a direct coupling to the battery for the pyrotechnic firing current and an ON/OFF switch. The switch and battery shall be capable of handling the following maximum current pulses: Lp = 30 A/50 ms Sp = 10 A/50 ms

* The radar altimeter average power for this report is estimated at 17 W, which is 5 W higher than the advertised average of 12 W by the experiment data book. We have assumed an additional 5 W as a means of accommodating a capacitor system to supply energy for the 35 W, 50 μsec spikes (150 cps rep rate) which are "on-top" of a 35 W, 1.75 second pulse which occurs every spacecraft revolution during the periapsis pass.

** Lp = 3 functional groups; Sp = 2 functional groups

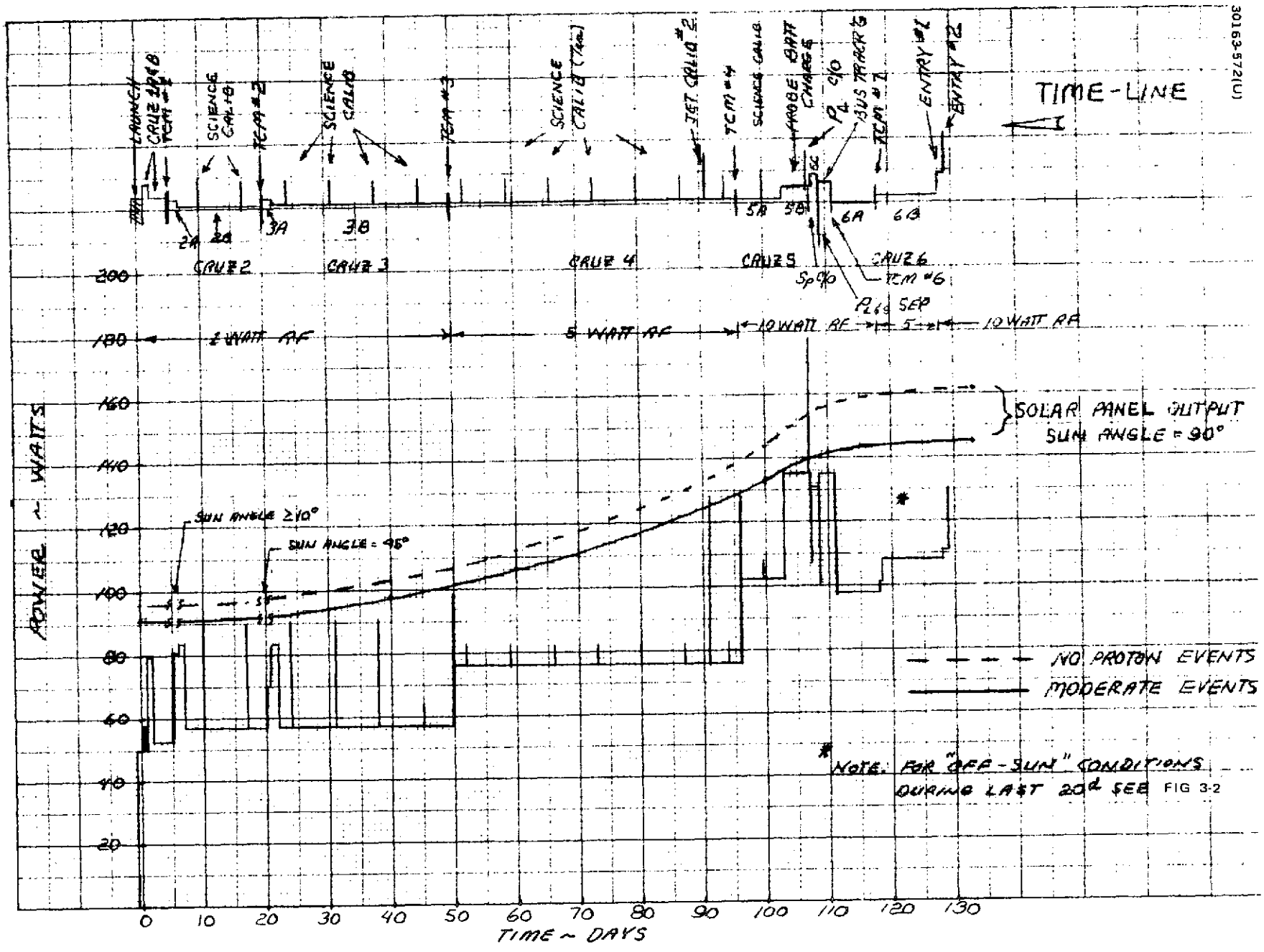

FIGURE 3-1. PROBE BUS POWER HISTOGRAM — TRANSIT PHASE

b.) The battery is sized by the long apoapsis eclipse which requires 145.9 W-hr and represents a 67.5 percent DOD to the battery. The specified time duration represents a midpoint between the worst case pneumbra and umbra for this mission. Additionally, the spacecraft is configured to provide sequential operation of the IR radiometer, solar wind probe, and magnetometer, at a 33-1/3 percent duty cycle, during the entire eclipse and storage of said data for subsequent playback.

3) Large Probe. The large probe descent time and operational configuration and assumptions as described in this section represent an energy requirement of 278.8 W-hr.

4) Small Probe. The small probe descent time and operational configuration and assumptions as described in Section 4 represent an energy requirement of 145.3 W-hr.

Probe Bus Power Budget

The power budget for the probe bus contains 25 standard operational modes which begin at prelaunch (T - 5 min) and continues through the mission to probe bus entry and destruction (Entry 2). The budget also contains a science calibration mode which is used throughout the mission on a weekly basis. For power entries, the budget lists seven subsystems and 27 units. For the power subsystem, an efficiency factor of 85 percent is used for determining battery discharge regulator losses. For battery charging, two current rates are used. For recharging appreciable depletions, a full or maximum rate of 1 A (approximately 32 V) is used, whereas 0.16 A (5.1 W) is used when very modest depletions have occurred or for trickle charging. In events where the solar panel does not support the entire load, the battery is used as a second source of energy in a share mode configuration. A 10 percent contingency is added to the required power. Figures 3-1 through 3-3 will explain the workings of each operational mode. Figures 3-1 and 3-2 are probe bus power histograms; Figure 3-1 described the transit phase in detail, while Figure 3-2 describes the last 20 days in detail. Figure 3-3 provides a battery depth of discharge and energy histogram of the entire mission. Table 3-6 contains the summary computer run of the power budget. Tables 3-7 and 3-8 will define the various entry and unit designators used by the computer program in printing out the detailed and summary power budgets for all four vehicles. The mode headings are for the most part self explanatory; however, the various histograms and the orbital power mode diagram will explain those headings which are not self explanatory.

Large Probe Power Budget

The power budget for the large probe contains ten standard power modes plus a checkout mode on the probe bus. The power entries contain 7 subsystems and 24 unit entries. An efficiency of 87.9 percent is used to determine battery discharge regulator losses and a 10 percent contingency is added to the total

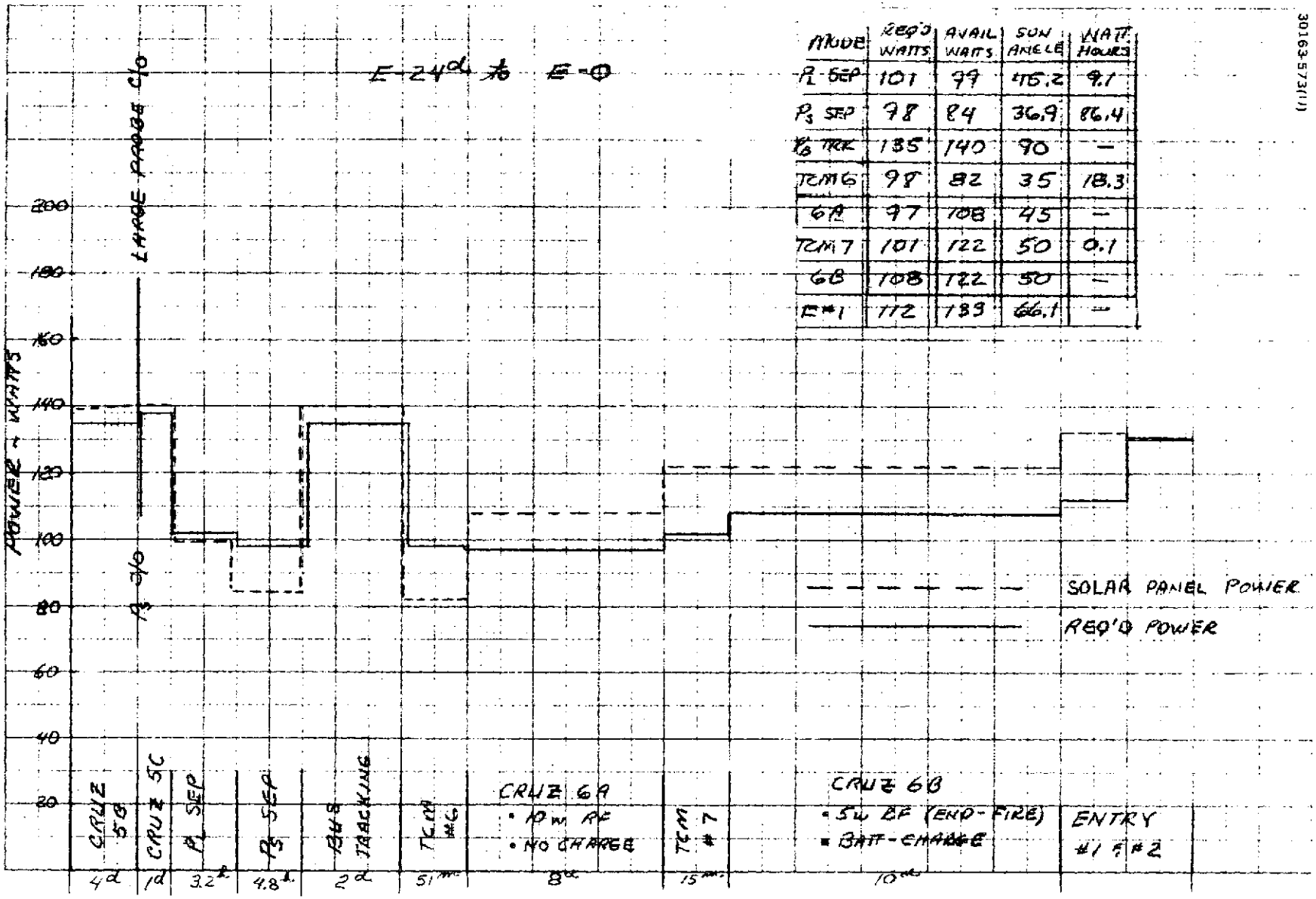

FIGURE 3-2. PROBE BUS POWER

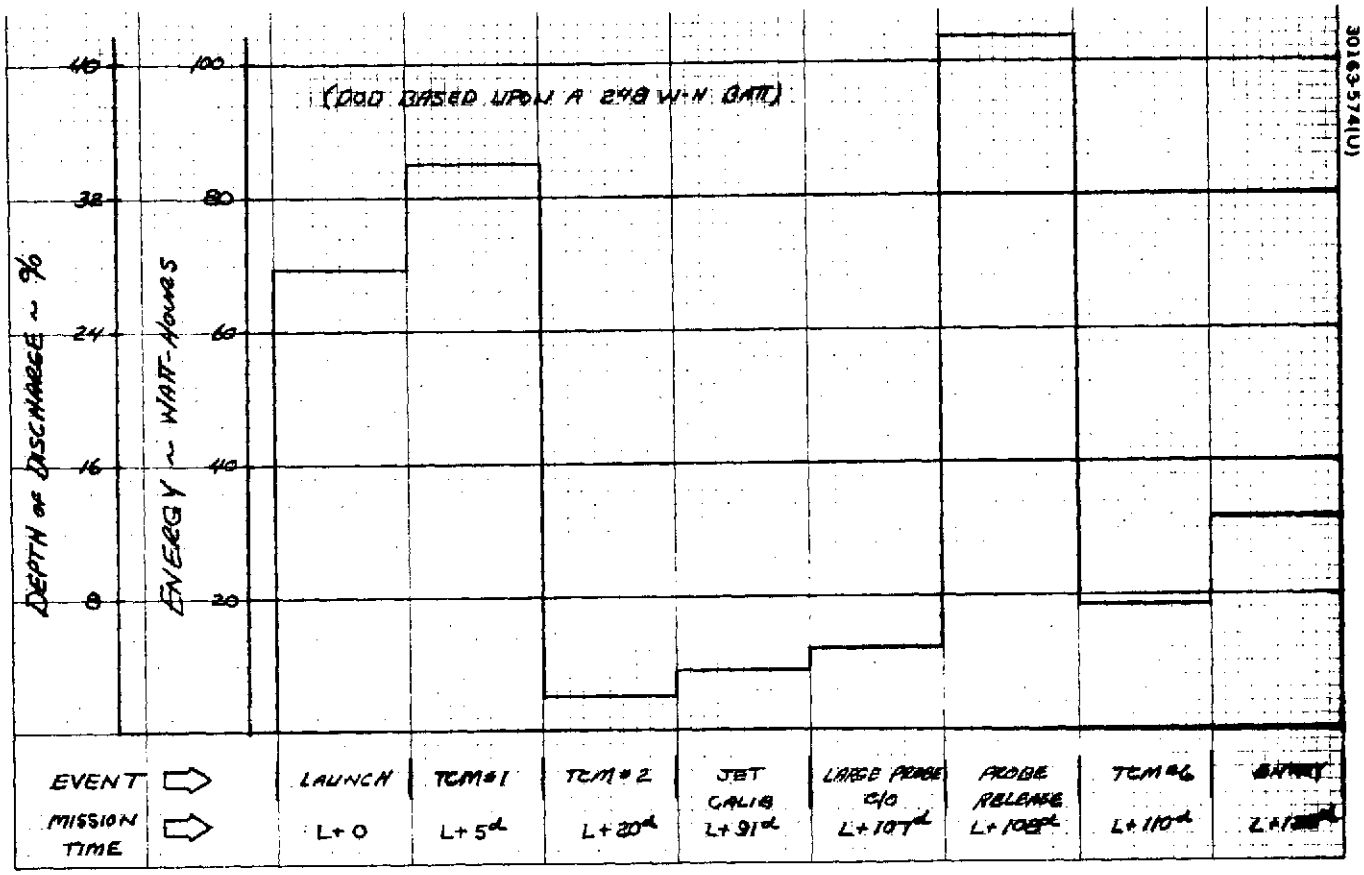

FIGURE 3-3. PROBE BUS BATTERY ENERGY AND DEPTH OF DISCHARGE HISTOGRAM

TABLE 3-6. PROBE BUS POWER PROFILE

	ON BATT	LNCH -SEP	SEP-ACQ.	ATT. DET.	JET CALB	CRUZ #1A
MODE DUR	0.08	0.68	0.51	2.00	6.20	24.00
TIME	0	0	0	0	1	0
SUNANGLE	0.	0.	0.	57.00	85.00	90.00
RF	18.6	18.6	18.6	18.6	18.6	18.6
DATA	8.5	8.5	8.5	8.5	8.5	8.5
CMD	3.8	3.8	3.8	3.8	3.8	3.8
AC	0.	0.	6.3	6.3	34.3	3.8
THER	3.5	3.5	3.5	3.5	3.5	3.5
SCI	0.	0.	0.	0.	0.	0.
PWR	4.9	4.9	4.9	4.9	4.9	36.9
CONTING.	3.9	3.9	4.6	4.6	7.3	7.2
SBTLWATTS	(43.2)	(43.2)	(50.2)	(50.2)	(79.9)	(79.5)
SOLAR PWR	0.	0.	0.	76.3	90.7	91.0
PWR MARG.	-43.2	-43.2	-50.2	26.2	10.8	11.5
WATT HRS	3.6	29.4	25.6	0.	0.	0.
TRANSIENT	0.	0.	0.3	0.3	0.	0.
DISC.REG.	0.6(7.6)	5.2(7.6)	4.6(8.9)	0. (0.)	0. (0.)	0. (0.)
UNREG.PWR	0. (0.)	0. (0.)	0. (0.)	0. (0.)	0. (0.)	0. (0.)
CONTING.	0. (0.)	0. (0.)	0. (0.)	0. (0.)	0. (0.)	0. (0.)
WTHRS TOT	4.2	34.6	30.4	0.3	0.	0.
TOT WATTS	(50.8)	(50.8)	(59.1)	(50.2)	(79.9)	(79.5
BATT CAP	248.0	248.0	248.0	248.0	248.0	248.0
DPTH-DSCH	1.7	13.9	12.3	0.1	?.	?.

	CRUZ #1B	TCM #1	CRUZ #2A	CRUZ #2B	TCM #2	CRUZ #3A
MODE DUR	96.00	0.05	24.00	336.00	0.58	24.00
TIME	1	5	5	6	20	20
SUNANGLE	90.00	0.	90.00	90.00	45.00	90.00
RF	18.6	36.8	18.6	18.6	36.8	18.6
DATA	8.5	8.5	8.5	8.5	8.5	8.5
CMD	5.0	3.8	2.0	5.0	3.8	2.0
AC	3.8	6.3	3.8	3.8	6.3	3.8
THER	2.5	3.5	2.5	2.5	3.5	2.5
SCI	0.	0.	3.5	3.5	0.	3.5
PWR	10.0	4.9	36.9	10.8	4.9	36.9
CONTING.	4.8	6.4	7.6	5.2	6.4	7.6
SBTLWATTS	(53.2)	(70.2)	(83.4)	(57.1)	(70.2)	(83.4)
SOLAR PWR	91.0	0.	91.0	91.0	65.1	92.0
PWR MARG.	37.8	-70.2	7.6	33.9	-5.1	8.6
WATT HRS	0.	66.7	0.	0.	3.2	0.
TRANSIENT	0.	6.3	0.	0.	8.5	0.
DISC.REG.	0. (0.)12.8(13.5)		0. (0.)	0. (0.)	0.6(1.1)	0. (0.)
UNREG.PWR	0. (0.)	0. (0.)	0. (0.)	0. (0.)	0. (0.)	0. (0.)
CONTING.	0. (0.)	0. (0.)	0. (0.)	0. (0.)	0. (0.)	0. (0.)
WTHRS TOT	0.	85.8	0.	0.	4.1	0.
TOT WATTS	(53.2)	(83.7)	(83.4)	(57.1)	(71.2)	(83.4
BATT CAP	248.0	248.0	248.0	248.0	248.0	248.0
DPTH-DSCH	0.	34.6	0.	0.	1.6	0.

TABLE 3-6. (Continued)

	CRUZ #3B	TCM #3	CRUZ #4	TCM #4	CRUZ #5A	CRUZ #5B
MODE DUR	696.00	0.23	1104.00	0.33	168.00	96.00
TIME	29	50	50	96	96	103
SUNANGLE	90.00	90.00	90.00	90.00	90.00	90.00
RF	13.6	36.8	36.8	62.0	62.0	62.0
DATA	8.5	8.5	8.5	8.5	8.5	8.5
CMD	5.0	3.8	2.0	3.8	0.0	5.0
AC	3.8	34.3	3.8	34.3	3.8	3.8
THER	2.5	2.5	2.5	2.5	2.5	2.5
SCI	3.5	0.	3.5	0.	3.5	3.5
PWR	10.0	4.9	10.2	4.9	13.0	36.9
CONTING.	5.2	9.1	6.7	11.6	9.2	12.2
SBTLWATTS	(57.1)	(99.9)	(73.8)	(127.6)	(101.5)	(134.4)
SOLAR PWR	92.0	101.2	131.2	129.0	139.0	139.0
PWR MARG.	34.9	1.1	27.2	1.4	27.5	4.6
WATT HRS	0.	0.	0.	0.	0.	0.
TRANSIENT	0.	0.	0.	0.	0.	0.
DISC.REG.	0. (0.)	0. (0.)	0. (0.)	0. (0.)	0. (0.)	0. (0.)
UNREG.PWR	0. (0.)	0. (0.)	0. (0.)	0. (0.)	0. (0.)	0. (0.)
CONTING.	0. (0.)	0. (0.)	0. (0.)	0. (0.)	0. (0.)	0. (0.)
WTHRS TOT	0.	0.	0.	0.	0.	0.
TOT WATTS	(57.1)	(99.9)	(73.8)	(127.6)	(101.5)	(134.4
BATT CAP	248.0	248.0	248.0	248.0	248.0	248.0
DPTH-DSCH	0.	0.	0.	0.	0.	0.

	LP C/O	SP C/O	CRUZ #5C	LP SEP	TCM #5	BUS TRKG
MODE DUR	0.25	0.75	23.50	3.20	4.82	48.00
TIME	107	107	107	108	108	108
SUNANGLE	92.00	90.00	90.00	45.20	36.90	90.00
RF	62.0	62.0	62.0	62.0	62.0	62.0
DATA	8.5	8.5	8.5	8.5	8.5	8.5
CMD	5.0	5.0	2.0	6.8	3.0	5.0
AC	3.8	3.8	3.8	6.3	6.3	3.8
THER	2.5	2.5	2.5	3.5	3.5	2.5
SCI	0.	0.	3.5	0.	0.	3.5
PWR	80.3	15.8	36.9	4.9	6.2	36.9
CONTING.	16.2	9.8	11.9	9.2	9.3	12.2
SBTLWATTS	(178.3)	(107.4)	(131.1)	(101.2)	(99.3)	(134.4)
SOLAR PWR	140.0	140.0	140.0	99.3	84.1	140.0
PWR MARG.	-38.3	32.6	8.9	-1.9	-15.3	5.6
WATT HRS	9.6	0.	0.	6.8	73.3	0.
TRANSIENT	0.	0.	0.	1.1	0.5	0.
DISC.REG.	1.7(6.7)	0. (0.)	0. (0.)	1.2(8.4)	13.0(2.7)	0. (0.)
UNREG.PWR	0. (0.)	0. (0.)	0. (0.)	0. (0.)	0. (0.)	0. (0.)
CONTING.	0. (0.)	0. (0.)	0. (0.)	0. (0.)	0. (0.)	0. (0.)
WTHRS TOT	11.3	0.	0.	8.3	86.8	0.
TOT WATTS	(135.1)	(107.4)	(131.1)	(101.6)	(100.0)	(134
BATT CAP	248.0	248.0	248.0	248.0	248.0	248.0
DPTH-DSCH	4.5	0.	0.	3.3	35.0	0.

←95.1 W-H, 38.3% DOD→

TABLE 3-6. (Continued)

	TCM #6	JET CALB	CRUZ #6A	TCM #7	CRUZ #6B	ENTR #1
MODE DUR	0.35	2.00	192.00	0.25	240.00	2.20
TIME	110	91	110	118	113	128
SUNANGLE	35.00	84.00	50.00	58.00	58.00	66.10
RF	62.0	62.0	62.0	62.0	36.8	62.0
DATA	8.5	8.5	8.5	8.5	8.5	8.5
CMD	3.8	3.8	2.0	6.8	5.0	3.8
AC	6.3	34.3	3.8	6.3	3.8	3.8
THER	3.5	2.5	3.5	3.5	3.5	2.5
SCI	0.	0.	3.5	0.	3.5	15.9
PWR	4.9	4.9	4.9	4.9	36.9	4.9
CONTING.	3.9	11.6	8.8	9.2	9.8	10.1
SBTLWATTS	(97.9)	(127.6)	(97.0)	(101.2)	(107.8)	(111.5)
SOLAR PWR	71.4	124.3	108.8	122.1	122.1	132.6
PWR MARG.	-16.5	-3.3	11.8	20.9	14.3	21.2
WATT HRS	14.3	6.6	0.	0.	0.	0.
TRANSIENT	0.4	0.	0.	0.1	0.	0.
DISC.REG.	2.5(3.7)	0. (0.)	0. (0.)	0. (0.)	0. (0.)	0. (0.)
UNREG.PWR	0. (0.)	0. (0.)	0. (0.)	0. (0.)	0. (0.)	0. (0.)
CONTING.	0. (0.)	0. (0.)	0. (0.)	0. (0.)	0. (0.)	0. (0.)
WTHRS TOT	16.9	6.6	0.	0.1	0.	0.
TOT WATTS	(100.9)	(127.6)	(97.0)	(101.2)	(107.8)	(111.5)
BATT CAP	248.0	248.0	248.0	248.0	248.0	248.0
DPTH-DSCH	6.8	2.6	0.	0.2	0.	0.

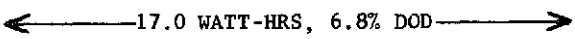

	ENTR #2	AAAA AAAA	AAAA AAAA	AAAA AAAA	AAAA AAAA	AAAA AAAA
MODE DUR	0.25	0.	0.	0.	0.	0.
TIME	128	0	0	0	0	0
SUNANGLE	0.	0.	0.	0.	0.	0.
RF	62.0	62.0	62.0	62.0	62.0	62.0
DATA	8.5	70.5	70.5	70.5	70.5	70.5
CMD	3.8	77.3	77.3	77.3	77.3	77.3
AC	3.8	81.1	81.1	81.1	81.1	81.1
THER	2.5	84.6	84.6	84.6	84.6	84.6
SCI	15.9	88.1	88.1	88.1	88.1	88.1
PWR	4.9	93.0	93.0	93.0	93.0	93.0
CONTING.	10.1	9.3	9.3	9.3	9.3	9.3
SBTLWATTS	(111.5)	(102.3)	(102.3)	(102.3)	(102.3)	(102.3)
SOLAR PWR	0.	0.	0.	0.	0.	0.
PWR MARG.	-111.5	-102.3	-102.3	-102.3	-102.3	-102.3
WATT HRS	27.9	0.	0.	0.	0.	0.
TRANSIENT	0.	0.	0.	0.	0.	0.
DISC.REG.	4.9(19.6)	0. (0.)	0. (0.)	0. (0.)	0. (0.)	0. (0.)
UNREG.PWR	0. (0.)	0. (0.)	0. (0.)	0. (0.)	0. (0.)	0. (0.)
CONTING.	0. (0.)	0. (0.)	0. (0.)	0. (0.)	0. (0.)	0. (0.)
WTHRS TOT	32.8	0.	0.	0.	0.	0.
TOT WATTS	(131.2)	(102.3)	(102.3)	(102.3)	(102.3)	(102.3)
BATT CAP	248.0	248.0	248.0	248.0	248.0	248.0
DPTH-DSCH	13.2	0.	0.	0.	0.	0.

TABLE 3-7. PRINTED ENTRY DESIGNATOR

Printed Entry	Explanation	Units
MODE DUR	Time required to perform that particular mode specified on the printout	hours
TIME	The start time of each particular mode from various mission milestones such as launch, probe separation, entry, etc. NOTE: Negative numbers represent a prior to event	m = minute h = hours d = days
SUNANGLE	Angle between the sun and the spacecraft spin axis with 90 defined as the sun being normal to the spin axis and the solar panel	degrees
CONTING	10 percent contingency	watts
SBTLWATTS	Total watts excluding discharge regulator	(watts)
SOLAR PWR	Solar panel output as a function of solar intensity and sun angle (that angle at top of printout)	watts
PWR MARG	The negative or positive margin existing between the watts required (not including discharge regulator) and panel output	watts
TRANSIENTS	Energy required for units that operate intermittently most notably the propulsion valves and solenoid drivers	watt-hours
DISC REG	Energy and power consumed by the battery discharge regulator, nominally 85 percent	watt-hours (watts)
UNREG PWR	Energy and power required for those units "tied" directly to the battery notably the window heaters in the probes (large and small)	watt-hours

TABLE 3-7. (Continued)

Printed Entry	Explanation	Units
CONTING	10 percent contingency of the UNREG PWR	watt-hours
WT HRS TOT	Total watt-hours required for that mode	watt-hours
BATT CAP	Total battery capacity in watt-hours NOTE: Does not account for specified DOD	watt-hours
DPTH-DSCH	Depth to which the battery has been discharged for that particular mode	percent
TOT WATTS	Peak watts required during this mode, i. e., sum of SBTLWATTS, DISC REG (watts), UNREG PWR (watts) and CONTING (watts)	(watts)

TABLE 3-8. COMPUTER PROGRAM SUBSYSTEM – UNIT DESIGNATOR KEY

Designator	Subsystem – Unit Name
RF	Radio subsystem
DATA	Data handling subsystem
CMD	Command subsystem
AC	Attitude control subsystem
THER	Thermal control subsystem
SCI	Science experiments
C&DH	Command and data handling subsystem
D/M	Deceleration Module
EQUP	Equipment subsystem
PWR	Power subsystem

required watts for all modes. All pyrotechnic transients are estimated and added as one lump sum under the heading of transients. Figure 3-4 contains an energy histogram for the complete large probe descent profile and Table 3-9 contains a summary power budget.

Small Probe Power Budget

The power budget for the small probe contains seven standard power modes plus a checkout mode on the probe bus. The power entries contain 5 subsystems and 14 units. An efficiency of 87 percent is used in determining battery discharge regulator losses and a contingency of 10 percent is added to the total required watts for all modes.

Figure 3-5 contains an energy histogram for the complete small probe descent profile and Table 3-10 contains a summary of the power budget.

Orbiter Spacecraft Power Budget

The detailed power budget for the orbiter spacecraft contains 22 standard operational modes for the transit phase of the mission. These modes extend from the T-5 minute mode on the launch pad up to and including orbit insertion in addition to a science calibration mode. The orbit phase of the mission is defined at three distinctly different 24-hour orbit periods. A worst cast periapsis eclipse (25 min) orbit has been selected and defined in the power budget; next, a worst case apoapsis eclipse (3-h) orbit has been selected and defined; this orbit also includes the worst case periapsis solar panel heating/power loss condition. Additionally, a typical orbit near the beginning of life (BOL) has been selected which also illustrates the solar panel heating and power losses during a periapsis pass at this period of time. It should be noted that the long eclipse orbit represents the worst possible condition in terms of periapsis solar panel heating and subsequent power loss at 28 Vdc. From this point in the mission, either toward BOL or EOL, the situation improves, which is somewhat of a midpoint between the two eclipse periods; i. e., solar azimuths of 0 and 180 deg.

For power entry purposes, the power budget includes 8 subsystems and 37 unit entries. The battery discharge regulator is assumed to be 85 percent efficient during all modes with one exception; i. e., during the long eclipse, an 80 percent efficient regulator is assumed because of the less than nominal power being "drawn". For battery charging purposes, the following rates have been chosen:

1) C/15 - to be used during cruise to provide the lowest possible load for the solar panel output.

2) C/10 - to be used during the orbital phase to provide a fully charged battery prior to the apoapsis midpoint and subsequent orbital correction maneuvers. This choice was rather arbitrary and is subject to change in the next iteration.

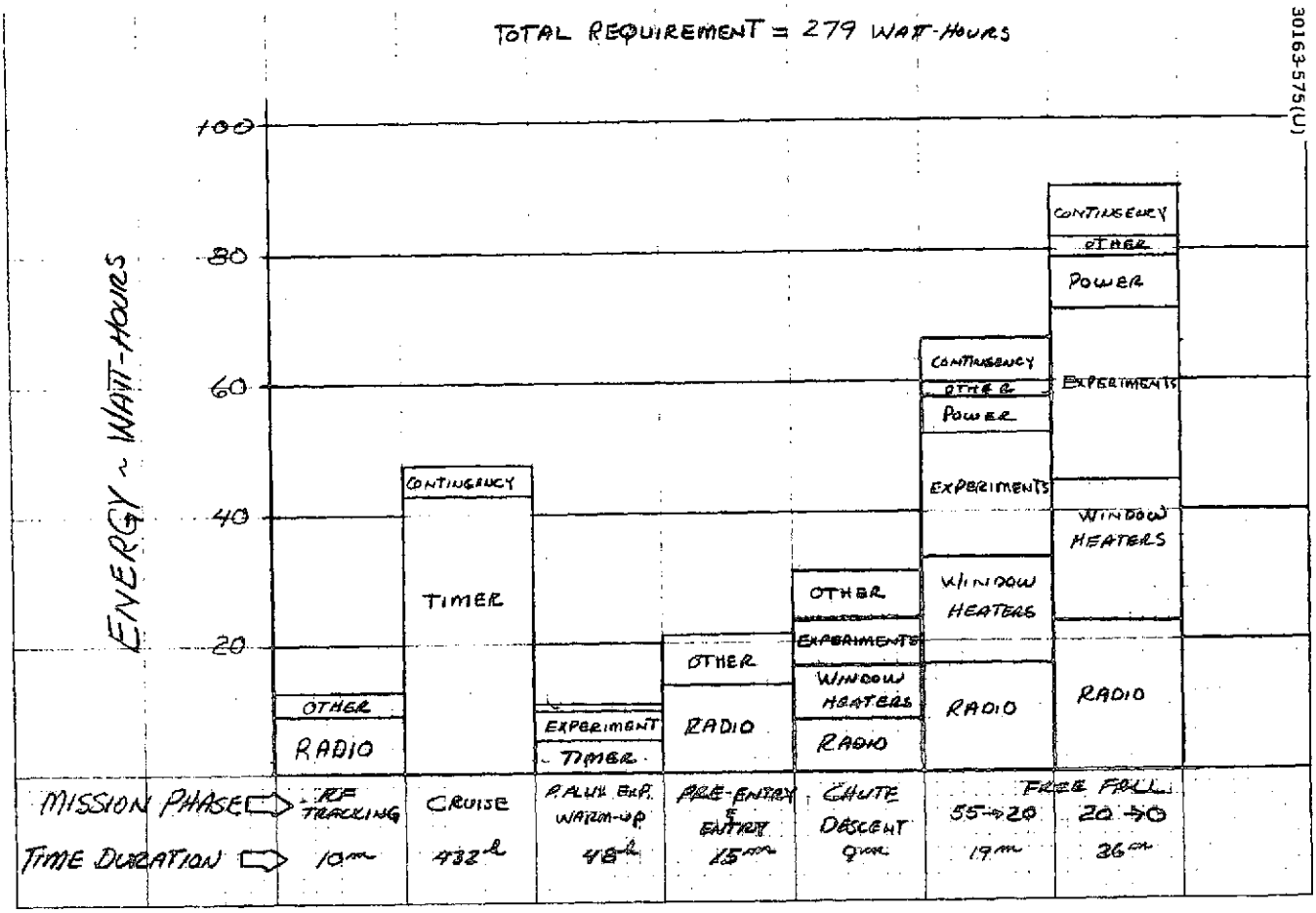

30163-575(U)

FIGURE 3-4. LARGE PROBE ENERGY HISTOGRAM

TABLE 3-9. LARGE PROBE POWER PROFILE

	SEP- C/O	SEP+ C/O	CRUZ #1	CRUZ #2	PRE- ENTR	PRE- ENTR
MODE DUR	0.	0.17	432.00	48.00	0.17	0.08
TIME	-21	-20	-20	-18	-15	-5
SUNANGLE	0.	0.	0.	0.	0.	0.
RF	0.	52.9	0.	0.	52.9	52.9
C&DH	4.5	4.5	0.1	0.1	4.5	4.5
D/M	1.5	0.	0.	0.	0.	1.5
EQUP	1.5	1.5	0.	0.	1.5	1.5
THER	0.	0.	0.	0.	0.	0.
SCI	60.6	0.	0.	0.1	4.4	4.4
PWR	0.4	0.4	0.	0.	0.4	0.4
CONTING.	6.8	5.9	0.0	0.0	6.4	6.5
SDTLWATTS	(75.3)	(65.2)	(0.1)	(0.2)	(70.1)	(71.7)
SOLAR PWR	0.	0.	0.	0.	0.	0.
PWR MARG.	-75.3	-65.2	-0.1	-0.2	-70.1	-71.7
WATT HRS	0.	10.9	47.5	10.6	11.7	6.0
TRANSIENT	0.	0.3	0.	0.	0.	0.
DISC.REG.	0. (0.)	1.7(10.1)	0. (0.)	0. (0.)	1.0(10.5)	0.9(13.0
UNREG.PWR	0. (0.)	0. (0.)	0. (0.)	0. (0.)	0. (0.)	0. (0.)
CONTING.	0. (0.)	0. (0.)	0. (0.)	0. (0.)	0. (0.)	0. (0.)
WTHRS TOT	0.	12.9	47.5	10.6	13.5	6.0
TOT WATTS	(75.3)	(75.3)	(0.1)	(0.2)	(83.6)	(82.5
BATT CAP	348.3	348.3	348.3	348.3	348.3	348.3
DPTH-DSCH	0.	3.7	13.6	3.0	3.9	2.0

	ENTR E=0	DEST #1	DEST #2	DEST #3	POST IMPT	AAAA AAAA
MODE DUR	0.01	0.15	0.31	0.43	0.86	0.
TIME	0	1	10	28	54	0
SUNANGLE	0.	0.	0.	0.	0.	0.
RF	52.9	52.9	52.9	52.9	52.9	52.9
C&DH	4.5	4.5	4.5	4.5	4.5	4.5
D/M	1.5	0.	0.	0.	0.	1.
EQUP	1.5	1.5	1.5	1.5	1.5	1.5
THER	0.	0.	0.	0.	0.	0.
SCI	0.4	54.6	60.6	60.6	4.3	4.3
PWR	0.4	0.4	0.4	0.4	0.4	0.4
CONTING.	6.9	11.4	12.0	12.0	6.4	6.4
SDTLWATTS	(76.1)	(125.3)	(131.9)	(131.9)	(70.0)	(70.0)
SOLAR PWR	0.	0.	0.	0.	0.	0.
PWR MARG.	-76.1	-125.3	-131.9	-131.9	-70.0	-70.0
WATT HRS	0.6	19.0	41.3	56.7	60.2	0.
TRANSIENT	0.	0.	0.	0.	0.	0.
DISC.REG.	0.1(11.4)	2.9(15.8)	6.2(19.8)	8.5(19.8)	9.0(10.5)	0. (0.)
UNREG.PWR	0. (0.)	8.4(55.0)	17.2(55.0)	21.9(51.0)	0. (0.)	0. (0.)
CONTING.	0. (0.)	0.8(5.5)	1.7(5.5)	2.2(5.1)	0. (0.)	0. (0.)
WTHRS TOT	0.7	31.1	66.4	89.3	69.2	0.
TOT WATTS	(87.5)	(204.6)	(213.2)	(207.3)	(82.5)	(70.0
BATT CAP	348.3	348.3	348.3	348.3	348.3	348.3
DPTH-DSCH	0.2	3.9	19.3	25.6	19.3	0.

MISSION TOTALS: 278.8 WATT-HOURS / 79.9% DOD

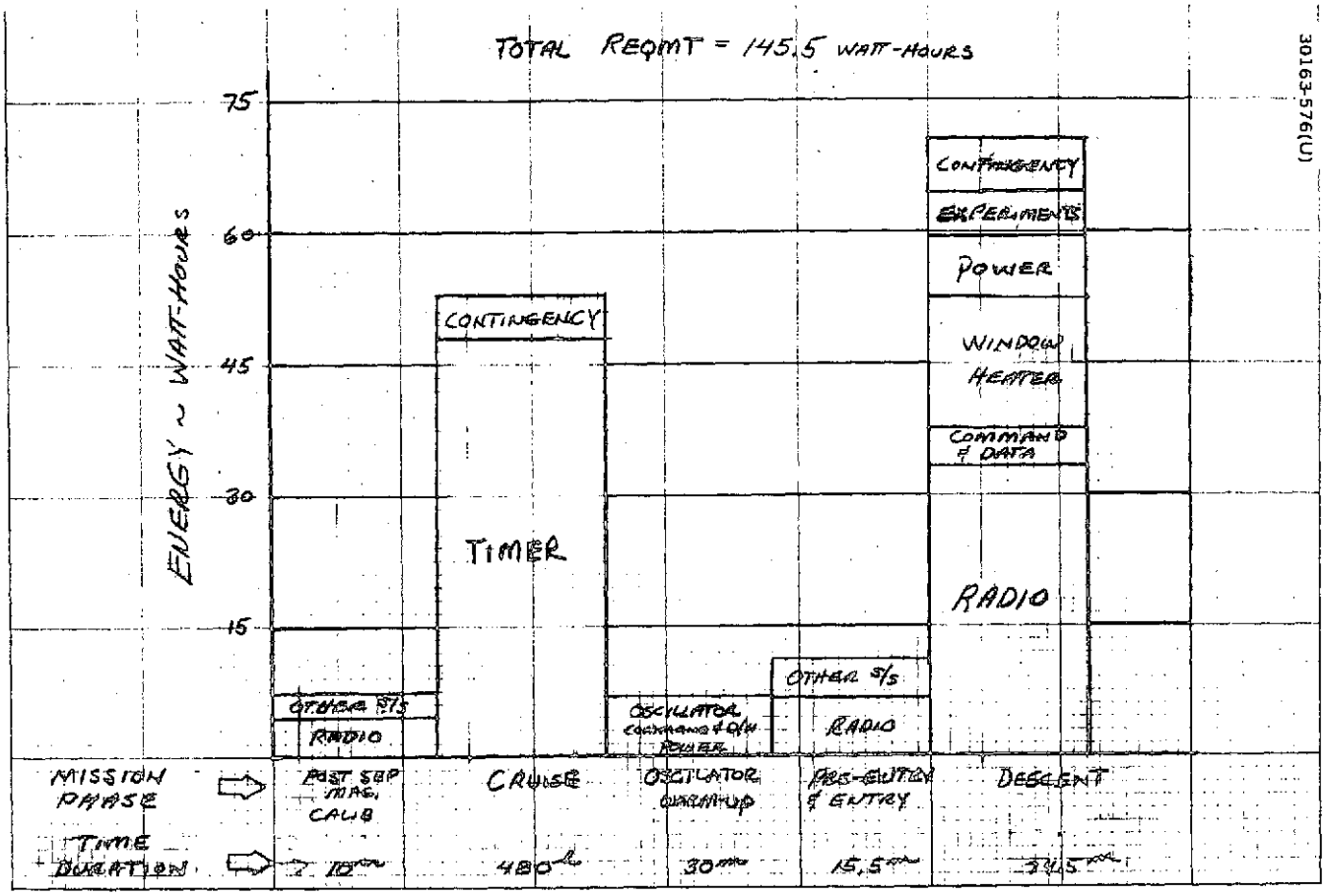

FIGURE 3-5. SMALL PROBE ENERGY HISTOGRAM

TABLE 3-10. SMALL PROBE POWER PROFILE

	SEP- C/O	SEP+ C/O	CRUZ	PRE- ENTR	PRE- ENTR	ENTR E=0
MODE DUR	0.	0.17	480.00	0.50	0.25	0.01
TIME	-21	-20	-20	-45	-15	0
SUNANGLE	0.	0.	0.	0.	0.	0.
RF	2.3	27.0	0.	2.0	27.0	0.3
C&DH	3.2	3.2	0.1	3.2	3.2	3.2
THER	0.	0.	0.	0.	0.	0.
SCI	4.0	4.0	0.	0.	4.0	3.4
POWR	0.4	0.4	0.	0.4	0.4	0.4
CONTING.	1.0	3.5	0.0	0.6	3.5	1.2
SBILWATTS	(10.9)	(38.1)	(0.1)	(6.2)	(38.1)	(13.5)
SOLAR PWR	0.	0.	0.	0.	0.	0.
PWR MARG.	-10.9	-38.1	-0.1	-6.2	-38.1	-13.5
WATT HRS	0.	6.4	52.8	3.1	9.5	0.1
TRANSIENT	0.	0.	0.	0.	0.	0.
DISC.REG.	0. (0.)	1.0(5.7)	0. (0.)	0.5(2.9)	1.4(5.7)	0.2(2.0
UNREG.PWR	0. (0.)	0. (0.)	0. (0.)	0. (0.)	0. (0.)	0.1(12.7
CONTING.	0. (0.)	0. (0.)	0. (0.)	0. (0.)	0. (0.)	0.2(1.2
WTHRS TOT	0.	7.3	52.8	3.5	13.9	0.2
TOT WATTS	(10.9)	(43.8)	(0.1)	(7.1)	(43.8)	(28.8
BATT CAP	132.0	132.0	132.0	132.0	132.0	132.0
DPTH-DSCH	0.	4.0	39.9	1.9	6.0	0.1

	DES- CENT	POST IMPT				
MODE DUR	1.24	0.84	0.	0.	0.	0.
TIME	1	75	0	0	0	0
SUNANGLE	0.	0.	0.	0.	0.	0.
RF	27.0	27.0	27.0	27.0	27.0	27.0
C&DH	3.2	3.2	3.2	3.2	3.2	3.2
THER	0.	0.	0.	0.	0.	0.
SCI	4.0	4.0	4.0	4.0	4.0	4.0
POWR	0.4	0.4	0.4	0.4	0.4	0.4
CONTING.	3.5	3.5	3.5	3.5	3.5	3.5
SBILWATTS	(38.1)	(38.1)	(38.1)	(38.1)	(38.1)	(38.1)
SOLAR PWR	0.	0.	0.	0.	0.	0.
PWR MARG.	-38.1	-38.1	-38.1	-38.1	-38.1	-38.1
WATT HRS	47.2	32.8	0.	0.	0.	0.
TRANSIENT	0.	0.	0.	0.	0.	0.
DISC.REG.	7.1(5.7)	4.8(5.7)	0. (0.)	0. (0.)	0. (0.)	0. (0.)
UNREG.PWR	14.9(12.0)	0. (0.)	0. (0.)	0. (0.)	0. (0.)	0. (0.)
CONTING.	1.5(1.2)	0. (0.)	0. (0.)	0. (0.)	0. (0.)	0. (0.)
WTHRS TOT	70.6	36.8	0.	0.	0.	0.
TOT WATTS	(57.0)	(43.8)	(38.1)	(38.1)	(38.1)	(38.1)
BATT CAP	132.0	132.0	132.0	132.0	132.0	132.0
DPTH-DSCH	38.8	20.2	0.	0.	0.	0.

MISSION TOTALS: 145.3 WATT-HOURS
79.8% DOD

3) C/4 - to be used during the long eclipse orbit season in order to recharge the battery in the allotted time between the long eclipse and the worst case periapsis solar panel heating power loss. This rate will not fully recharge the battery but will provide sufficient recharge to support the periapsis pass without exceeding the 70 percent DOD limit.

For contingency purposes, a 10 percent factor is added to all modes to obtain the total required watts for each specific mode.

Propellant valve operation is treated in two distinctly different manners. When sufficient power margin exists from the solar panel, the power requirements for the valves and valve drivers is entered as a steady-state value. However, for the most part, the propellant valve operations are determined on the basis of the actual length of operation and added as required watt-hours under the watt-hour transient entry.

The reader should remember that the modes presented in this document are derived from the mission sequence; however, in some instances, the division of modes or operational configuration may be slightly altered to keep the number of configurations to a reasonable number. An example of this is the star sensor which is turned OFF when not in use for maneuvers or attitude determination; however, in the power budget it remains ON throughout the mission because of: 1) its low power drain, and 2) the desire not to proliferate the number of operational modes for this iteration of the power budget.

Figures 3-6 through 3-9 provide the reader with a summary of the power profile for the orbiter mission. Figure 3-6 presents a histogram of the transit portion of the mission, while Figure 3-7 presents the perigee pass for a typical 24-h orbit at the BOL; Figure 3-8 presents a worst case short eclipse periapsis pass, and Figure 3-9 presents a full 24-h orbit during the worst case apoapsis eclipse. Figure 3-10 presents a graphical description of orbital power nomenclature. Table 3-11 presents the orbiter power summary.

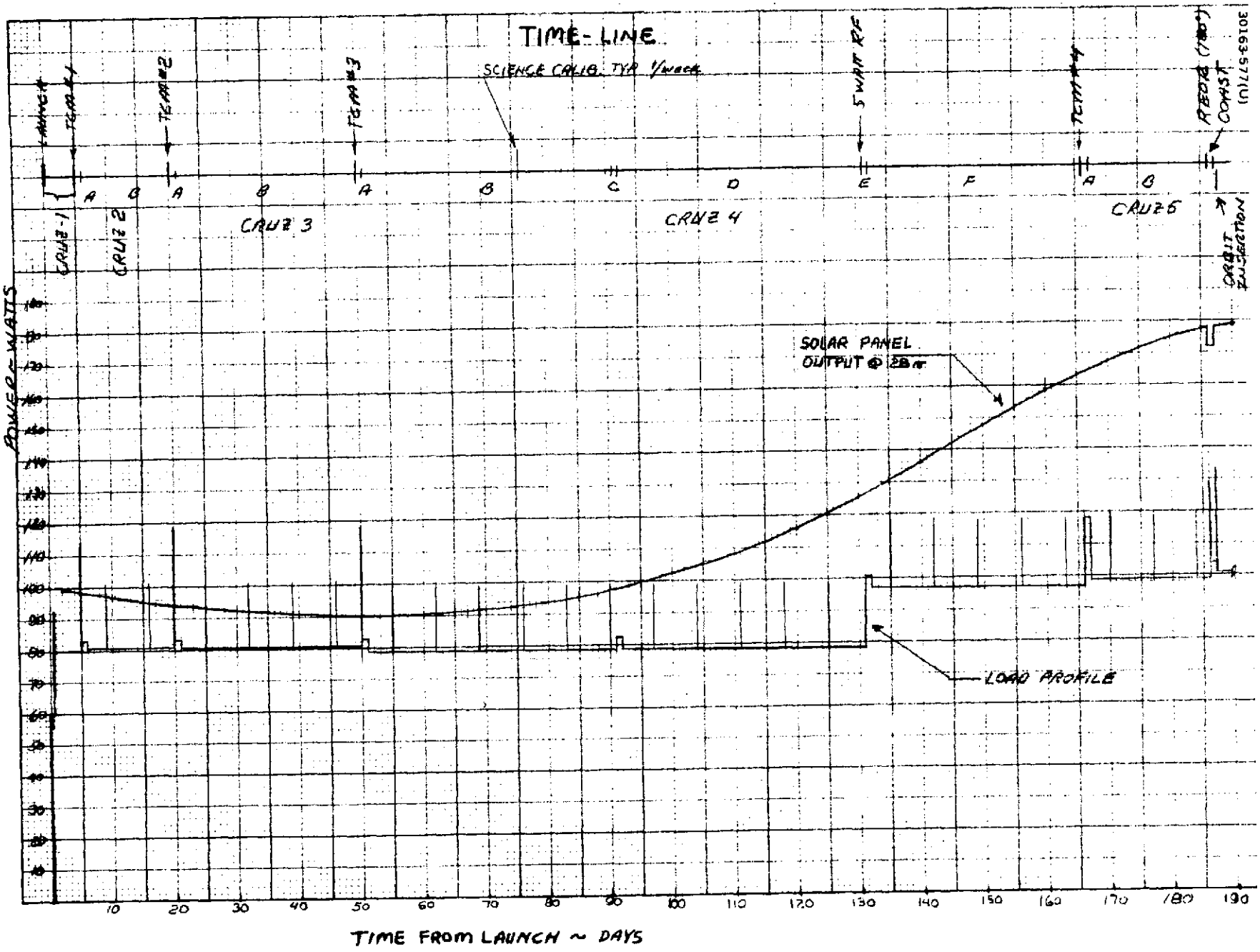

FIGURE 3-6. ORBITER SPACECRAFT TRANSIT PHASE POWER HISTOGRAM

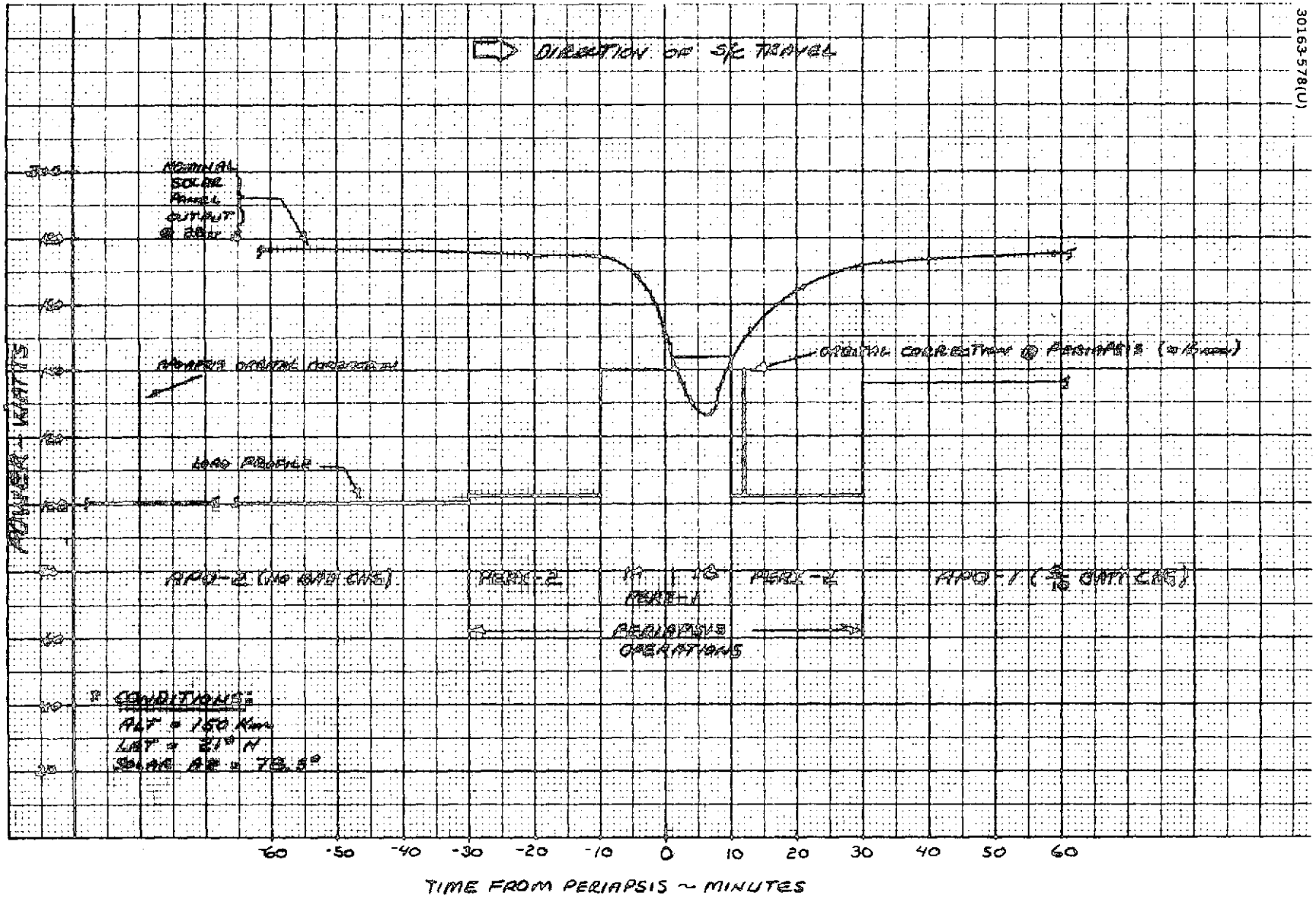

30163-578(U)

FIGURE 3-7. BEGINNING OF LIFE ORBIT PERIAPSIS PASS POWER HISTOGRAM

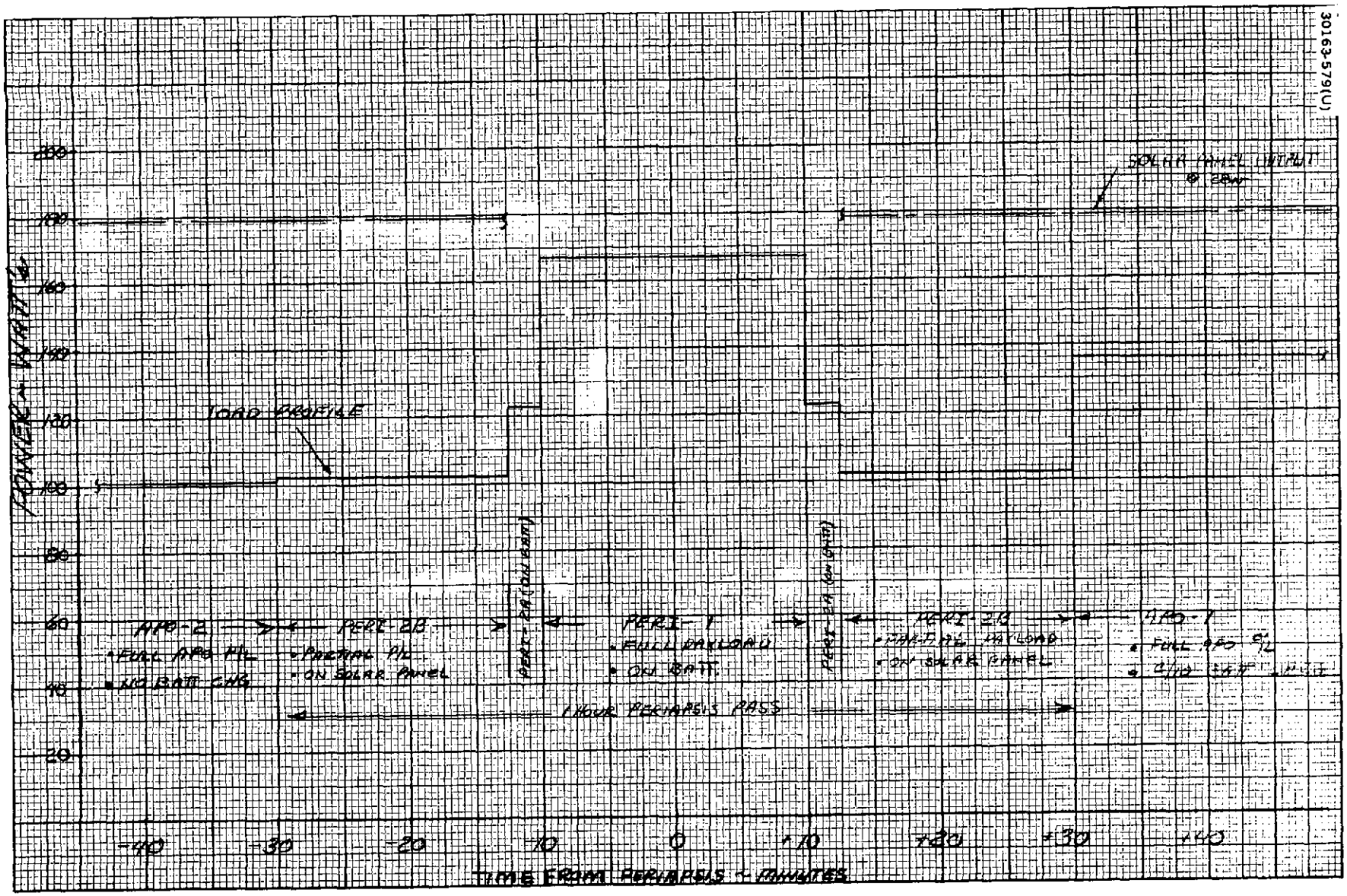

FIGURE 3-8. SHORT ECLIPSE PERIAPSIS PASS POWER HISTOGRAM

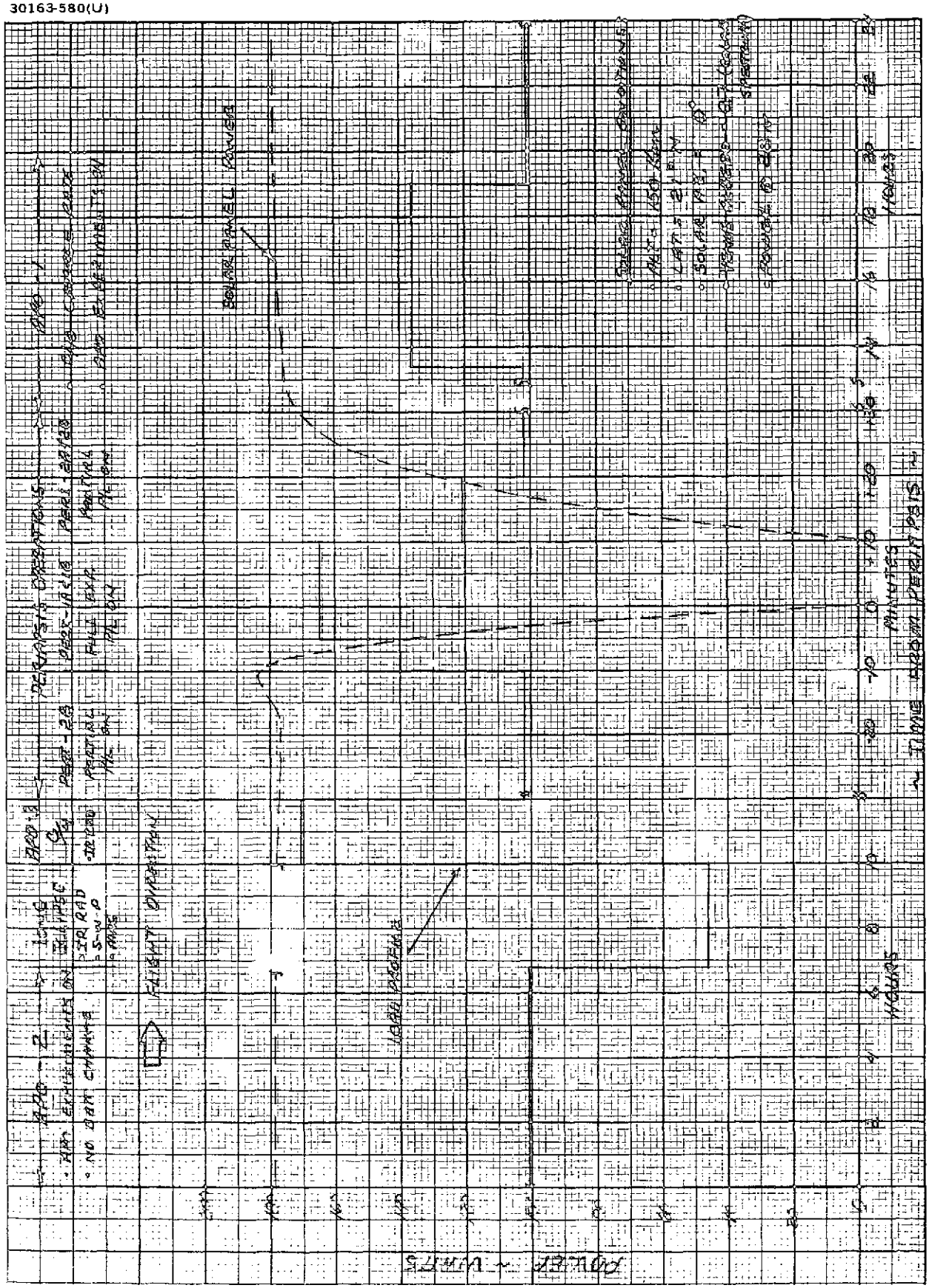

FIGURE 3-9. LONG ECLIPSE (APOAPSIS) ORBIT POWER HISTOGRAM

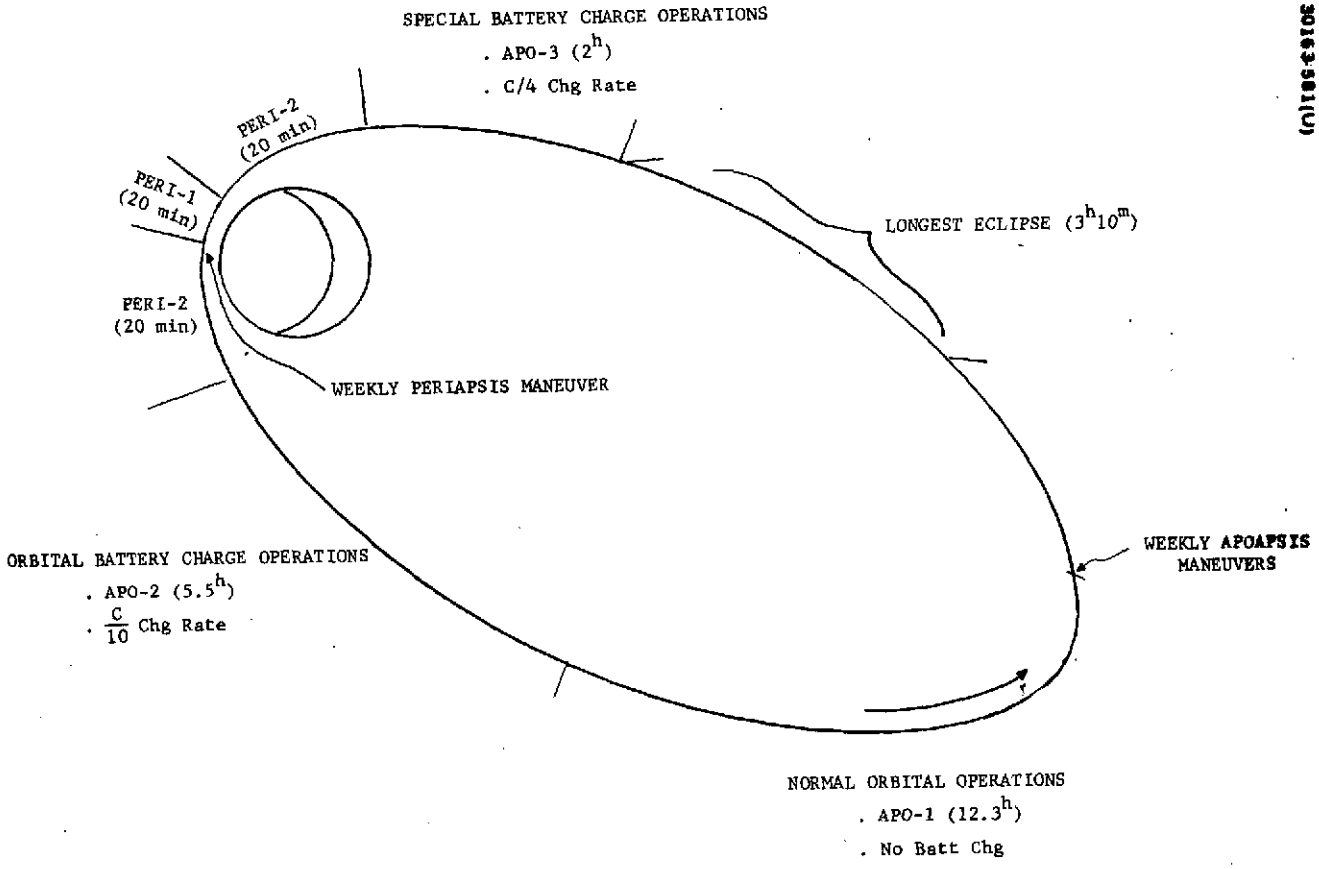

FIGURE 3-10. ORBITAL POWER MODES – TYPICALLY AT 187 DAYS

TABLE 3-11. ORBITER POWER PROFILE

	ON BATT	LNCH	S/C SEP	SUN ACS	JET CALD	CRUZ #1
MODE DUR	0.08	1.12	0.59	2.38	6.20	4.50
TIME	0	0	0	0	0	0
SUNANGLE	0.	0.	0.	64.00	85.00	90.00
RF	18.6	18.6	18.6	18.6	18.6	18.6
C&DH	12.7	12.7	12.7	12.7	12.7	13.9
A.C	0.	0.	0.	5.0	11.0	4.5
PROP	0.3	0.3	0.3	0.3	28.3	0.3
THER	10.8	10.8	10.8	10.8	10.8	10.8
SCI	0.	0.	0.	0.	0.	0.
POWR	3.4	3.4	3.4	3.4	3.4	24.7
CONTING.	4.6	4.6	4.6	5.1	8.5	7.3
SBTLWATTS	(50.4)	(50.4)	(50.4)	(55.9)	(93.3)	(80.1)
SOLAR PWR	0.	0.	0.	89.0	98.6	89.0
PWR MARG.	-50.4	-50.4	-50.4	33.1	5.3	18.9
WATT HRS	4.0	56.4	29.7	0.	0.	3.
TRANSIENT	0.	0.	0.	0.3	0.	0.
DISC.REG.	0.7(3.9)	9.9(8.9)	5.2(8.9)	0. (0.)	0. (0.)	0. (0)
UNREG.PWR	0. (0.)	0. (0.)	0. (0.)	0. (0.)	0. (0.)	0. (0)
CONTING.	0. (0.)	0. (0.)	0. (0.)	0. (0.)	0. (0.)	0. (0.)
WTHRS TOT	4.7	66.4	35.8	0.3	0.	0.
TOT WATTS	(59.3)	(59.2)	(59.2)	(55.9)	(93.3)	(80)
BATT CAP	216.0	216.0	216.0	216.0	216.0	216.0
DPTH-DSCH	2.2	30.7	16.2	0.1	0.	0.

← 106.4 WATT-HRS, 49.2% DOD →

	TCM #1	CRUZ #2A	CRUZ #2B	TCM #2	CRUZ #3A	CRUZ #3B
MODE DUR	0.27	24.00	336.00	0.68	24.00	696.00
TIME	5	5	6	20	20	21
SUNANGLE	0.	90.00	90.00	45.00	90.00	90.00
RF	36.7	18.6	18.6	36.7	18.6	18.6
C&DH	12.7	13.9	13.9	12.7	13.9	13.9
A.C	5.0	10.5	10.5	11.0	10.5	10.5
PROP	0.3	0.3	0.3	0.3	0.3	0.3
THER	10.8	10.8	10.8	10.8	10.8	10.8
SCI	2.	0.	15.0	0.	0.	15.0
POWR	3.4	24.7	4.6	3.4	24.7	4.6
CONTING.	6.9	7.6	7.4	7.5	7.6	7.4
SBTLWATTS	(75.9)	(83.4)	(81.1)	(82.5)	(83.4)	(81.1)
SOLAR PWR	0.	98.0	94.0	66.5	94.0	94.0
PWR MARG.	-75.9	14.6	12.9	-16.0	10.6	12.9
WATT HRS	66.0	0.	0.	10.9	0.	0.
TRANSIENT	5.4	0.	0.	0.9	0.	0.
DISC.REG.	12.6(14.5)	0. (0.)	0. (0.)	2.1(3.1)	0. (0.)	0. (0)
UNREG.PWR	0. (0.)	0. (0.)	0. (0.)	0. (0.)	0. (0.)	0. (0)
CONTING.	0. (0.)	0. (0.)	0. (0.)	0. (0.)	0. (0.)	0. (0)
WTHRS TOT	84.0	0.	0.	13.9	0.	0.
TOT WATTS	(96.4)	(83.4)	(81.1)	(85.6)	(83.4)	(81)
BATT CAP	216.0	216.0	216.0	216.0	216.0	216.0
DPTH-DSCH	38.9	0.	0.	6.4	0.	0.

TABLE 3-11. (Continued)

	TCM #3	CRUZ #4A	CRUZ #4B	CRUZ #4C	CRUZ #4D	CRUZ #4E
MODE DUR	0.27	24.00	960.00	24.00	960.00	24.00
TIME	50	50	51	91	92	132
SUNANGLE	90.00	90.00	90.00	90.00	90.00	90.00
RF	36.8	18.6	18.6	18.6	18.6	18.6
C&DH	12.7	10.9	13.9	10.9	13.9	10.9
A.C	11.0	10.5	10.5	10.5	10.5	10.5
PROP	0.3	0.3	0.3	0.3	0.3	0.3
THER	10.8	10.8	10.8	10.8	10.8	10.8
SCI	0.	0.	15.0	0.	15.0	15.0
POWR	3.4	24.7	4.6	24.7	4.6	25.9
CONTING.	7.5	7.6	7.4	7.6	7.4	9.2
SBTLWATTS	(82.5)	(83.4)	(81.1)	(83.4)	(81.1)	(101.2)
SOLAR PWR	89.0	89.0	89.0	97.0	97.0	127.0
PWR MARG.	6.5	5.6	7.9	13.6	15.9	25.8
WATT HRS	0.	0.	0.	0.	0.	0.
TRANSIENT	0.2	0.	0.	0.	0.	0.
DISC.REG.	0. (0.)	0. (0.)	0. (0.)	0. (0.)	0. (0.)	0. (0)
UNREG.PWR	0. (0.)	0. (0.)	0. (0.)	0. (0.)	0. (0.)	0. (0)
CONTING.	0. (0.)	0. (0.)	0. (0.)	0. (0.)	0. (0.)	0. (0)
WTHRS TOT	0.2	0.	0.	0.	0.	0.
TOT WATTS	(82.5)	(83.4)	(81.1)	(83.4)	(81.1)	(101.2
BATT CAP	216.0	216.0	216.0	216.0	216.0	216.0
DPTH-DSCH	7.1	0.	0.	0.	0.	0.

	CRUZ #4F	TCM #4	CRUZ #5A	CRUZ #5B		
MODE DUR	720.00	0.29	24.00	480.00	0.	0.
TIME	133	166	166	167	0	0
SUNANGLE	90.00	90.00	90.00	90.00	0.	0.
RF	36.8	36.8	36.8	36.8	18.6	18.6
C&DH	13.9	12.7	10.9	13.9	12.7	12.7
A.C	10.5	17.0	10.5	10.5	11.0	11.0
PROP	0.3	28.3	0.3	0.3	0.3	0.3
THER	3.8	3.8	3.8	3.8	10.8	10.8
SCI	15.0	0.	15.0	15.0	0.	0.
POWR	4.6	3.4	25.9	4.6	3.4	3.4
CONTING.	9.0	10.7	10.9	9.0	5.7	5.7
SBTLWATTS	(98.9)	(117.7)	(119.0)	(98.9)	(62.5)	(62.5)
SOLAR PWR	127.0	159.0	159.0	159.0	0.	0.
PWR MARG.	28.1	41.3	40.0	60.1	-62.5	-62.5
WATT HRS	0.	0.	0.	0.	0.	0.
TRANSIENT	0.	0.	0.	0.	0.	0.
DISC.REG.	0. (0.)	0. (0.)	0. (0.)	0. (0.)	0. (0.)	0. (0)
UNREG.PWR	0. (0.)	0. (0.)	0. (0.)	0. (0.)	0. (0.)	0. (0)
CONTING.	0. (0.)	0. (0.)	0. (0.)	0. (0.)	0. (0.)	0. (0)
WTHRS TOT	0.	0.	0.	0.	0.	0.
TOT WATTS	(98.9)	(117.7)	(119.0)	(98.9)	(62.5)	(625
BATT CAP	216.0	216.0	216.0	216.0	216.0	216.0
DPTH-DSCH	0.	0.	0.	0.	0.	0.

TABLE 3-11. (Continued)

/←——— BOL ORBIT

	PRE-INS.	COAST	ORB-INS.	APO #2	PERI #2	PERI #1A
MODE DUR	0.18	24.00	1.80	22.50	0.67	0.18
TIME	186	186	187	0	0	0
SUNANGLE	13.00	90.00	77.00	90.00	90.00	90.00
RF	62.0	36.8	62.0	36.8	36.8	36.8
C&DH	13.9	13.9	12.7	13.9	14.1	14.1
A.C.	11.0	10.5	11.0	10.5	10.5	10.5
PROP	0.3	0.3	28.0	0.3	0.3	0.3
THER	3.8	3.8	3.8	3.8	3.8	3.8
SCI	0.	15.0	0.	21.0	22.0	53.0
POWR	3.4	24.7	3.4	5.5	5.5	8.7
CONTING.	9.9	11.0	12.1	9.2	9.3	12.7
SBTLWATTS	(109.3)	(121.0)	(133.0)	(101.0)	(102.3)	(139.9)
SOLAR PWR	30.9	178.0	173.4	179.0	140.2	140.0
PWR MARG.	-78.4	57.0	40.4	78.0	37.7	0.1
WATT HRS	14.1	0.	0.	0.	0.	0.
TRANSIENT	0.3	0.	0.	0.	0.	0.
DISC.REG.	2.5(14.1)	0. (0.)	0. (0.)	0. (0.)	0. (0.)	0. (0)
UNREG.PWR	0. (0.)	0. (0.)	0. (0.)	0. (0.)	0. (0.)	0. (0)
CONTING.	0. (0.)	0. (0.)	0. (0.)	0. (0.)	0. (0.)	0. (0)
WTHRS TOT	17.0	0.	0.	0.	0.	0.
TOT WATTS	(123.4)	(121.0)	(133.0)	(101.0)	(102.3)	(139
BATT CAP	216.0	216.0	216.0	216.0	216.0	216.0
DPTH-DSCH	7.3	0.	0.	0.	0.	0.

BOL ORBIT——→/←— SHORT ECLIPSE ORBIT

	PERI #1B	APO #1	APO #2	PERI #2A	PERI #2A	PERI #1
MODE DUR	0.15	0.50	19.50	0.58	0.08	0.33
TIME	0	0	0	0	0	0
SUNANGLE	90.00	90.00	90.00	90.00	90.00	0.
RF	36.8	36.8	36.8	36.8	36.8	36.8
C&DH	14.1	13.9	13.9	14.1	14.1	14.1
A.C.	10.5	10.5	10.5	10.5	10.5	10.5
PROP	0.3	0.3	0.3	0.3	0.3	0.3
THER	3.8	3.8	3.8	3.8	5.8	5.8
SCI	53.0	21.0	21.0	22.0	22.0	53.0
POWR	8.7	37.5	5.5	5.5	5.5	8.7
CONTING.	12.7	12.4	9.2	9.3	9.5	12.9
SBTLWATTS	(139.9)	(136.2)	(101.0)	(102.3)	(104.5)	(142.1)
SOLAR PWR	126.0	179.0	179.0	179.0	0.	0.
PWR MARG.	-13.9	42.8	78.0	76.7	-104.5	-142.1
WATT HRS	2.1	0.	0.	0.	8.7	47.3
TRANSIENT	0.	0.	0.	0.	0.	0.
DISC.REG.	0.4(2.4)	0. (0.)	0. (0.)	0. (0.)	1.5(13.4)	8.3(25
UNREG.PWR	0. (0.)	0. (0.)	0. (0.)	0. (0.)	0. (0.)	0. (0)
CONTING.	0. (0.)	0. (0.)	0. (0.)	0. (0.)	0. (0.)	0. (0)
WTHRS TOT	2.5	0.	0.	0.	13.2	55.7
TOT WATTS	(142.4)	(136.2)	(101.0)	(102.3)	(122.9)	(167
BATT CAP	216.0	216.0	216.0	216.0	216.0	216.0
DPTH-DSCH	1.1	0.	0.	0.	4.7	25.8

/←65.9 W-H, 30.5% DOD→/

TABLE 3-11. (Continued)

SHORT ECLIPSE ORBIT → ← LONG ECLIPSE ORBIT

	APO #1	APO #2	LONG ECLS	APO #3	PERI #2B	PERI #1A
MODE DUR	3.50	12.30	3.17	2.00	0.50	0.08
TIME	0	0	0	0	0	0
SUNANGLE	90.00	90.00	0.	90.00	90.00	90.00
RF	36.8	36.8	7.0	36.8	36.8	36.8
C&DH	13.9	13.9	11.1	13.9	14.1	14.1
A.C.	10.5	10.5	1.0	10.5	10.5	10.5
PROP	0.3	0.3	0.3	0.3	0.3	0.3
THER	3.8	3.8	5.8	3.8	3.8	3.8
SCI	21.0	21.0	4.3	6.0	22.0	53.0
POWR	37.5	5.5	4.0	84.0	5.5	8.7
CONTING.	12.4	9.2	3.3	15.5	9.3	12.7
SBTLWATTS	(136.2)	(101.0)	(36.8)	(170.8)	(102.3)	(139.9)
SOLAR PWR	179.0	179.0	0.	179.0	179.0	179.0
PWR MARG.	42.8	78.0	-36.8	8.2	76.7	39.1
WATT HRS	0.	0.	116.7	0.	0.	0.
TRANSIENT	0.	0.	0.	0.	0.	0.
DISC.REG.	0. (0.)	0. (0.)	29.2(9.3)	0. (0.)	0. (0.)	0. (0.)
UNREG.PWR	0. (0.)	0. (0.)	0. (0.)	0. (0.)	0. (0.)	0. (0.)
CONTING.	0. (0.)	0. (0.)	0. (0.)	0. (0.)	0. (0.)	0. (0.)
WTHRS TOT	0.	0.	145.9	0.	0.	0.
TOT WATTS	(136.2)	(101.0)	(46.1)	(170.8)	(102.3)	(139
BATT CAP	216.0	216.0	216.0	216.0	216.0	216.0
DPTH-DSCH	0.	0.	67.5	0.	0.	0.

LONG ECLIPSE ORBIT →

	PERI #1B	PERI #2A	APO #1	PERI O/C	APO O/C	
MODE DUR	0.25	0.17	5.50	0.	0.	0.
TIME	0	0	0	0	0	0
SUNANGLE	0.	0.	90.00	90.00	90.00	0.
RF	36.8	36.8	36.8	36.8	36.8	36.8
C&DH	14.1	14.1	13.9	14.1	13.9	14.1
A.C.	10.5	10.5	10.5	17.0	17.0	10.5
PROP	0.3	0.3	0.3	28.3	28.3	0.3
THER	3.8	3.8	3.8	3.8	3.8	3.8
SCI	53.0	22.0	21.0	22.3	21.0	22.0
POWR	8.7	5.5	37.5	5.5	5.5	5.5
CONTING.	12.7	9.3	12.4	12.7	12.6	9.3
SBTLWATTS	(139.9)	(102.3)	(136.2)	(140.2)	(138.9)	(102.3)
SOLAR PWR	0.	0.	179.0	149.2	179.0	0.
PWR MARG.	-139.9	-102.3	42.8	8.8	40.1	-102.3
WATT HRS	35.0	17.1	0.	0.	0.	0.
TRANSIENT	0.	0.	0.	0.	0.	0.
DISC.REG.	6.2(24.6)	3.0(18.0)	0. (0.)	0. (0.)	0. (0.)	0. (0.)
UNREG.PWR	0. (0.)	0. (0.)	0. (0.)	0. (0.)	0. (0.)	0. (0.)
CONTING.	0. (0.)	0. (0.)	0. (0.)	0. (0.)	0. (0.)	0. (0.)
WTHRS TOT	41.1	20.1	0.	0.	0.	0.
TOT WATTS	(164.5)	(120.3)	(136.2)	(140.2)	(138.9)	(102
BATT CAP	216.0	216.0	216.0	216.0	216.0	216.0
DPTH-DSCH	19.0	9.3	0.	0.	0.	0.

← 61.2 W-H, 28.3% DOD →

4. TRADE AND DESIGN STUDIES

Studies and tradeoffs were performed to optimize the power subsystem design in terms of cost, performance, and reliability. Key areas of investigation were specified in the Statement of Work (SOW). Additional items to supplement those specified in the SOW are discussed in this section.

One of the primary environmental factors influencing the design study was temperature. Initially, it was thought that welded solar cell interconnects would be necessary, since high solar panel temperatures would be experienced in and around the planet Venus. However, once the temperatures were defined, it was determined that conventional materials and fabrication techniques could be employed, resulting in a lower cost design. Operating and storage temperatures of both the bus batteries and probe batteries was taken into consideration in finally selecting the type of battery and charge/discharge methods to be used.

The magnetometer experiment on board the orbiter causes a requirement for low magnetic fields. The high remnant fields of the nickel cadmium cells is undesirable. However, silver-cadmium cells with low remnant fields and low cycle life (for good mission success probability) were considered, but were ruled out in the early stages of the study. Since one of the main considerations in this study was cost, newly developed techniques or devices (i. e., long life silver-zinc or low magnetic nickel-cadmium) were ruled out. Development costs for this mission would be prohibitive.

Operation of the probe components at high g levels was investigated. Batteries are more vulnerable than other components and special care must be used in their design construction and mounting. It was determined that all other components could be expected to survive high g forces if they are properly selected and packaged.

4.1 REGULATED VS. UNREGULATED POWER DISTRIBUTION

Probe Bus and Orbiter Power Subsystem

Early in the Pioneer Venus study, it was decided to use an unregulated power bus distribution configuration for the probe bus and orbiter. This decision was made prior to a detailed mission definition. An unregulated bus requires that each subsystem and science instrument provides its own

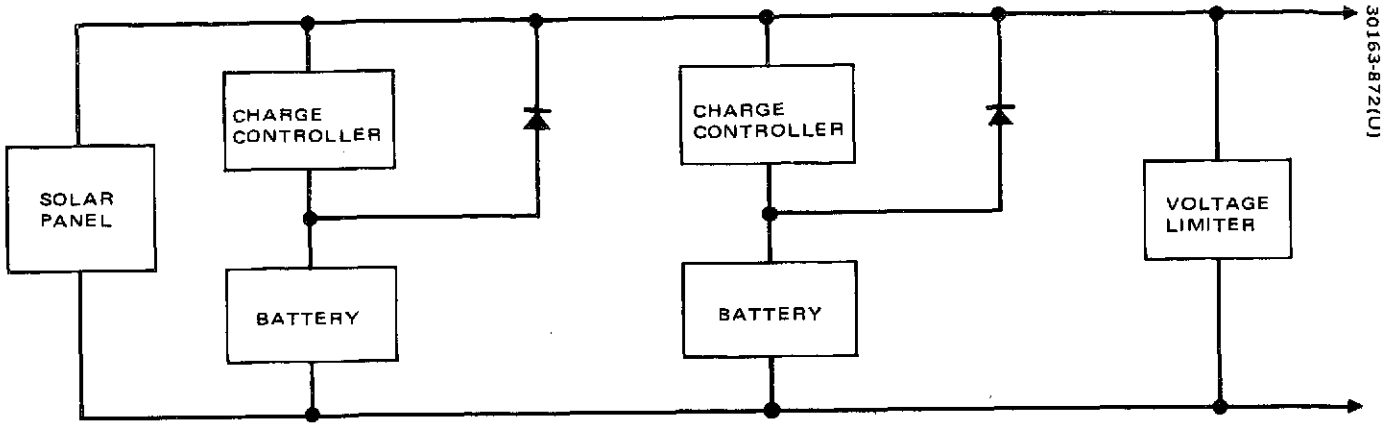

FIGURE 4-1. POWER DISTRIBUTION CONFIGURATION A – UNREGULATED

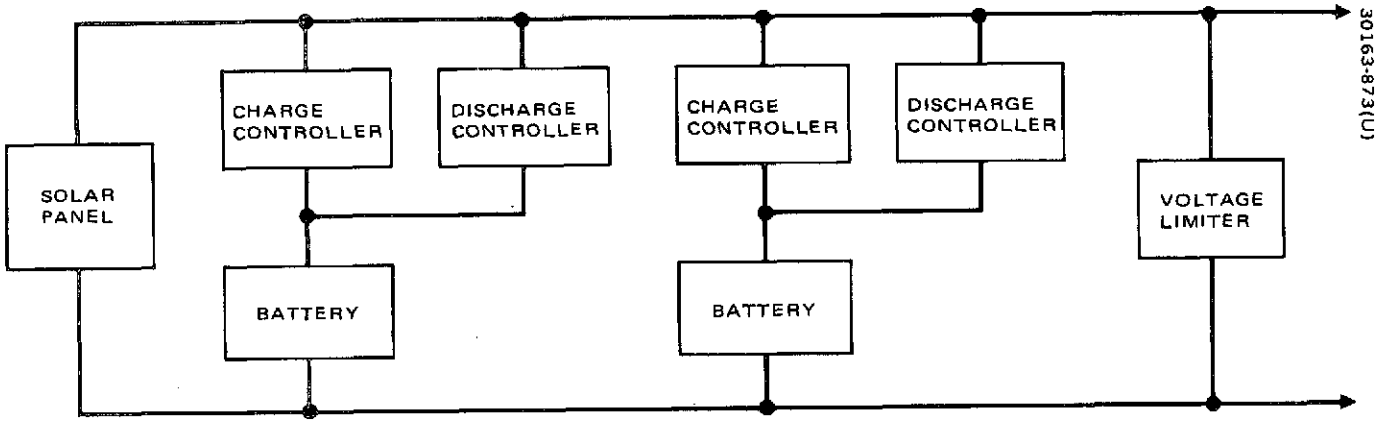

FIGURE 4-2. POWER DISTRIBUTION CONFIGURATION B – SEMIREGULATED

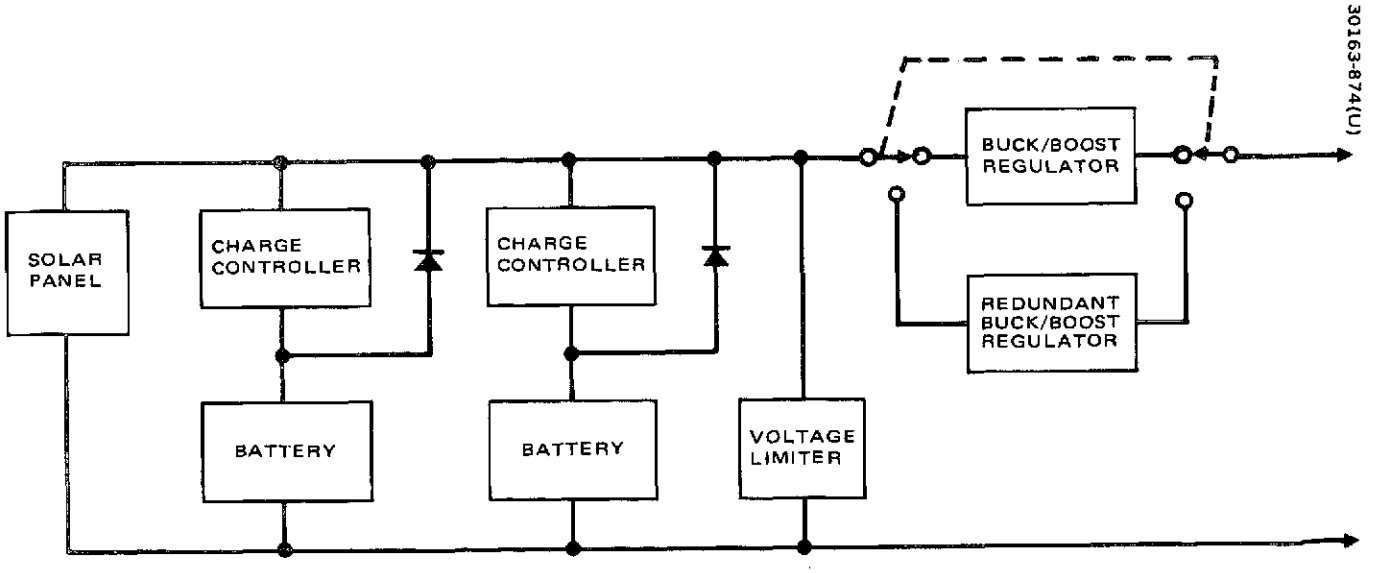

FIGURE 4-3. POWER DISTRIBUTION CONFIGURATION C – REGULATED

regulation. Because the solar panel is subjected to a wide temperature range, this results in a power mismatch between the panel and the spacecraft loads for some mission phases. A centralized switching regulator can eliminate this problem but introduces other problems. Since the choice was not certain, a tradeoff was performed to reassess this decision. Shortly after this tradeoff was initiated, the decision to utilize the Atlas/Centaur launch vehicle was made. The Atlas/Centaur approach is more conservative and utilizes two batteries (Thor/Delta configuration uses one battery to minimize weight). Therefore the tradeoff was conducted for two battery systems.

Three different types of power distribution configurations were studied for the Pioneer Venus orbiter and probe bus. These are shown in Figures 4-1, 4-2, and 4-3. Configuration A uses no electronic regulation units. The solar panel voltage at any given time is a function of solar panel temperature, solar constant and spacecraft loads. The minimum bus voltage of 23V occurs when the 21 cell battery is close to complete discharge. The solar panel voltage is clamped at 33V by the OSO-I type voltage limiters to prevent excessive bus voltage levels when the solar panel is cold and lightly loaded. This voltage is dictated by the maximum battery voltage under charge (21 x 1.5 = 31.5V) plus a drop of 1.5V across the battery charger.

Configuration B shows a semiregulated configuration. It utilizes a boost regulator type discharge controller that boosts the 18 cell battery voltage up to a minimum bus voltage of 26V. The discharge controller starts to provide current to the bus when the solar panel voltage drops below 28V. The maximum solar panel voltage is again limited by OSO-I type voltage limiters to 33V. However, if tighter regulation were required, the upper voltage could be limited to a value as low as (18 x 1.5) + 1.5 = 28.5V by adjusting the set point of the voltage limiters downwards.

The main disadvantage of Configurations A and B is that the solar panel can be power matched or optimized only for a specific panel temperature. If the maximum power point moves away from 28V due to a temperature change, a power mismatch must be tolerated. Since the Pioneer Venus solar panels will be subjected to a very wide temperature variation, this factor must be considered in the design of the power subsystem.

The orbiter is subjected to the widest temperature range. In a Type II orbit, the spacecraft initially moves away from the sun and reaches a minimum temperature of 10°C approximately 50 days from launch. Near Venus, a high solar constant, high albedo and aerodynamic heating drive the solar panel temperature up to 120°C during some periapsis passes. The solar panel is designed to provide maximum power at the required 28V level at approximately 70°C. A significant mismatch occurs at the high and low temperature extremes. This requires extra solar cells (and additional honeycomb substrate also) to compensate for this power loss.

A similar problem occurs for the probe bus. The probe release and bus retargeting sequences must be conducted with the spin axis at a sun angle of approximately 30 deg. This results in a substantial solar power reduction

TABLE 4-1. ORBITER POWER SUBSYSTEM MASS TRADEOFF, Kg
(TYPE II ORBIT)

Unit	A Unregulated	B Semi Regulated	C Regulated
Solar panel (including substrate)	14.6	13.6	11.0
Batteries	9.8	9.8	9.8
Charge Controllers	2.9	2.9	3.4
Discharge controller	0.5	8.2	—
Boost-buck regulator	—	—	10.0
Bus limiter	1.5	1.5	0.8
Limiter resistors	1.0	1.0	0.5
Undervoltage switch	0.8	0.8	0.8
Current sensors	0.4	0.4	0.4
Power interface unit	2.8	2.8	2.8
Subsystem regulators	0.2	0.2	—
Totals	34.5	41.2	39.5

from that obtainable for the nominal transit attitude (perpendicular to sunline). During these off-sun periods the batteries must augment the solar panels for several hours. The low sun angle causes the solar panel temperature to go to a low value. This moves the panel maximum power voltage above 28V and results in a power mismatch. This restricts the maximum time at this attitude.

A more efficient utilization of the available solar panel power over a wide range of panel temperatures and bus voltages would be a distinct advantage if it could be accomplished without offsetting disadvantages. The way to obtain maximum power from a solar panel over a wide range of voltages is to use a centralized switching regulator. This is shown in Configuration C. The regulators provide a power match over a wide range of voltages: approximately 40V near earth and approximately 20V near Venus. The buck-boost regulator supplies regulated +28V.

In order to determine which of the three configurations described above is the best choice for the orbiter and probe bus, they were evaluated on the basis of:

- Weight
- Subsystem and science instrument interfaces
- Mission operation problems
- Thermal impact
- Cost
- Reliability
- Prior spacecraft experience

Weight

Tables 4-1 and 4-2 summarize the power subsystem weight for the three configurations. Battery efficiency for all three configurations is approximately equal. The unregulated configuration requires extra cells (15%) to compensate for voltage falloff as the battery discharges. The discharge controller of Configuration B and buck-boost regulator of Configuration C operate at an efficiency of approximately 85%. Therefore, battery weight for all configurations is the same.

Solar panel efficiency is optimum for Configuration C, resulting in a lighter solar panel. However, the associated electronics weight more than offsets this advantage. The buck-boost regulator is a complex and heavy unit.

Although Configuration A requires the largest solar panel, no electronics are required for discharge control or solar panel operation. This results in the lowest overall weight. If regulator redundancy were not required for

TABLE 4-2. PROBE BUS POWER SUBSYSTEM MASS TRADEOFF, kg

Unit	A Unregulated	B Semi Regulated	C Regulated
Solar panel (including substrate)	13.6	12.9	11.7
Batteries (Ni Cd)*	5.5	5.5	5.5
Charge controllers	2.9	2.9	3.4
Discharge controller	0.5	8.2	—
Boost-buck regulator	—	—	10.0
Bus limiters	1.2	1.2	0.8
Limiter resistors	0.7	0.7	0.5
Undervoltage switch	0.8	0.8	0.8
Current sensors	0.4	0.4	0.4
Probe battery charger	1.8	1.8	1.8
Subsystem regulators	0.2	0.2	—
Power interface unit	2.7	2.7	2.7
Totals	30.3 kg	37.3 kg	37.6 kg

*For reasons of commonality and lowest price, the orbiter batteries will probably be used on the probe; this will increase the weight of the power subsystem an equal amount for all subsystems.

Configuration C, it would be a more attractive choice from a weight standpoint. Also, Configuration B would be more attractive for a single battery configuration that did not require discharge controller redundancy.

Subsystem Interfaces

Configurations A and B require all power users to perform their own regulation. Configuration C performs this function in a centralized regulator. However, eliminating the regulation requirement for the subsystem units results in very little simplification of their respective units. The regulators are relatively small and simple units that also perform other functions besides voltage regulation. Each subsystem regulator has a current limiter that protects the power bus from overloads. Also, each regulator incorporates a power on/off switch circuit. Finally, the regulator also provides EMI isolation protection between loads, whereas, common impedance coupling through a centralized regulator can be a severe problem.

A centralized regulator does not automatically eliminate the need for regulation by individual power users. The Philco transponder already has a regulator. The rf power amplifiers have a regulator that must drop at least 1V, even with a regulated bus. This regulator serves to protect high frequency rf transistors that are sensitive to power transients. In addition, there are some users that must regulate to a higher degree than that achieved by the centralized regulator. Experimenters sometimes provide additional and unneeded internal regulation as a safeguard against the possibility that the central regulator will not perform adequately and also as a safeguard against interference from other experimenters or spacecraft subsystems.

In summary, elimination of a requirement for individual subsystem and experiment regulators is not a strong positive factor in favor of a centralized regulator. On the contrary, there are strong compelling arguments for the utilization of individual regulators.

Mission Operations

There are several mission phases where large shifts of solar panel temperature result in power mismatches that puts additional burdens on mission operations personnel. During orbiter periapsis passes, solar panel temperatures reach very high values due to planetary albedo and aerodynamic heating. This drives the solar panel voltage to very low levels and the battery must augment the solar panel. This means that the battery must often be utilized and then recharged, even though there is an excess of solar power available. This is no problem for Configuration C, because it is capable of operating down to low voltage limits.

The power mismatch problem that occurs with the probe bus also incurs mission restraints. During probe bus and bus targeting maneuvers, the sun angle is approximately 30 deg, resulting in a small power deficit for Configurations A and B that limits maneuver time due to a power mismatch with a cold panel. For Configuration C, this deficit is much smaller.

TABLE 4-3. REGULATED VERSUS UNREGULATED SPACECRAFT SUMMARY

Regulated	Unregulated (or Semiregulated)
Tiros	Pioneers (A thru E)
Nimbus	ATS (A thru E)*
Mariners (All)	Intelsat II*
OAO	Intelsat IV*
Skylab	Tacsat*
Viking Orbiter	OGO
Intelsat III	Anik*
Surveyor*	OSO-H
	FleetSatCom
Mixed	HS-318*
OSO-I*	HS-350*

*Hughes spacecraft

A regulated bus would provide more mission operations flexibility for the probe bus and require less battery charging on the orbiter. However, neither of these restrictions with the unregulated bus is a serious drawback. Also, a small increase in solar panel area could remove these restrictions completely.

Thermal Impact

An unregulated bus system utilizes several distributed regulators that must dissipate surplus power available above their minimum operational voltage. This dissipation is a function of load level and solar panel temperature. When the panel is cold, the bus voltage is high and the distributed regulator dissipation is maximum.

A central regulator, on the other hand, dissipates a large amount of power in one concentrated location. However, its dissipation is relatively constant and independent of the panel temperature. This makes thermal analysis somewhat easier. Distributed subsystem and science instrument regulator dissipations vary with solar panel temperature, resulting in a more dynamic thermal environment that is a little more difficult to analyze. However, none of the three configurations has a significant thermal control limitation or advantage in relation to the other two configurations.

Cost

The unregulated configuration is the lowest in cost due to the elimination of relatively complex switching regulator electronic units needed in the other two configurations. This is true in spite of the fact that each power user must provide its own regulator. The subsystem regulators are simple, small, and inexpensive devices. As indicated above, these regulators perform other functions, also. Although precise costing data was not developed, Configuration A is at least $100K lower in cost than the other two configurations.

Reliability

The discharge controller and buck-boost regulator of Configurations B and C, respectively, can be designed with a low failure rate. However, the unregulated configuration is more reliable due to its simplicity and has a slight advantage for this reason.

Prior Spacecraft Experience

Previous spacecraft designs have utilized both regulated and unregulated power systems. Each spacecraft designer makes this decision based on his analysis of the mission goals, spacecraft environment, and also previous experience with techniques that worked satisfactorily in the past. Table 4-3 is a summary of previous spacecraft designs. This list is almost evenly divided. However, the preference at Hughes has definitely favored unregulated power buses.

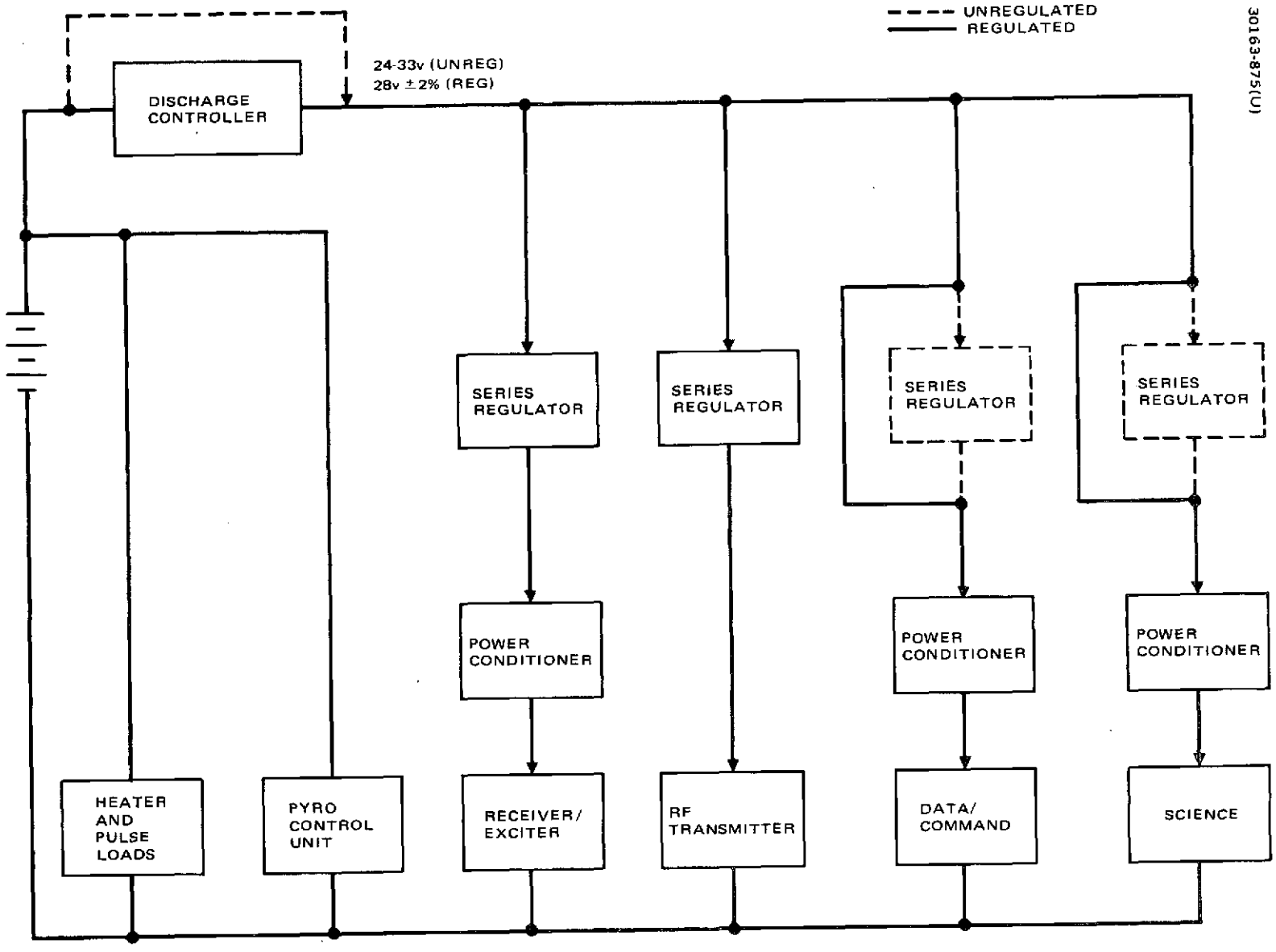

FIGURE 4-4. PROBE POWER DISTRIBUTION

Summary

The unregulated bus configuration has been selected for the Pioneer Venus probe bus and orbiter. In spite of the fact that a larger solar panel is required for this configuration and individual subsystem and experiment regulators are required, it has many compensating desirable features. These include low weight due to elimination of heavy electronic units, low cost, simplicity, reliability, and better EMI protection.

Spacecraft load changes were made late in the program that required an increase in near-earth solar panel power. These were the elimination of the low power 1W transmitter mode (5W is the minimum transmitter power now) and an increase in heater power. These changes forced the panel size to increase to the point where the panel is now capable of providing power to the spacecraft loads without the battery during probe separation maneuvers.

Probe Power Subsystems

A tradeoff was conducted to evaluate an unregulated versus regulated bus for the probes. These two configurations were evaluated on the basis of weight, cost, volume, subsystem and science experiment interfaces, thermal impact, and reliability.

Figure 4-4 shows a functional block diagram of the regulated configuration. The dotted lines indicate the manner in which it is converted to an unregulated configuration. All power users, with a few exceptions, need not only regulated power, but also additional power conditioning to develop the specific positive and negative voltages required by that user.

The central switching regulator provides a voltage boost from a 13 cell 35 A-hr silver zinc battery (nominal 18.2V) to a voltage level of 28V $\pm$2 percent. This voltage is applied to all loads with the exception of heaters and high current pulse loads. The unregulated configuration provides power directly from an 18 cell 20 A-hr silver zinc battery. A silver zinc battery provides good regulation over the plateau region of its discharge curve. Except for the initial tailup for a fully charged battery and near full discharge, it maintains the bus at 26.5 $\pm$1V (Figure 4-5).

Subsystem and Science Interfaces

Many of the same interface considerations that were factors in the regulated versus unregulated tradeoff for the probe bus and orbiter are present in this tradeoff also.

All of the subsystem and science users must perform their own regulation with an unregulated bus. These are simple and small dissipative regulators. These individual regulators also provide a high degree of isolation between loads. This is especially important when some of the loads require large pulse currents. Common impedance coupling through the discharge controller can introduce interference signals to the other loads on the power bus.

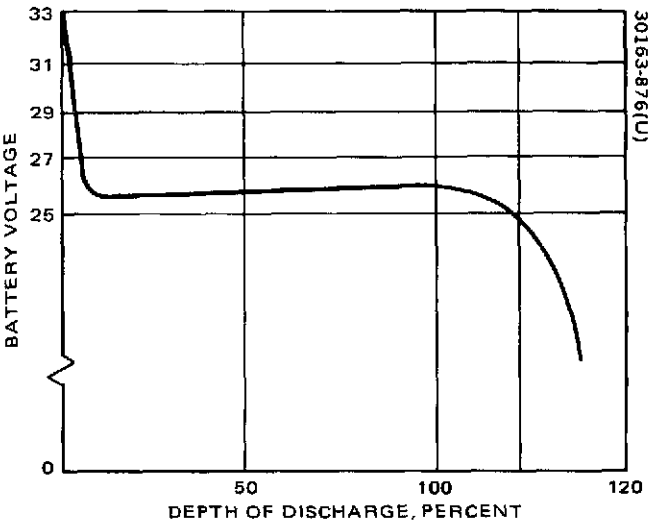

FIGURE 4-5. PROBE UNREGULATED BUS VOLTAGE

Some power users require an additional regulator even with a central regulator. Some loads require regulation to a higher degree than can be conveniently provided by a central regulator. The Viking transponder that has been selected for the large probe already has a regulator that operates over the range of 24 to 37V. The largest power user in the probes is the rf transmitter. The transmitter will require a regulator that must drop at least 1V to protect sensitive high frequency transistors from power transients and ripple. This type of noise appears at the output of switching regulators unless prohibitively large filters are used.

Thus, it appears that many users would provide additional regulation for finer voltage control or bus isolation even if a regulated bus were provided. The use of individual regulators appears to be unavoidable for many power users. In their case, the use of a discharge controller is wasteful.

Weight

The discharge controller has an efficiency of approximately 85 percent. That is, 15 percent of the battery energy is dissipated in this unit. Since many of the power users must provide additional regulation, as explained above, overall battery discharge efficiency is approximately 80 percent for a regulated bus.

With an unregulated bus, the nominal bus voltage is 26.5V and the minimum bus voltage is 25V. Therefore, the user regulators must be set at approximately 24.5V. This results in a nominal 2V drop across the regulators or a battery discharge efficiency of 90 to 91 percent. The flat plateau region of the silver zinc cells is responsible for this high figure of merit. Thus, the battery weight for an unregulated configuration is somewhat smaller (see Table 4-4).

The major weight saving, however, with an unregulated bus is due to the elimination of the heavy discharge controllers. These units use large power transistors, capacitors, inductors, and EMI filters. Although several small regulators will have to be supplied by the power users, their combined extra weight should not exceed 0.3 kg for each probe. Table 4-4 shows a large net weight saving for the unregulated power bus configuration.

Cost

An unregulated bus will eliminate the need for one large and three small discharge controllers. This represents a substantial cost saving.

An unregulated bus allows the rf transmitters, pyrotechnic control units, and power interface units to work over the same 24 to 33V range on the probe bus, orbiter, and probes. This equipment commonality also results in a cost saving.

Using a discharge controller in the probes would require special packaging to conform to the available space in the spherical pressure vessel.

TABLE 4-4. BATTERY MASS COMPARISON, Kg

	Large Probe		Small Probe	
	Regulated	Unregulated	Regulated	Unregulated
Batteries				
Number of cells	13	18	13	18
Weight	12.0	11.5	3.75	3.60
Discharge controller	5.1	—	2.35	—
Subsystem regulators	—	0.3	—	0.3
Total	17.1	11.8	6.07	3.90

Elimination of these units also eliminates the costs associated with this task. All of the above cost savings are shown in Table 4-5.

The unregulated configuration requires an increase in the number of cells from 13 to 18. Although each cell is smaller, the overall battery cost will increase.

Increasing the number of cells also requires charging the probe batteries at a higher potential. This means that the probe bus charger must incorporate a voltage boost circuit at additional cost.

Finally, an unregulated bus will require additional user regulators. The additional costs for all of the above items are shown in Table 4-5. Combining savings and additional costs results in a substantial net cost saving.

Volume

Volume is an important parameter in the probes. Table 4-6 summarizes volume changes for those elements that are affected by the tradeoff. The table indicates that an unregulated power bus results in a volume advantage for both large and small probes.

Reliability

The discharge controller is in series with almost all probe loads and represents a potential single point failure. Elimination of this unit results in an increase in reliability. An unregulated bus, however, requires an increase in the number of battery cells which, in turn, reduces the battery

reliability. These are offsetting factors and the overall system reliability for both configurations is approximately equal.

Thermal Impact

Total probe heat dissipation is a function of load requirements and regulator losses. The regulated configuration discharge controllers develop a large amount of heat in a single concentrated location; the user regulators, on the other hand, dissipate a relatively small amount of power. As indicated above, total regulation losses are approximately 10 percent less for the unregulated system and they are distributed among the user regulators. Therefore, the overall bulk temperature for the unregulated configuration is lower and makes the thermal control task easier.

Summary

An unregulated bus has been selected for the probes. This configuration results in the lowest weight, cost, volume and heat dissipation and fewer EMI problems.

TABLE 4-5. UNREGULATED BUS COST SAVINGS
(THOUSANDS OF DOLLARS)

Item	
Deletion of discharge controller	
Large	-125
Small (3)	-110
Conformal pack	
Large	- 9
Small	- 6
Equipment commonality	- 10
Additional cells	+ 25
Add boost charge	+ 50
Add subsystem regulators	+ 25
Total Saving	150

TABLE 4-6. BATTERY VOLUME COMPARISON, CM^3

Unit	Large Probe		Small Probe	
	Regulated	Unregulated	Regulated	Unregulated
Batteries				
Number of cells	13	18	13	18
Volume	7,000	6,800	2,700	3,500
Discharge controller	3,040	—	1,360	—
Subsystem regulators	—	250	—	250
Total Volume	10,040	7,025	4,060	3,750

4.2 POWER SUBSYSTEM LOSSES AND REQUIRED MARGINS

This subsection describes the power subsystem losses and system margins as a function of the system loads versus mission modes as defined in Section 3 of this volume. Sufficient solar panel power capability exists for all intransit phases of the mission, except during periods of science calibration and trajectory correction maneuvers. To handle these periods, the alternate methods of switching loads in sequence or using available battery energy are employed.

The largest demand on the probe bus battery occurs during the probe separation sequence, when approximately 96 W-hr are required. This value was used to size the 13.6 A-hr battery, assuming 40 percent depth-of-discharge (DOD). On the other hand, the orbiter battery was sized to accommodate the 3 hr eclipse periods. A 70 percent DOD is incurred by the 10 A-hr battery during the approximately nine long (≤ 3 hr) eclipses towards the end of mission.

The energy demands required by both large and small probes are adequately met utilizing silver zinc batteries. Detail mission sequences have been established and an 80 percent DOD is used to determine battery size requirements. This applies to both Atlas/Centaur and Thor/Delta probes. The resulting margins appear adequate to compensate for any unforseen uncertainties that might be encountered.

Primary Power Source

Primary power for both the orbiter and probe bus is supplied by the solar array. The array has been sized for the worst case load conditions to be encountered, assuming normal orientation and solar illumination. Table 4-7 summarizes the panel characteristics for both Thor/Delta and Atlas/Centaur and probe buses. The parameters of the panel have been selected during the solar panel study (see subsection 4.4) to maximize panel performance on the Thor/Delta at minimum weight. The battery meets momentary peak transient load power requirements and is used for power when off-sun or large angular excursions from sun normal are experienced.

Secondary Power Sources

Secondary power is supplied by silver-zinc and nickel-cadmium batteries on the probe and orbiter bus, respectively. In each case, the battery has been sized for the worst case W-hr requirement, which on the probe bus, occurs at probe separation and for the orbiter at the 3 hr apoapsis eclipse. Sufficient capacity exists to insure against inadvertent delays in sun acquisition during the launch/acquisition sequence. The required power is supplied by the solar panel and supplemented by the battery. Since adequate battery capacity has been designed into the system, it is only necessary to assure that a full charge has been completed prior to the maneuver. The same applies to the orbiter bus during the long eclipse season.

TABLE 4-7. SOLAR PANEL CHARACTERISTICS

Solar Cell	
Cell type	2 by 2, N/P, 2 0.20 mm, (8 mils) thick
Coverglass	0.15 mm (6 mil) thick, 0211 microsheet
Cell output at 25°C at 1 sun	119.5 A at 460 V
Cell adhesive	GE RTV-566
Coverglass adhesive	Down Corning 93-500
Interconnect	0.05 (2 mil), chem-etched copper, solder placed

Solar Panel Item	Orbiter		Probe	
	Thor/Delta	Atlas/ Centaur	Thor/Delta	Atlas/ Centaur
Total cells	8586	9072	6930	7812
Series X parallel	81 x 106	84 x 103	77 x 90	84 x 93
Power at 28V				
Earth without rad	105	107	96	100
Earth with rad	99	101	91	95
Venus without rad	202	213	162	183
Venus without rad	179	193	145	170
Panel length, cm (in.)	58.2 (22.9)	52.1 (20.5)	47.8 (18.8)	45.7 (18.0)
Panel mass, Kg (lb.)	4.99 (11.0)	5.76 (12.7)	4.04 (8.9)	5.17 (11.4)
(less substrate)				
Area m^2, (ft^2)	3.76 (40.5)	3.99 (43.0)	3.07 (33.0)	3.25 (35.0)

Because of their high energy density, a silver-zinc battery system has been chosen for the Thor/Delta probe bus. The Atlas/Centaur baseline utilizes two nickel-cadmium batteries on both orbiter and probe bus. Table 4-8 summarizes the batteries utilized on each bus.

The losses of each element comprising the power subsystem for the orbiter and probe buses are tabulated in Table 4-9. Losses for elements comprising the large and small probes are tabulated in Table 4-10. Where appropriate, standby and operating losses have been listed. The bus limiters have a standby loss of 0.3 W each as long as the bus voltage is below 33V dc or the particular set point of the limiter. In the limiting mode, each limiter has the capacity of limiting 66W. The Thor/Delta discharge regulator has a standby loss of 6.0W; however, when operating, the efficiency is a function of the load and, hence, the loss of power through the regulator varies as the load and efficiency changes. A curve depicting the variation in efficiency of a typical regulator as a function of load is shown in Figure 4-6. This curve also shows the effect on the output voltage of a typical regulator. The loss of power in the cabling and harness is estimated to be 1.7W and 1.4W in the Thor/Delta orbiter and probe bus, respectively. Power losses in the large and small probes are negligible. The losses in the Atlas/Centaur version are about the same as those on the Thor/Delta.

Tables 4-11 through 4-14 contain a summary of the battery energy needed during intervals when the solar array is not sun oriented or the peak power exceeds the panel capability.

TABLE 4-8. BATTERY TYPES AND CAPACITY

	Thor/Delta		Atlas/Centaur	
Vehicle	Type	Capacity, W-hr	Type	Capacity, W-hr
Orbiter	Nickel-cadmium	216	Nickel-cadmium	353
Probe bus	Silver-zinc	248	Nickel-cadmium	353

TABLE 4-9. THOR/DELTA AND ATLAS/CENTAUR ORBITER AND PROBE BUS UNIT POWER DISSIPATIONS, W

Unit	Thor/Delta Power Dissipations				Atlas/Centaur Power Dissipations			
	Orbiter		Probe Bus		Orbiter		Probe Bus	
Bus limiter	Standby	0.3	Standby	0.3	Standby	0.3	Standby	0.3
	Electronics	3.5	Electronics	3.5	Electronics	3.5	Electronics	3.5
	Power resistor	66	Power resistor	66	Power resistor	66	Power resistor	66
Battery charger	Charging at 3 A	18.0	Charging at 0.4 A	5.4	Charging at 3 A	18.0	Charging at 0.4 A	5.4
Discharge regulator	Standby	6.0	Standby	6.0	Standby	0	Standby	0
	Operating	29.0	Operating	18.0	Operating	7.0	Operating	6.2
Current sensor		0.4		0.4		0.4		0.4
Experiment overload control	Standby	1.05	---		Standby	1.05	---	
	Operating (68 W load)	5.45	---		Operating (30 W load)	3.05	---	
Power interface	---		Standby	0	---		Standby	0
Undervoltage switch	---		---		Operating	2.12	Operating	2.12
Probe battery charger	---		Charging	5.4	---		Charging	5.4
			Standby	1.4			Standby	1.4
Heater switch	---		Standby	0	---		Standby	0
			Operating	0.05			Operating	0.05
Harness loss		1.70		1.40		1.90		1.7

TABLE 4-10. THOR/DELTA AND ATLAS/CENTAUR LARGE AND SMALL PROBE UNIT POWER DISSIPATION, W

Unit	Thor/Delta Power Dissipations				Atlas/Centaur Power Dissipations			
	Large Probe		Small Probe		Large Probe		Small Probe	
Discharge regulator	Standby	6.0	Standby Off	0.05	Standby Off	0	Standby Off	0.05
	Operating	42.0	Standby On	6.9	Standby On	6.0	Standby On	6.9
			Operating	11.3	Operating	48.0	Operating	13.7
Power interface unit	Standby	0	Standby	0	Standby	0	Standby	0
	On	1.0	On	0.02	On	1.0	On	0.02
Pyro switch unit (for 50 ms)	Standby Off	0	Standby Off	0	Standby Off	0	Standby Off	0
	Standby On	4.0	Standby On	4.0	Standby On	4.0	Standby On	4.0
	Operating	65	Operating	65	Operating	65	Operating	65
	25 amp load							
Harness	Negligible		Negligible		Negligible		Negligible	

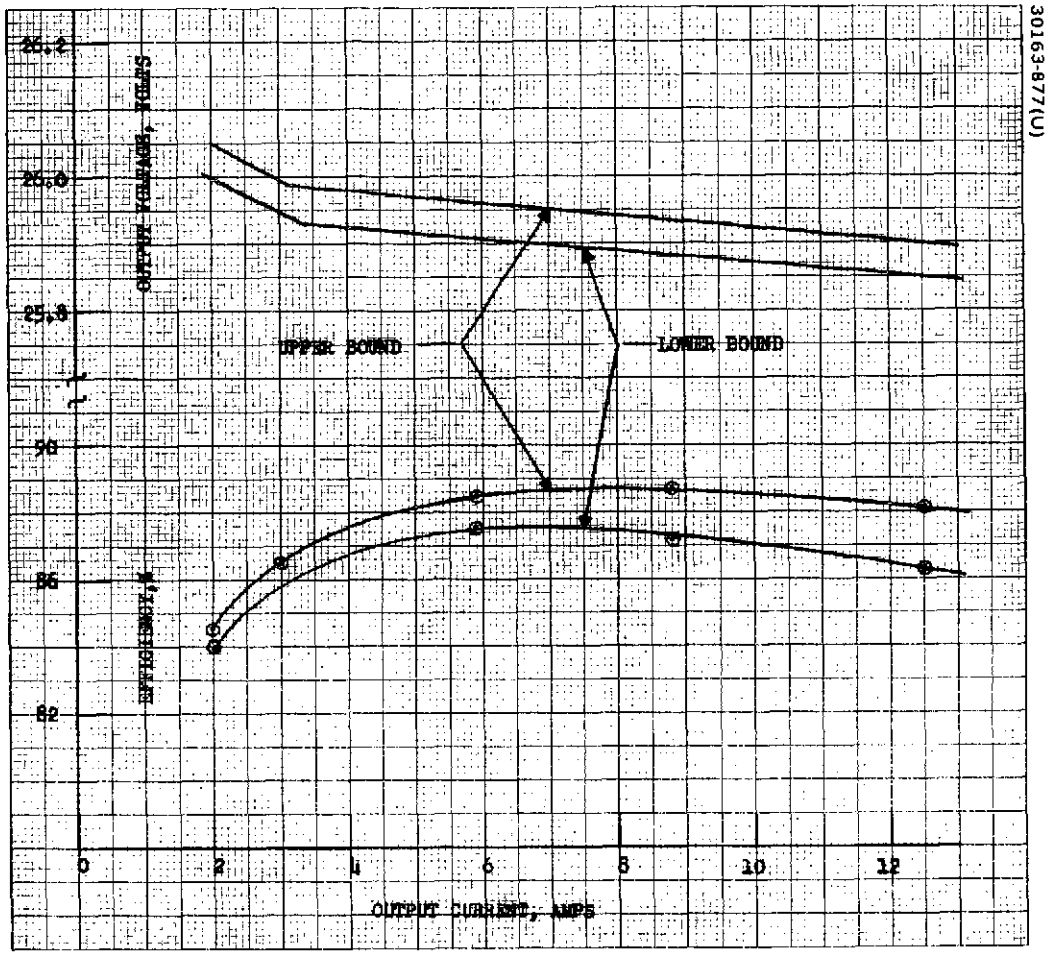

FIGURE 4-6. BATTERY DISCHARGE REGULATOR EFFICIENCY VERSUS LOAD

TABLE 4-11. T/D PROBE BUS POWER REQUIREMENT SUMMARY

Interval	Power Required, W	Battery Energy Required, W-hr
Launch to spacecraft separation	50.8	69.4
Spacecraft separation to sun acquisition	59.0	
First cruise period	79.5	
TCM No. 1	82.5	84.7
TCM No. 4	128.9	
Cruise No. 5B	134.4	
Large probe checkout	178.3	12.4
Probe separation (large)	101.2	96.0
Probe separation (small)	98.0	
Final cruise period	108.0	
Entry	111.5	

TABLE 4-12. THOR/DELTA LARGE PROBE POWER AND ENERGY SUMMARY

Interval	Power Required W	Battery Energy Required, W-hr
Postseparation rf tracking	74.6	12.5
Cruise mode No. 1	0.11	47.5
Cruise mode No. 2	0.22	10.8
Preentry mode No. 1	80.5	13.4
Preentry mode No. 2	82.5	6.9
Entry	87.6	1.0
Descent mode No. 1	204.6	31.1
Descent mode No. 2	212.2	66.4
Descent mode No. 3	207.8	89.4
		279 Total

TABLE 4-13. THOR/DELTA SMALL PROBE POWER AND ENERGY SUMMARY

Interval	Power Required, W	Battery Energy Required, W-hr
Postseparation	43.8	7.3
Cruise	0.11	52.8
Oscillator warmup	7.0	3.5
Preentry	43.8	11.0
Entry	28.8	0.2
Descent	57.0	70.7
		145.5 Total

TABLE 4-14. THOR/DELTA ORBITER BUS POWER REQUIREMENT SUMMARY

Interval	Power Required W	Battery Energy Required, W-hr
Launch to spacecraft separation	50.4	105.8
Spacecraft separation to sun acquisition	50.4	
Jet calibration (first cruise)	93.3	
TCM No. 1	75.9	84.0
Cruise No. 5A	119.0	
Orbit insertion	133.0	
Eclipse (0.5 hr maximum periapsis)	167.1	66.0
Apoapsis cruise	136.2	
Eclipse (3 hr apoapsis)	36.8	144.0
Apoapsis cruise	170.8	

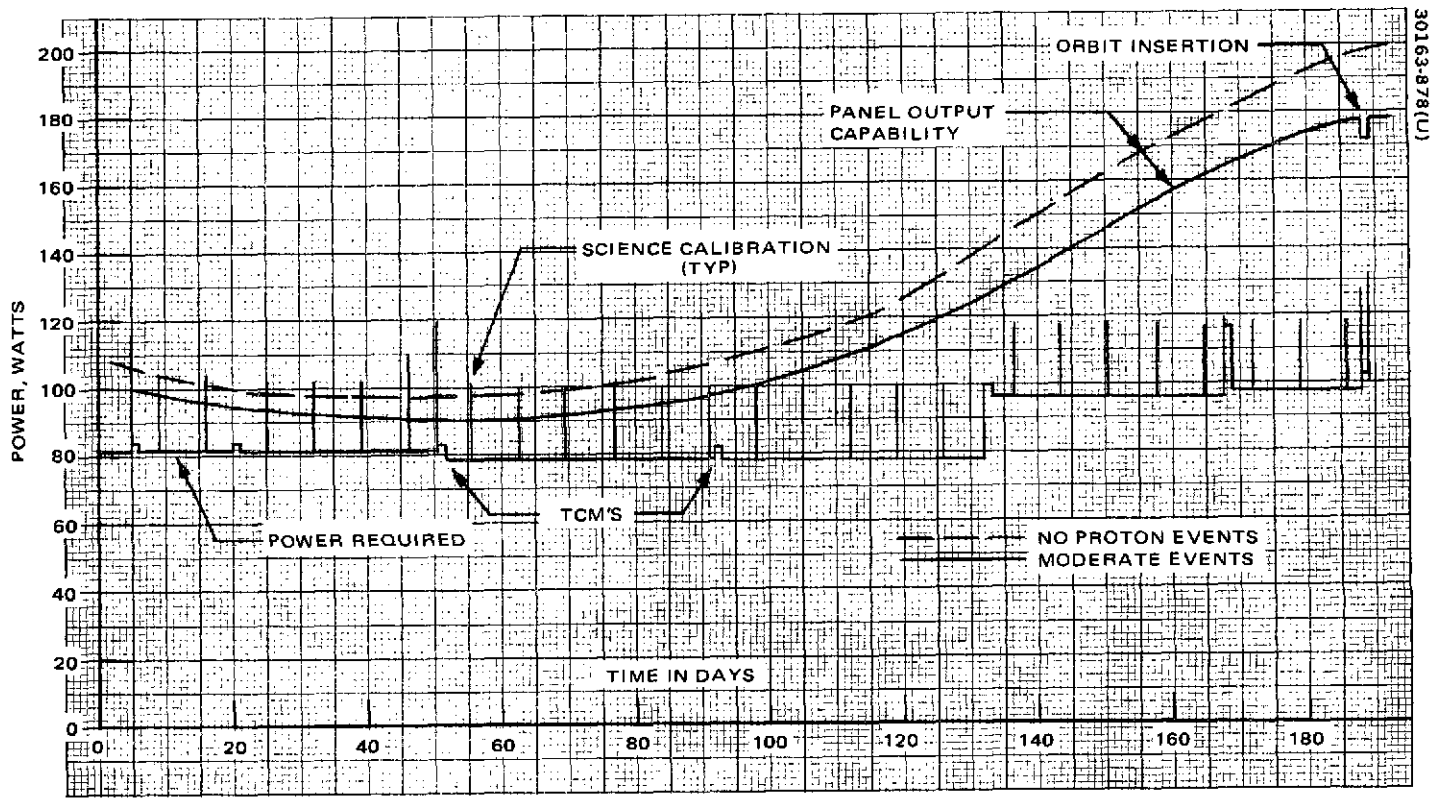

FIGURE 4-7. ORBITER BUS POWER REQUIREMENT AND SOLAR ARRAY OUTPUT CAPABILITY (IN-TRANSIT) – THOR/DELTA

Margins

The power requirements have been analyzed and reported in Section 3. The Thor/Delta orbiter bus power intransit requirements are plotted in Figure 4-7, and the panel output capability with and without the effects of solar flare degradation are presented on the same graph. Similar data are presented in Figure 4-8 for the Thor/Delta probe bus. The transients on the power required line represent either science calibrations or trajectory correction maneuvers. Where transients exceed the panel output capability, the battery will be used.

In summary, adequate solar array power is available in all cases, except when science calibrations and trajectory correction maneuvers are being performed and in the case of the probe bus during probe separation and checkout, in which case, panel output will be augmented with the battery. The orbiter bus panel power decreases from the initial near earth level due to the Type II trajectory, which takes the spacecraft farther away from the sun. After about 60 days, the power output starts to increase, resulting in an even greater margin. In the case of the probe bus, the panel output power gradually increases from its near earth value, and a sufficient margin exists with the exception of trajectory correction maneuvers and probe separation at approximately 107 days. The battery has been sized to provide the necessary energy to meet the demands of probe separation. After probe separation, the bus battery is recharged and readied for the bus entry phase 19 to 20 days later.

A detailed study and design analysis of the solar array is presented in subsection 4. 4. One of the major factors that influences the design of the panel and, hence, the margins is temperature. As the temperature increases, the output of the panel decreases. The loss of power at the maximum power point is approximately 0. 5 percent/^{o}C. The most pronounced effect of temperature will be experienced on the orbiter bus during the low altitude periapsis passes. The predicted panel temperature will vary from 90^{o}C to approximately 130^{o}C from the beginning of the mission to the time where the periapsis point approaches the subsolar point. The difference in the orbiter panel output as a function of the two extremes in temperature is illustrated in Figure 4-9. The deficit in power will be supplied by the battery. The energy demand varies from 10 to 25 W-hr for the upper curve, which is easily within the capabilities of the battery that has a 215 W-hr capacity. The dashed curve illustrates the worst case temperature effect that will occur during the mission. As the panel power decays, the battery energy demand increases to sustain the loads. If the full panel output or the equivalent power is required during this period of time, the battery must supply 59 to 87 W-hr, representing a worst case battery depth-of-discharge of 41 percent. During the smaller energy demand of 10 to 25 W-hr, to maintain the bus at the same power capability, a battery DOD (worst case) of less than 12 percent will be experienced.

A computer program has been prepared that sums all power requirements and computes the margins for the solar panel, as well as the battery depth-of-discharge. Tables 4-15 through 4-18 present the results of these computer generated data in terms of total power required, the available panel

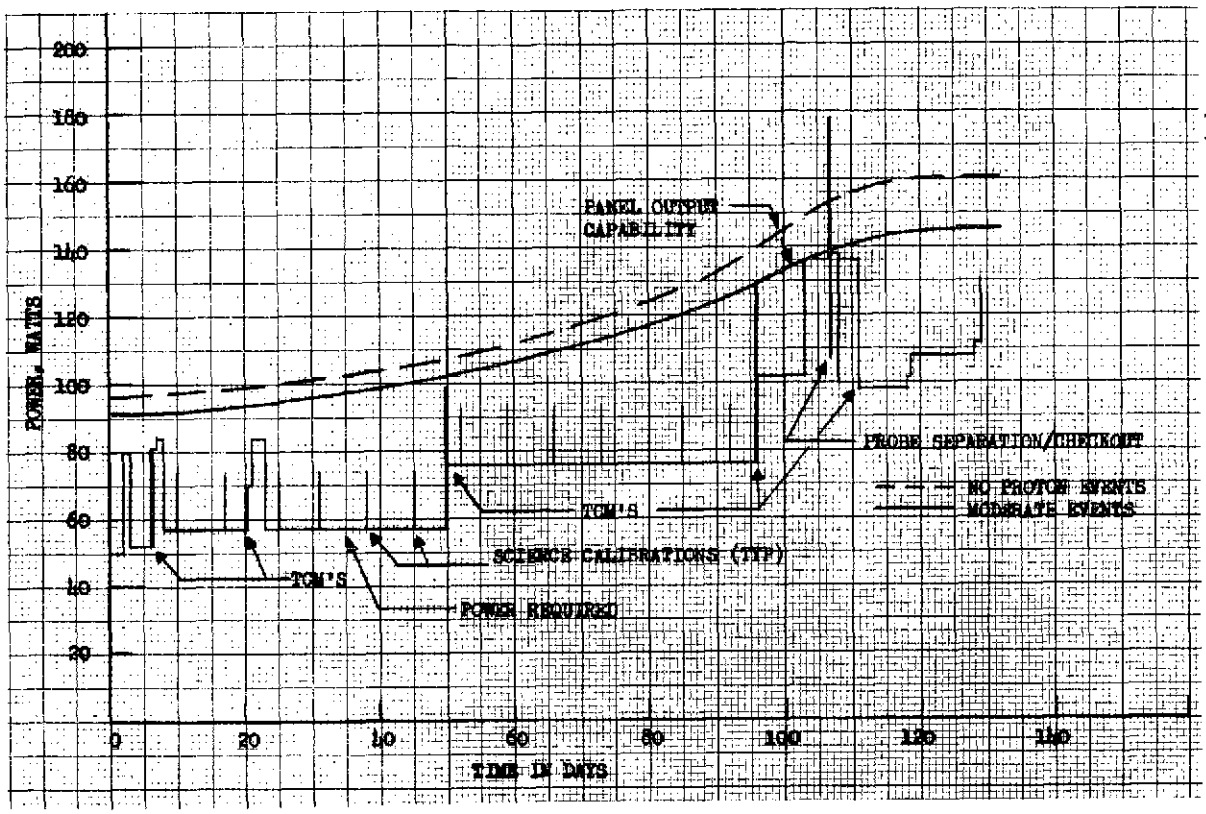

FIGURE 4-8. THOR/DELTA PROBE BUS POWER REQUIREMENT AND SOLAR ARRAY OUTPUT

power (which is a function of sun angle) battery energy and depth-of-discharge. Again, a 10 percent contingency has been included in the required power levels.

4.3 BATTERY SELECTION

Batteries for each vehicle have been selected considering charge/discharge cycle requirements, the effect of battery generated magnetic fields on the science complement, battery energy density, and the environmental conditions in which the batteries must operate. Most of the spacecraft flown today use nickel-cadmium batteries to supply multicycle energy demands of transient and eclipse periods of operation. However, batteries other than nickel-cadmium had to be considered in an attempt to minimize magnetic field interference with the magnetometer experiment. In the case of large and small probes, where only a single discharge cycle is required, the silver-zinc system becomes a logical choice also because of the low weight and ability to operate at elevated temperatures. As indicated in Table 4-19, the silver-zinc system has the highest energy density which is of primary importance considering probe volume constraints. Further, the cycle lofe of the silver-zinc is adequate to meet all testing and flight operating conditions. As shown in Table 4-19, the silver cadmium battery is magnetically clean compared to the nickel-cadmium; however, it has about one-fifth the useful life. Additionally, the silver cadmium battery requires a more precise environment and precision charge termination circuitry.

Special consideration has been given to separator materials for the silver and nickel battery systems to design a highly, reliable system, especially since the large and small probe batteries wet stand life will be strongly dependent upon separator material.

Although initially thought to be a significant part of the battery problem, investigation has indicated the g levels to be encountered during probe deceleration to be easily accommodated through case design and cell mounting. Several designs exist that exceed the Pioneer Venus requirement.

This battery study has corroborated the preliminary results of the proposal effort. Based on the mission requirements, the vehicle battery selection remains unchanged from those selected initially and are listed in Table 4-20.

Commonality of Design

In considering the commonality of design of all battery systems, three factors must be taken into account. Namely, the requirements of the magnetometer experiment on all vehicles, except the large probe, and temperature environment during operation and the high g environment of the large and small probes. Any commonality examination must of necessity consider the cost factor associated with each design and the possible weight penalty.

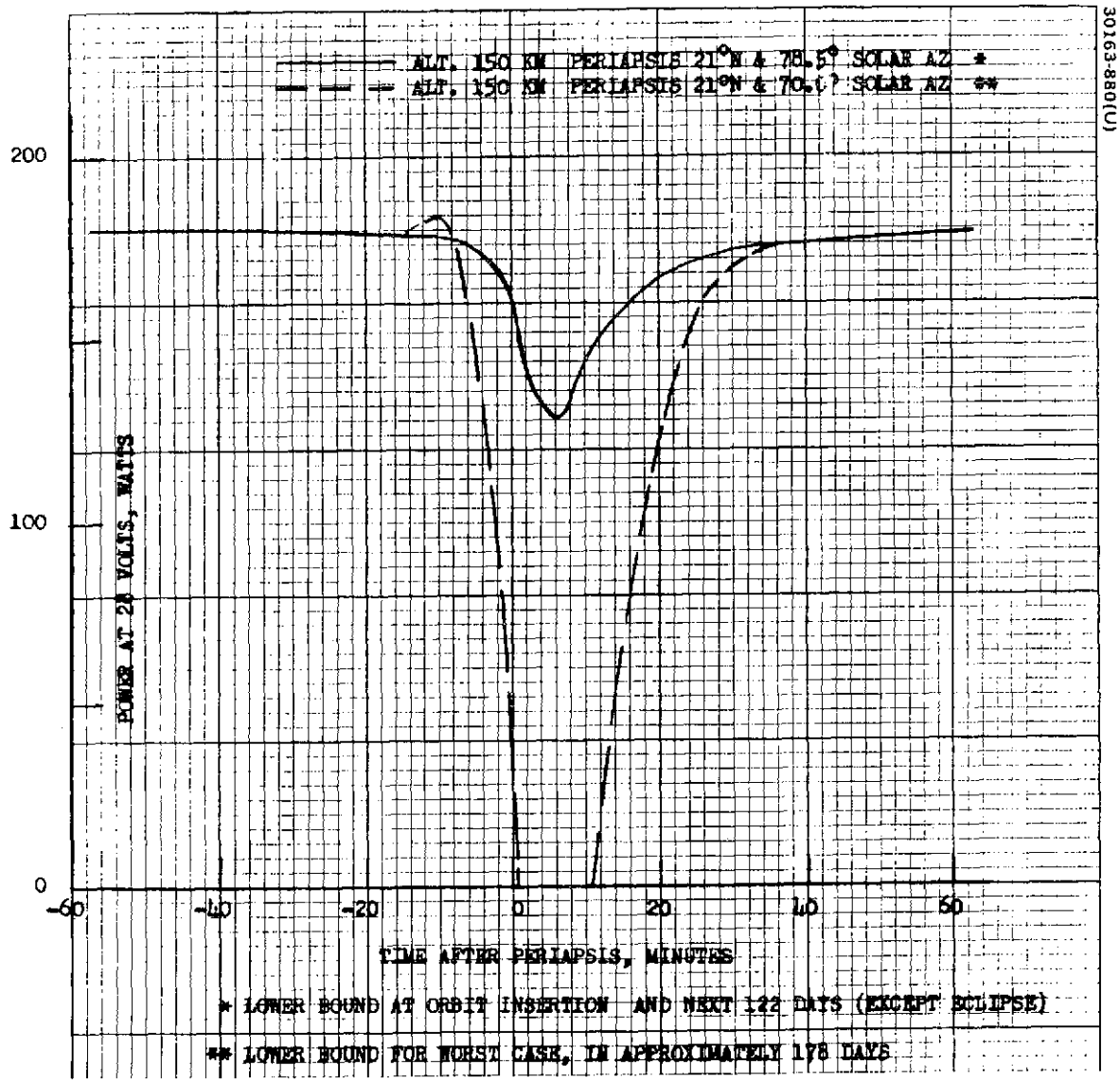

FIGURE 4-9. THOR/DELTA ORBITER SOLAR PANEL OUTPUT NEAR PERIAPSIS

TABLE 4-15. THOR/DELTA ORBITER POWER MARGINS

	ON BATT	LNCH	S/C SEP	SUN ACQ	JET CALB	CRUZ #1	TCM #1	CRUZ #2A	CRUZ #2B	TCM #2	CRUZ #3A	CRUZ #3B	TCM #3	CRUZ #4A	CRUZ #4B	CRUZ #4C	CRUZ #4D	CRUZ #4E	CRUZ #4F	TCM #4	CRUZ #5A	CRUZ #5B		
MODE DUR	0.08	1.12	0.59	0.	0.	0.	0.87	0.	0.	0.68	0.	0.	0.	0.	0.	0.	0.	0.	0.	0.	0.	0.	0.	0.
LNCH-DAYS	0	0	0	0	0	0	5	5	6	20	20	21	50	50	51	91	92	132	133	166	166	167	0	0
SUNANGLE	0.	0.	0.	64.00	85.00	90.00	0.	90.00	90.00	45.00	90.00	90.00	90.00	90.00	90.00	90.00	90.00	90.00	90.00	90.00	90.00	90.00	0.	0.
TOT WATTS	50.4	50.4	50.4	55.9	93.3	80.1	75.9	83.4	81.1	82.5	83.4	81.1	82.5	83.4	81.1	83.4	81.1	101.2	98.9	117.7	119.0	98.9	62.5	62.5
SOLAR PWR	0.	0.	0.	89.0	98.6	99.0	0.	98.0	94.0	66.5	94.0	98.0	89.0	89.0	89.0	97.0	97.0	127.0	127.0	159.0	159.0	159.0	0.	0.
PWR MARG	-50.4	-50.4	-50.4	33.1	5.3	18.9	-75.9	14.6	12.9	16.0	10.6	16.9	6.5	5.6	7.9	13.6	15.9	25.8	28.1	41.3	40.0	60.1	-62.5	-62.5
WT HRSTOT	4.7	66.4	35.0	0.	0.	0.	84.0	0.	0.	13.9	0.	0.	0.	0.	0.	0.	0.	0.	0.	0.	0.	0.	0.	0.
BATT CAP	216.0						216.0						216.0						216.0					
DPTH-DSCH	2.2	30.7	16.2	0.	0.	0.	38.9	0.	0.	13.9	0.	0.	0.	0.	0.	0.	0.	0.	0.	0.	0.	0.	0.	0.

	PRE-INS.	COAST	ORB-IRS.	APO #2	PERI #2	PERI #1A	PERI #1B	APO #1	APO #2	PERI #2B	PERI #2A	PERI #1	APO #1	APO #2	LONG ECLS	APO #3	PERI #2B	PERI #1A	PERI #1B	PERI #2A	APO #1	PERI O/C	APO O/C	
MODE DUR	0.18	0.	1.80	0.	0.	0.	0.15	0.	0.	0.	0.08	0.33	0.	0.	3.17	0.	0.	0.	0.25	0.17	0.	0.	0.	0.
LNCH-DAYS	186	186	187	0	0	0	0	0	0	0	0	0	0	0	0	0	0	0	0	0	0	0	0	0
SUNANGLE	10.00	90.00	77.00	90.00	90.00	90.00	90.00	90.00	90.00	90.00	90.00	0.	90.00	90.00	0.	90.00	90.00	90.00	0.	0.	90.00	90.00	90.00	0.
CONTING	9.9	11.0	12.1	9.2	9.3	12.7	12.7	12.4	9.2	9.3	9.5	12.9	12.4	9.2	3.3	15.5	9.3	12.7	12.7	9.3	12.4	12.7	12.6	9.3
TOT WATTS	109.3	121.0	133.0	101.0	102.3	139.9	139.9	136.2	101.0	102.3	104.5	142.1	136.2	101.0	36.8	170.8	102.3	139.9	139.9	102.3	136.2	140.2	138.9	102.3
SOLAR PWR	30.9	178.0	173.4	179.0	140.0	140.0	126.0	179.0	179.0	179.0	179.0	0.	179.0	179.0	0.	179.0	179.0	179.0	0.	0.	179.0	179.0	179.0	0.
PWR MARG	-78.4	57.0	40.4	78.0	37.7	0.1	-13.9	42.8	78.0	76.7	74.5	-142.1	42.8	78.0	-36.8	8.2	76.7	39.1	-139.9	-102.3	42.8	8.7	40.1	-102.3
WT HRSTOT	17.0	0.	0.	0.	0.	0.	2.5	0.	0.	0.	0.	55.7	0.	0.	144.0	0.	0.	0.	41.1	17.1	0.	0.	0.	0.
BATT CAP	216.0						216.0						216.0						216.0					
DPTH-DSCH	7.8	0.	0.	0.	0.	0.	1.1	0.	0.	0.	0.	25.8	0.	0.	66.7	0.	0.	0.	19.0	7.9	0.	0.	0.	0.

TABLE 4-16. THOR/DELTA PROBE BUS POWER MARGINS

	ON BATT	LNCH -SEP	SEP. ACQ.	ATT. DET.	JET CALB	CRUZ #1A	CRUZ #1B	TCM #1	CRUZ #2A	CRUZ #2B	TCM #2	CRUZ #3A	CRUZ #3B	TCM #3	CRUZ #4	TCM #4	CRUZ #5A	CRUZ #5B
MODE DUR LNCH-DAYS SUNANGLE	0.08 0 0.	0.63 0 0.	0.51 0 0.	2.00 0 57.00	6.20 1 85.00	24.00 0 90.00	96.00 1 90.00	0.95 5 0.	24.00 5 90.00	336.00 6 90.00	0.58 20 45.00	24.00 20 90.00	696.00 29 90.00	0.23 50 90.00	1104.00 50 90.00	0.33 96 90.00	163.00 96 90.00	96.00 103 90.00
CONTING	3.9	3.9	4.6	4.6	7.3	7.2	4.8	6.4	7.6	5.2	6.4	7.6	5.2	9.1	6.7	11.6	9.2	12.2
TOT WATTS	43.2	43.2	50.2	50.2	79.9	79.5	53.2	70.2	83.4	57.1	70.2	83.4	57.1	99.9	73.8	127.6	101.5	134.4
SOLAR PWR	0.	0.	0.	76.3	90.7	91.0	91.0	0.	91.0	91.0	46.0	92.0	92.0	101.0	101.0	129.0	129.0	139.0
PWR MARG.	-43.2	-43.2	-50.2	26.2	10.8	11.5	37.8	-70.2	7.6	33.9	-24.2	8.6	34.9	1.1	27.2	1.4	27.5	4.6
WT HRSTOT	4.2	34.6	30.5	26.5	0.	0.	0.	84.7	0.	0.	17.1	0.	0.	0.	0.	0.	0.	0.
BATT CAP	248.0						248.0						248.0					
DPTH-DSCH	0.	0.	0.	0.	0.	0.	0.	0.	0.	0.	0.	0.	0.	0.	0.	0.	0.	0.

	LP C/O	SP C/O	CRUZ #5C	LP SEP	TCM #5	BUS TRKG	LP C/O	SP C/O	CRUZ #5C	LP SEP	TCM #5	BUS TRKG
MODE DUR LNCH-DAYS SUNANGLE	0.25 107 90.00	0.75 107 90.00	23.50 107 90.00	4.80 108 45.20	4.80 108 36.90	48.00 108 90.00	0.25 107 90.00	0.75 107 90.00	23.50 107 90.00	4.80 108 45.20	4.80 108 36.90	48.00 108 90.00
CONTING	16.2	9.5	11.9	9.2	9.0	12.2	16.2	9.8	11.9	9.2	9.0	12.2
TOT WATTS	178.3	107.4	131.1	101.2	99.3	134.4	178.3	107.4	131.1	101.2	99.3	134.4
SOLAR PWR	140.0	140.0	140.0	99.3	84.1	140.0	140.0	140.0	140.0	99.3	84.1	140.0
PWR MARG.	-38.3	32.6	8.9	-1.9	-15.3	5.6	-38.3	32.6	8.9	-1.9	-15.3	5.6
WT HRSTOT	11.3	0.	0.	11.8	86.8	0.	11.3	0.	0.	11.8	86.8	0.
BATT CAP	248.0						248.0					
DPTH-DSCH	4.5	0.	0.	4.8	35.0	0.	4.5	0.	0.	4.8	35.0	0.

	TCM #6	JET CALB	CRUZ #6A	TCM #7	CRUZ #6B	ENTRY #1	ENTR #2
MODE DUR LNCH-DAYS SUNANGLE	0.85 110 35.00	2.00 91 84.00	192.00 110 50.00	0.25 118 58.00	240.00 118 58.00	2.20 128 66.10	0.25 128 0.
CONTING	8.9	11.6	8.8	9.2	9.8	10.1	10.1
TOT WATTS	97.9	127.6	97.0	101.2	107.8	111.5	111.5
SOLAR PWR	81.4	141.2	108.8	122.1	122.1	132.6	0.
PWR MARG.	-16.5	13.6	11.8	20.9	14.3	21.0	-111.5
WT HRSTOT	16.9	0.	0.	0.1	0.	0.	32.8
BATT CAP	248.0						248.0
DPTH-DSCH	6.0	0.	0.	0.0	0.	0.	13.2

TABLE 4-17. SMALL PROBE POWER MARGINS

Parameter	Pre-separation Checkout	Pre-separation Checkout	Cruise	Preentry	Preentry	Entry E-0	Descent
Mode duration	0.25	0.17	430.00	0.50	0.25	0.01	1.24
Launch days	-21	-20	-20	-45	-15	0	1
Sun angle	0.	0.	0.	0.	0.	0.	0.
Total W	10.9	33.1	0.1	6.2	38.1	13.5	33.1
Solar Power	0.	0.	0.	0.	0.	0.	0.
Power maraging	-10.9	-33.1	-0.1	-6.2	-38.1	-13.5	-38.1
W-hours total	0.	7.3	52.8	3.5	10.9	0.2	70.6
Battery capability	182.0						182.0
Depth of discharge	0.	4.0	29.0	1.9	6.0	0.1	38.8

maximum DOD = 79.8 percent

TABLE 4-18. LARGE PROBE POWER MARGIN

Parameter	Pre-Separation Checkout	Post-Separation Checkout	Cruise No. 1	Cruise No. 2	Preentry	Preentry
Mode duration	120.00	0.17	432.00	43.00	0.17	0.08
Launch days	-21	-20	-20	-18	-15	-5
Sun angle	0.	0.	0.	0.	0.	0.
Total W	75.3	65.2	0.1	0.2	70.1	71.7
Solar power	0.	0.	0.	0.	0.	0.
Power margin	-75.3	-65.2	-0.1	-0.2	-70.1	-71.7
W hr total	398.3	12.9	47.5	10.6	13.5	6.8
Battery capacity	348.8					
Depth discharge	0.	3.7	13.6	3.0	3.9	2.0

	Entry	Descent No. 1	Descent No. 2	Descent No. 3	
Mode duration	0.01	0.15	0.31	0.43	
Launch days	0	1	10	28	
Sun angle	0.	0.	0.	0.	
Total W	76.1	125.3	131.9	131.9	
Solar power	0.	0.	0.	0.	
Power Margin	-76.1	-125.3	-131.9	-131.9	
W hr total	0.7	31.1	66.4	89.3	
Battery capacity	343.8				
Depth discharge	0.2	8.9	19.0	25.6	

Maximum DOD 79.5 percent.

TABLE 4-19. COMPARISON OF CANDIDATE BATTERIES

Parameter	Silver-Zinc	Nickel-Cadmium	Silver-Cadmium
Useful life, months	12+	Over 36	18+
Energy density, W-hr (lb)	66 (30)	25 (12)	40 (18)
Magnetically clean	Yes	No***	Yes
Useful life at maximum depth of discharge, cycles*	50	500	100
Compatible environments requirements**	Yes	Yes+	Marginal

*Special shielding (mu-metal), location, or cell design required

**Approximately 95 cycles required on orbiter bus

***Packaging required for high g

+Unsatisfactory for high temperature probe environment

TABLE 4.20. BATTERY SELECTION (THOR/DELTA)

Launch Vehicle	Vehicle	Couple	No. of Cells	Maximum Depth of Discharge Percentage
Thor/ Delta	Probe bus	Silver-Zinc	13	40
	Small probes	Silver-Zinc	18	80
	Large probe	Silver-Zinc	18	80
	Orbiter	Nickel-Cadmium	18	70
Atlas/ Centaur	Probe bus	Nickel-Cadmium	21	57
	Small probes	Silver-Zinc	18	80
	Large probe	Silver-Zinc	18	80
	Orbiter	Nickel-Cadmium	21	70

As indicated earlier, the cycle life and mission duration of the orbiter can be met reliably only with a nickel-cadmium battery. There is a possible impact on the science due to the high magnetic field of the nickel-cadmium battery, but by use of a boom of sufficient length, this deficiency can be overcome. While no battery design exists that exactly meets the orbiter requirement, it is only necessary to scale down existing Hughes designs. When weight is not a factor, as on Atlas/Centaur, the orbiter battery could be used on the probe bus. Some over design will exist, but a cost savings could result at the expense of additional battery weight. Average values of energy density for the silver-zinc battery is about 66 W-hr/kg (30 W-hr/lb) compared to 25 W-hr/kg (12 W-hr/lb) for the nickel-cadmium.

In the case of the probes, the only logical contender is the silver-zinc battery when one considers probe size, payload capability, and most importantly, the temperature profile from launch to probe impact. The silver-zinc battery can operate reliably at the elevated temperature of 52°C (125°F) maximum (during descent) without excessive loss of capacity. The W-hr efficiency on discharge for the silver-zinc battery is higher at 52°C (125°F) than at 21°C (70°F), whereas, the W-hr efficiency on discharge of the nickel-cadmium battery decreases at temperatures over 32°C (90°F).

Nonoperating conditions in excess of 35°C (95°F) could result in excessive self discharge of the nickel system. The larger power requirement difference between large and small probe precludes use of the same battery system. The present battery complement appears to be a reliable and realistic approach to each vehicle requirement, in terms of weight and reliability.

Battery Charge/Termination Control

Orbiter Spacecraft

Battery charge control is a critical design element in a battery system that is used for long term spacecraft operations. The basic function of battery charge control can be separated into two interrelated tasks. The first task is to obtain a fully charged battery under the normal range of operating conditions. The second task is a protective function (which allows completion of the first task) with built-in provisions for eliminating or limiting detrimental gassing and overtemperature conditions that can occur during charge. Alternative charge control methods are discussed in the following paragraphs.

Initial uncontrolled and subsequent voltage limit charging offers the advantage of providing good charge efficiency with protection against pressure build-up at low temperatures, if the voltage limit is properly selected. However, as the battery approaches full charge, its temperature increases, its voltage then decreases, and the charge current would increase, possibly resulting in "thermal runaway." With this method, "thermal runaway" is prevented by causing the limiting voltage setting to decrease as the battery temperature increases.

Constant current charging without a voltage limit must be utilized within a relatively narrow band of charge rates and battery temperatures. The rate must be low enough to prevent detrimental overcharge and overpressure, but must be high enough to obtain full battery charge/overcharge status. Wide battery temperature variations could seriously affect the capability of this system to fully charge the battery, while increasing the possibility of overpressure. However, between temperature limits of 0°C to 35°C, rates between C/10 and C/15 are feasible. Implementation of a voltage limit which can be used to reduce the charge rate is relatively simple and allows rapid recharge within a given temperature range. However, as with the other methods discussed, the single voltage limit can be detrimental if wide temperature excursions occur.

The voltage limit and constant current charge techniques can be coupled with a variety of control signals. These signals may be a voltage limit, a temperature limit, a coulometer, or a timing device. It is also possible (and in some instances, necessary) to compensate these control signals for varying environmental and orbital cyclic conditions. Other control signals employed are third electrode or auxiliary electrode voltage and direct pressure measurements.

The approach tentatively selected for the Pioneer Venus orbiter mission is initial uncontrolled and then voltage limit to a temperature biased end voltage followed by a taper to a trickle current. Multiple levels can be used that are selectable by ground command. The reliability of the battery is increased by greater flexibility with this charge control method. It can accommodate changes in the battery or environment during mission life.

Probe Bus and Probes

The probe bus and probe silver-zinc batteries can use various methods of charge control. Some of these methods are:

1) Constant current charge to a voltage cutoff followed by open-circuit stand.

2) Constant current charge to a regulating voltage value where the current is allowed to taper to a predetermined value, followed by a voltage clamp at 1.87 V.

3) Constant current (0.4 amp) charge to a voltage limit of 1.93 V/cell and current is allowed to taper to 2 to 10 mA - commanded off at a predetermined time or current level.

The silver-zinc battery systems do not typically tolerate relatively high rates of overcharge as do nickel-cadmium batteries and, therefore, the charge control method must be selected to minimize overcharge except at very low rates that remain below the limited capability for oxygen recombination on the negative electrode and approach the shelf-discharge rate. Method 3 has been selected.

Probe battery temperature during the 110 days between launch and separation will remain between -40 and +4°C. During operation, battery temperature will be between 4 and 52°C, the former temperature expected primarily during the 20 day cruise after separation and the latter temperature achieved at impact.

Typical silver-zinc battery capacity loss rates are negligible at temperatures such as those expected during the cruise. If the probe batteries are charged and topped off from ground support equipment through the umbilical interface with the probe bus/probes, just prior to launch, full battery capacity will be available at separation. Therefore it is entirely feasible to fly the probes without inflight charging.

Orbiter Battery Considerations

Nickel-cadmium cells have been selected for use on the orbiter mission. The 95 charge-discharge cycles and 13 month mission life requirements do not present any performance limitation problems for nickel-cadmium batteries nor is there a need for special cell or battery packaging designs to meet the requirements of the Pioneer Venus orbiter mission. Cell designs similar to those flown on numerous Hughes satellites such as Intelsat II and IV, ATS, Tacsat, and Anik I will be used. Battery package design could change slightly to accommodate slightly different balances between thermoradiative and thermally conductive heat dissipation modes associated with the Pioneer Venus orbiter spacecraft versus the above named earth orbiting satellites. The magnetic interference problem is discussed in detail later.

Selection of separator material will be in accordance with the components listed below taking into consideration all mission requirements. Hughes is presently working with flight nickel-cadmium batteries in the range of 1 to 22 A-hr and technology program nickel-cadmium batteries of 50 A-hr size. Appropriate data from these and other programs will be utilized in the design of the Pioneer Venus orbiter battery.

Separator Materials

To satisfy the requirement of the orbiter mission, the nickel-cadmium battery will utilize a polyamide nonwoven separator material. This material has been found acceptable for the temperature regime, cycle life, and mission duration.

Under the conditions of a temperature of 36°C, oxygen gas, and 34 weight percent potassium hydroxide electrolyte solution, polyamide separators will readily thermally depolymerize by hydrolysis reaction at the carbon-nitrogen bonds. In addition, oxidative hydrolysis of the polyamide separator occurs at temperatures below 36°C at the positive plate-electrolyte-separator interface, especially during overcharge.

TABLE 4-21. PERMANENT MAGNETIC FIELD OF BATTERY CELLS

Item	Type	Electrodes	Magnetic Field Magnitudes in Gammas				
			30.5 cm (12.0 in.)			Max* at 1.1 m (3.5 ft)	Max* at 3.2 m (10.5 ft)
			Initial	Post Exposure	Post Deperming	Post Exposure	Post Exposure
Electric Storage Battery Company	5AH	SilCad	1.6	1.9	1.4	<0.4	<0.002
Yardney Electric Corporation	5AH	SilCad	<0.5	<0.5	<0.5	<0.1	<0.005
Gulton Industries, Inc.	4AH	NiCad	13.5	333.0	4.1	7.8	0.3
General Electric Co.	12AH	Nicad	333.6	864.0	14.4	20.2	0.7
General Electric Co.	4AH	NiCad	55.1	113.6	0.3	2.7	0.1
Sonotone Corporation	3AH	NiCad	6.8	171.7	0.6	4.0	0.1

* Extrapolated strengths using $f_r = \frac{f_{PE}}{\left(\frac{r_2}{r_m}\right)^3}$

Where

f_r = maximum radial component at r_2

f_{PE} = measured radial component post exposure

r_2 = radial distance

r_m = radial distance of measurements

The main concern regarding polyamide separator hydrolysis depolymerization, is that oxygen is consumed in this reaction that otherwise would have been recombined at the negative plates. This results in increased precharge at the expense of overcharge protection, $Cd(OH)_2$, which is a battery life limiting phenomenon. However, for the orbiter mission duration (approximately 13 months), the rate of this latter depolymerization is not considered significant. Therefore, provided battery baseplate temperature remains equal to or below 25°C, Pellon 2505 separator will be used in the Pioneer Venus orbiter nickel-cadmium battery design.

Magnetic Cleanliness

The Pioneer Venus orbiter spacecraft will carry a highly sensitive magnetic field measuring experiment (magnetometer). Even though such devices are generally removed from close proximity to the spacecraft by mounting on a long boom, they are still susceptible to the influence of magnetic fields generated or existing within the spacecraft. Obviously, it is highly desirable to reduce or totally eliminate, where practicable, the influence on the magnetometer by the spacecraft systems. A 5 gamma maximum at the magnetometer was established as an upper limit earlier in the program and less than a gamma is desirable. In addition, the 5 gamma spec limit at the magnetometer still applies after the spacecraft has been exposed to a 25 G field.

Based solely on optimum lifetime and cycle life capability, with depth of discharge a weight influencing parameter, the most reliable and cost effective battery cell for use on the orbiter bus is clearly the nickel-cadmium type. Considered here also as a feasible backup to the nickel-cadmium approach for purposes of this study is the silver-cadmium type cell.

Sealed nickel-cadmium cells, with their relatively high mass to volume ratio and large mass percentage of high permeability material, are a potential source of significant residual magnetic fields, before and after exposure to the 25 G field and the other normal spacecraft environments. In addition, all cells, even those with little or no magnetic or highly permeable material, such as the silver-cadmium cells, are potential sources of stray magnetic fields while undergoing charge and discharge. Table 4-21 shows measured permanent magnetic field data for various nickel-cadmium and silver-cadmium cells, and includes extrapolated field strength effects on the magnetometer if a single cell were placed at the nearest or farthest possible mounting points on the spacecraft bus. At the single cell level, it is clear that the worst permanent magnet effect occurs after "perming" the cells in a high strength field, and that the nickel-cadmium cells exhibit field strengths one to two orders of magnitude higher than the silver-cadmium cells. However, the extrapolated field strengths at 3.2 m (10.5 ft) show that the worst single nickel-cadmium cells would represent less than 15 percent of the maximum allowable background at the magnetometer. Obviously, the matter of greatest concern then is to determine the extent of change in magnetic field strength from the single cell level to the battery assembly level.

TABLE 4.22 LUNAR ORBITER BATTERY - RCA No. 1756837-502

10 Cells, 12 AH, Nickel-Cadmium, Hermetically Sealed

Measurement	Magnetic Moment Magnitude in CGS Units	Maximum Radial Component Extrapolated at 0.91M (3 Ft.)*	Maximum Radial Component at 30M (1 Ft.) $f_r(3)^3$
Initial - open circuit	120 g-cm^3	30 gammas	810 gammas
Deperm at 40 G (3 axes)	35	9	261
25 G perming (1 axis)	377	94	2540
Deperming	36	9	261
10 A discharge	131	33	890
1 A charge	71	18	486
Final - open circuit	64	16	432

*Magnetic moment converted to maximum radial component using $f_r = \frac{2M}{r^3}$

The nickel-cadmium batteries used on the OGO spacecraft were comprised of 22 series connected 12 Ah Gulton cells. After exposure to a 25 G magnetic field, the "permanent" or residual magnetic field strength measured as high as 100 gamma at 0.3 m (1 ft) distance. This condition is independent of wiring layout and is primarily dependent on the quantity of nickel present in the cells and cell layout, assuming a very limited amount of ferromagnetic material is used in the battery package. If a battery of the OGO type were to be mounted along the same axis as the boom longitudinal axis, the battery influence at 1.1 m (3.5 ft) would be 2.3 gamma and $1000/(10.5)^3 = 0.9$ gamma at 3.2 m (10.5 ft). Since mounting a battery of this type on the boom side of the spacecraft would result in nearly 50 percent of the allowable background to exist at the magnetometer, it is apparent that all effort should be made to locate the spacecraft battery as far from the magnetometer as possible.

Measurements obtained on a lunar orbiter battery show permanent magnetic effects even higher than those noted for OGO nickel-cadmium batteries. Table 4-22 shows magnetic moment magnitude measurements in CGS units at 0.91 m (3 ft) for various battery conditions, while Figure 4-10 represents a plot of field strength versus distance. Extrapolations are made for maximum radial component at 0.91 m (3 ft) and at 0.3 m (1 ft). The permanent magnetic influence at the magnetometer using these data for both near and far mounting are:

Mounted at boom attach point = 59.5 gamma

Mounted opposite boom attach point = 59.5 gamma

In this instance, the best case condition results in the battery providing nearly 50 percent of the allowable background at the magnetometer, while the worst case situation clearly exceeds the limits. Additional data for various spacecraft nickel-cadmium batteries are shown in Table 4-23, including maximum postperming gammas at 0.30 m (1 ft) for comparison with the lunar orbiter battery measurements. Based on comparison of these data, the lunar orbiter battery appears to represent a worst-case package with the highest measured and extrapolated permanent magnetic moment magnitudes and radial components.

A second major area of consideration in the determination of a battery's magnetic field strength is that of stray fields. In addition to the permanent residual magnetism exhibited by batteries containing ferromagnetic materials, batteries on charge or discharge generate magnetic fields proportional to the current and uncompensated loop areas represented by the particular cell/battery/wiring harness. As noted in Tables 4-21 and 4-22, the stray field measurements on nickel-cadmium and silver-cadmium batteries show no advantage of one cell type over the other. However, it is clear that stray field effects are considerably less than the permanent magnetic effects in nickel-cadmium batteries, while the converse is true for silver-cadmium batteries. Cancellation or reduction of the stray field can be achieved by aligning the cells in the battery pack in an alternate polarity back-to-back so that the induced field from each cell will be cancelled by the next one. End

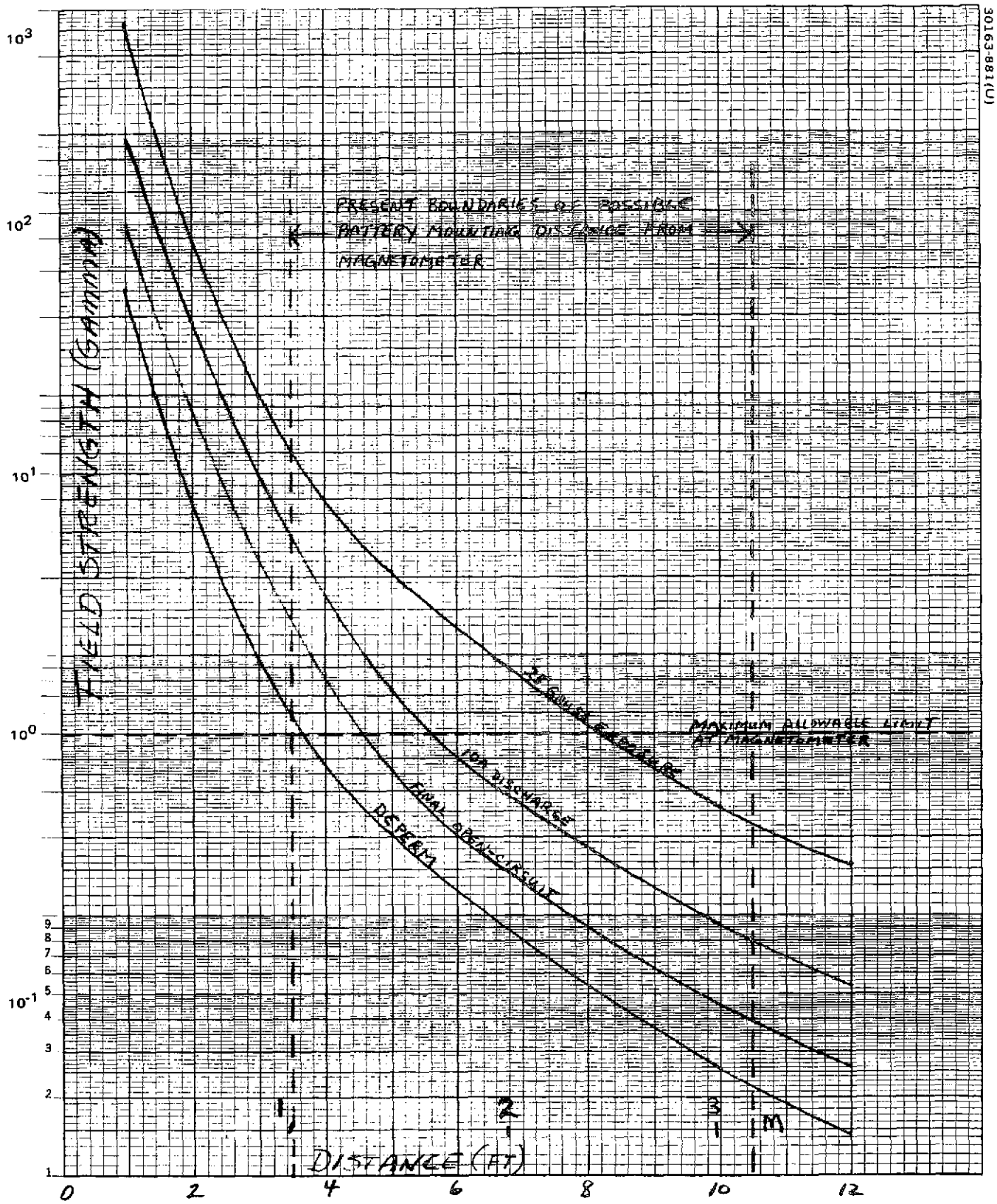

30163-881(U)

FIGURE 4-10. LUNAR ORBITER BATTERY MAGNETIC CHARACTERISTICS, FIELD STRENGTH VERSUS DISTANCE

TABLE 4-23. PERMANENT MAGNETIC MOMENTS OF BATTERIES

Spacecraft Program	Battery Type	Voltage and Current		Number of Cells	Perming	Moment Magnitude in CGS Units			Extrapolated Maximum Gamma Post Exposure
		V	A			Post Exposure	Post Deperming	Stray Field	
UK-2	NiCad	1.3	–	10	23	180	14	–	45
OAO	NiCad	28.0	12.0	3	168	2521	49	679	630
OGO	NiCad	28.0	–	22	42-378	–	–	–	–
OGO	SilCad	28.0	5.0		5	–	–	1106	–
IMP	SilCad	13.5	3.0	13	≪1	≪1	≪1	45***	≪1
IMP	NiCad**	13.5	3.0	13	19	1052	3	62	263
RAE*	NiCad	14.0	4.0	12	24	251	<1	10	63
RAE*	NiCad	16.0	4.0	12	23	481	6	46	120
ATS	NiCad	-9.0	1.2		40	180	5	5	45

* Test unit
** <4 gammas compensated
*** Both units contained 11 6 AH NiCad cells but were from different manufacturers

cells or isolated cells, where an odd number are used, may be compensated for by a loop cemented to the cell. The loop size would be proportional to the size of the cell. Additional loops may be added in the area of the electrical interconnections or the wiring harness of the battery may be routed in a manner that provides compensation for the various directions of current flow within the assembly. As an example of the effifacy of compensating with loops and proper assembly wiring layout, a 95 percent reduction in stray field strength was achieved on the 13 cell 5 Ah IMP silver-cadmium batteries, from 101.5 gammas at 45.72 cm (18 in.) to 4.9 gammas at 45.72 cm (18 in.). A single loop was used to reduce the assembly field in conjunction with a small loop for 1 of the 13 cells in the circular package. It was found that a rectangular 13 cell package could show comparable reductions utilizing two small side loops. If required, it appears that nearly complete compensation could be achieved by laboratory measurements and addition of small loops on individual assemblies.

After deperming the lunar orbiter battery showed a stray field at 1 ft of 629 gamma above the permanent magnetic field. This corresponds to a field strength of 14.7 gamma at 1.07 m (3.5 ft) (closest Pioneer Venus orbiter battery/magnetometer distance) and 0.5 gamma at 3.20 m (10.5 ft) (farthest Pioneer Venus orbiter battery/magnetometer distance). When compared with the permanent magnetic effects after perming at the same distances on the same battery, i.e., 59.5/14.7 and 2.2/0.5, it is clear that the permanent magnetic effects are more significant than those associated with the stray field effects.

Shielding the battery or cells has been considered as an additional means to reduce the background field at the magnetometer. Data recently presented at the 1972 NASA/GSFC Battery Workshop, based on work performed under NASA/ARC direction, has indicated that mu-metal could be effective as a nickel-cadmium cell case material if the interior components were depermed prior to cell assembly. However, the constituents of the mu-metal alloy are presently incompatible with the cell interior environment. More effective use of such shielding, at present, could possibly be achieved if utilized as the battery case material. Since the presently known spacecraft requirements specify maximum magnetic field strengths must not be exceeded after exposing the spacecraft to a 25 G perm, the shielding would not be as effective since it too would be magnetized, in addition to the increase in battery field strength, and act as a magnetic field source whose strength is proportional to the mass and geometry of the mu-metal required. Therefore, until actual test data is available related to the specific geometry and interfaces between the battery/spacecraft/magnetometer, shielding requirements are quite uncertain and the battery should be designed and specified with the unshielded postperm magnetic field strength values assumed and allowed for in the spacecraft design. Shielding the battery, however, could be considered and could be practical and effective if the requirement for perming the spacecraft (and the battery) were reduced or eliminated in the future, or when sufficient hardware is available for accurate determination of the weight and geometry required for the worst case situation.

The data indicate that stray fields can be compensated and reduced sufficiently, in both nickel-cadmium and silver-cadmium batteries. The major portion of the battery magnetic field background at the magnetometer will be contributed by the permanent magnetic field of the nickel-cadmium system. The data also indicate that the silver cadmium batteries are magnetically "cleaner" than nickel cadmium batteries, especially when compensated. However, if the condition is imposed that the nickel-cadmium battery be mounted on the opposite side of the spacecraft from the magnetometer, the battery worst-case magnetic field at the magnetometer can be held to less than 50 percent of the allowable limit. The battery packaging, wiring, and associated hardware would consist of nonferromagnetic material, therefore, the major field contributor would be solely the cells. Since the most practical and cost-effective battery for the orbiter bus will consist of an assembly having standard nickel-cadmium cells, requiring virtually no development or special testing, it seems impractical to attempt any further reduction in the battery magnetic field by changing cell materials. The analysis for the nickel-cadmium batteries is very worst case, in that the battery will never fly at the postperm residual field level, with the whole spacecraft being diagnosed prior to flight. For the lunar orbiter battery, the degaussed state shows a 0.23 gamma level at 3.20 m (10.5 ft) and a 0.37 gamma level after charge/discharge cycling. This is less than 8 percent of the maximum allowable limit at the magnetometer, and probably represents a more typical level of battery permanent magnetic field on the spacecraft.

Probe Bus and Probe Battery Considerations

The silver-zinc cells required for the Thor/Delta probe bus will be typical of those flown on many scientific planetary probe and earth orbiting satellites in the past. There are no unusual high g requirements associated with the multiprobe mission. The suggested separator configuration is detailed in Section 5. Presently, it is anticipated that these cells will be manufactured either by Yardney or ESB Inc.

The probe bus battery must incur approximately ten charge-discharge cycles during its mission usage. This is not a high cycle life requirement for secondary silver-zinc cells. Depending upon the cell manufacturer selected, a decision must be made whether to use individual cells or monoblocks in the design. The individual cells would be contained either in an aluminum or magnesium case. Further, in this case, massive epoxy potting will be used to effect hermetic sealing of the individual cells. Monoblocks would use multiple epoxy potting of all leads from the inside of each cell outward. A minimum of three epoxy seals in series would be used to accomplish the necessary hermetic sealing. Massive epoxy potting external to the cells would not be required in this case.

The probe batteries would be constructed almost identical to the probe bus batteries, except that the cell plate stack would be retained in its case by internal epoxy bonding with possible use of an injection molded restraint plate at the top of each cell to withstand the high g environment. The purpose of locking the cell plate stack into its case is to minimize any relocation of the plates during descent.

Orientation of the battery such that the g forces are not directed through the cell in a plane from the bottom of the plate stack to the cell terminals will further ensure battery survival.

Separator Materials

The low cycle and calendar life requirement for the silver-zinc batteries does not present a difficult separator selection problem. The primary function of the separator system is to physically separate the positive and negative plates and still have sufficient porosity to allow electrolyte to pass through. The separator system must of necessity impede the failure mechanisms characteristic of silver systems, namely, silver migration, zinc plate dendrite formation, and zinc plate shape changes. The basic separator system selected for both probe bus and probe batteries will incorporate cellulosics and absorber around the positive plates, and possibly a retainer on the negative plates.

Consideration was given to the possible use of irradiation cross-linked polyethylenes and semiflexible inorganic separators that have been under development for silver-zinc batteries over the past five years. It has been found that the cross-linked polyethylenes reduce significantly the amount of silver migration and prevents zinc dendrite penetration of the separator system. One deficiency does, however, exist in that the cross-linked polyethylenes swell only 5 to 10 percent in thickness when wet with 40 percent potassium hydroxide electrolyte solution compared with 300 to 500 percent swell factors associated with cellulosic materials.

The low swell factor associated with cross linked polyethylene separators in potassium hydroxide electrolyte solutions does not offer enough mechanical support for zinc plates. Therefore, severe zinc plate slumping problems result from use of polyethylene separators if cellulosics or potassium titanates or other high swell factor of supportive auxiliary material is not used in conjunction with this separator. Zinc plate slumping has been shown to be a concentration gradient problem. This is especially true at the top and side plate edges where active material goes into solution and reelectroplates elsewhere back onto the zinc plates resulting in shape changes. This shape change problem is enhanced by a separator system that does not provide maximum mechanical support for the zinc plates.

The semiflexible inorganic separators offer rigid support for zinc plates and also are effective in preventing silver migration and zinc dendrite penetration through the separator system. However, there has not been enough long term testing of this separator to consider its use for the Pioneer Venus application. Silver-zinc cell manufacturers must do more development work prior to incorporating this ceramic type of separator into their cells if they are to achieve long term reliability.

Because the wet life mission flight requirements for the probe bus and probe batteries does not exceed 130 days, and the cycle life requirements are extremely low, there is no advantage to using any separator system such as irradiation cross-linked polyethylene (R.A.I. Permion 2291) or

semiflexible inorganic separator (NASA-Lewis/Astropower/Yardney). A separator system such as the following is recommended for Pioneer Venus probe bus and probe silver-zinc batteries:

1) Absorber, one layer, on silver plates, such as:

   a) Kendall Dynel EM 470
   b) Pellon 2505 K

2) Separator, four layers, such as:

   a) DuPont Cellophane, 193 PUDO
   b) Yardney, C-19 (silver treated cellulosic)

3) Retainer, one layer on zinc plates, such as:

   a) Visking
   b) Viskon

The wet life capability of a separator system of this type should easily approach 2.5 times the flight duration requirements for the probe bus and probes. There does not appear to be a need to use other separator systems to accommodate the high 500 g requirement associated with probe descent to Venus.

Magnetic Cleanliness

At one time during the study, it was proposed to carry a magnetometer on the probe bus and the small probes. The magnetometer to be carried on the probe bus was to be mounted similarly to that of the orbiter bus and also have an established maximum allowable background of 5 gamma. The magnetometer on the small probe was to be mounted within the 30.5 cm (12 in.) diameter body and have a maximum allowable background limit of 100 gamma.

Since the probe bus battery will be the silver-zinc type, it is expected that the extremely low permanent magnetic field of this type battery will present little problem for the probe bus magnetometer. Silver-zinc batteries are essentially similar to silver-cadmium batteries magnetically, with virtually no ferromagnetic materials utilized in cell construction. Typical battery packaging can also eliminate most ferromagnetic material and result in silver-zinc batteries (or silver-cadmium batteries) having less than 1 gamma permanent magnetic field at 0.3 m (12 in.). This means that the background level at the magnetometer between 1.1 m (3.5 ft) and 1.2 m (10.5 ft), as a result of battery contribution would vary between 0.02 gamma and 0.0009 gamma, respectively. The probe bus battery could potentially have a greater effect on the small probe magnetometers (the large probe carries no magnetometer) than on the probe bus magnetometer since it is closer to the small probes prior to separation. However, there is no requirement for small probe magnetometer measurements to be taken prior to separation, only functional checkout of the instrument. In addition, since the

small probe magnetometer maximum allowable background limit is 100 gamma it is apparent that the probe bus battery, with less than 1 gamma field at 0.3 m (12 in.) could not contribute more than 1 percent of the allowable background level at the Thor/Delta small probe magnetometer. The same reasoning applies to the large probe battery since it too is a silver-zinc type. The worst case permanent magnetic field interaction between the probe bus battery/large probe battery and the probe bus magnetometer/small probe magnetometer will be negligible.

The major effects of battery magnetic field on the probe bus magnetometer will be due to stray fields generated during battery charge and discharge. The probe bus magnetometer will be operating during the entire mission, therefore, it is apparent that the probe bus battery must be magnetically compensated to minimize stray fields during charge and discharge. As with the orbiter bus battery, cells should be combined back to back in pairs, and odd numbered cells should have a magnetic loop added with an enclosed area approximating the cell face area. Single or double side loops on a rectangular package, or a single loop on a circular package could keep the maximum field strength below 5 gamma at 45.72 cm (18 in.). Since these results were achieved on the IMP 13 cell 5 AH silver-cadmium batteries, these data should be essentially applicable to the 13 cell 10 AH probe bus battery since the field is proportional to current and the IMP data was measured at 3 A discharge rate, similar to the typical discharge rates for the probe bus battery. The 5 gamma level extrapolates to 0.12 gamma at 1.07 m (3.5 ft) and 0.0043 gamma at 3.20 m (10.5 ft). It is apparent that this is a negligible effect on the probe bus magnetometer and the small probe magnetometer. The large probe battery, mounted near the spin axis will also have a field strength similar to that of the probe bus battery and will fall between the 1.07 m (3.5 ft) and 3.20 m (10.5 ft) levels cited for stray field effect at the bus magnetometer. Again, since the small probe magnetometers will not be required for measurements prior to separation, there will be no effect from any stray field emanating at the probe bus or large probe batteries.

The greatest potential problem area is related to the proximity of the small probe batteries to the small probe magnetometer. The small probe diameter is only 30.48 cm (12 in.) and assuming the battery and magnetometers are mounted as far apart as possible, the maximum distance will be less than 12 in. Using the IMP silver-cadmium battery data, since it utilizes the same number and approximate cell size as the small probe silver-zinc battery, the 5 gamma (3 A discharge rate) field extrapolates to 16.8 ganna at 30.48 cm (12 in.). This is a 17 percent contribution to the maximum allowable limit of 100 gamma at the magnetometer. However, the discharge rate on the small probe batteries will not exceed 1.6 A, and thus result in approximately one-half the 5 gamma field at 18 in. and extrapolates to 8.4 gamma at 30.48 cm (12 in.) less than 8.5 percent contribution to the maximum allowable magnetometer limit.

The probe bus, large probe and small probe batteries will have negligible permanent magnetic effects on the spacecraft magnetometers due to their use of nonferromagnetic materials throughout. However, stray field effects present the greatest potential problem, although compensation with cell arrangement and wiring/loop layout will keep the battery effects at the probe bus magnetometer to less than 4 percent and at the small probe magnetometer to less than 8.5 percent. Again, as with the orbiter batteries, every effort must be made to mount the spacecraft batteries as far from the magnetometers as possible.

Entry Acceleration

During the entry phase, the axial deceleration for any of the probes can approach 600 g, depending on the entry angle. The duration of the peak g level will be 1 to 2 sec, with deceleration forces acting for at least 6 to 8 sec. The batteries for both the large and small probes must be designed to meet performance requirements during and after exposure to the severe entry deceleration. Entry axial loads for the large and small probes for specific entry angles (γ_e) are presented in Volume 5, Section 5.

Designing the probe batteries to meet the deceleration requires that:

1) the cell itself must be made capable of undergoing exposure to the decelerative forces with no degradation in performance, and

2) the packaged battery comprised of numerous cells must maintain its integrity during the decelerative period.

The specific designs for both the cells and the battery package are interactive, since certain restrictions in the cell design are a possibility due to mass, volume, and form factor requirements imposed by the probe, which in turn may impose requirements or restrictions on the battery package itself to enhance the cell performance during the peak axial load period.

The results of this study indicate that the design of large and small probe batteries to withstand the high g environment is a realizable goal. A literature survey shows that higher levels have been accommodated. Some of these designs utilized specially designed cell plates to allow for flexing, and unique wrapping of the separator material around the plates to form a completed cell. In turn, the cell case was milled with slots in both sides and bottom to minimize plate pack movement. Epoxy was then used to facilitate holding and sealing the top of the cell assembly. Adequate strain relieving of terminal to internal cell wiring was employed to preclude breakage of the electrical connection. These and other techniques reported on in the references allowed battery packs to successfully undergo high g levels of impact testing.

To ensure that the selected design is adequate qualification test levels will be performed at 1.25 times the calculated flight levels.

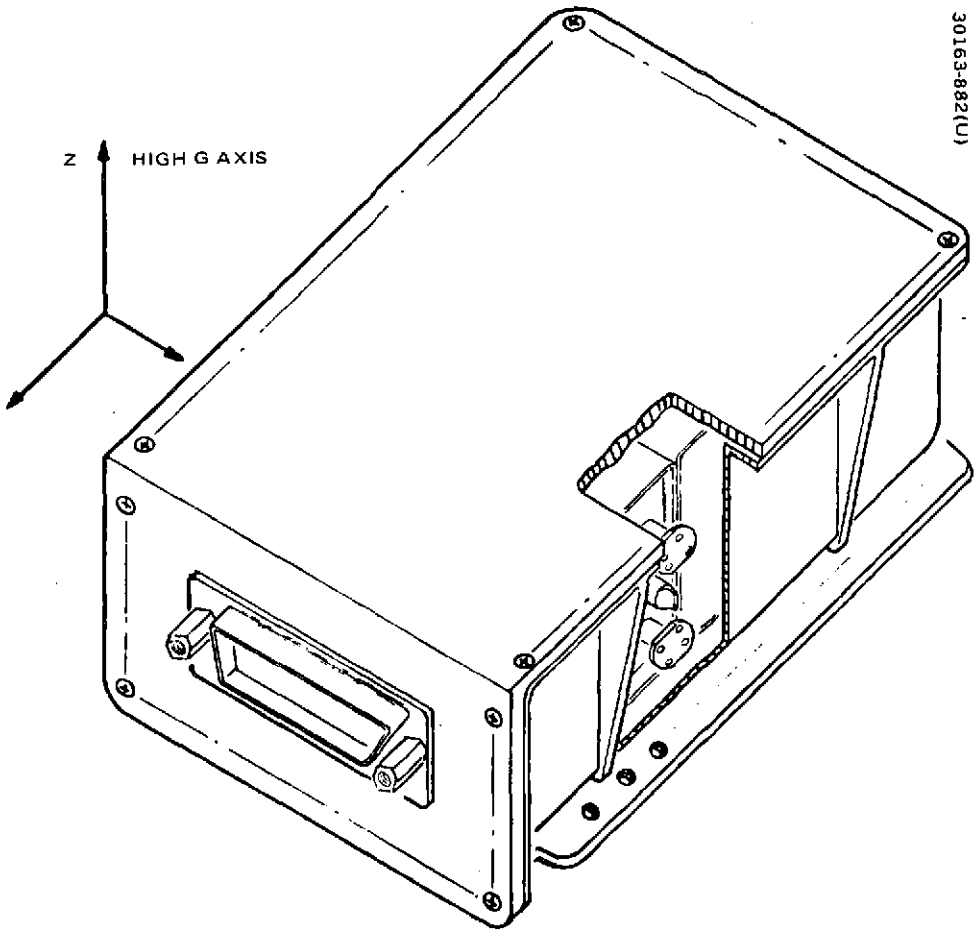

FIGURE 4-11. HIGH G BATTERY PACK DESIGN

Minor modifications to the basic cell assembly will have to be made to minimize or restrict plate pack movement. The total mass of a single assembly must be kept to a minimum (this implies multiple battery packs consistent with allowable packaging volume in each probe) and the proper orientation of the terminals maintained. It has been concluded that the most desirable orientation is such that the axial g forces pass through the narrow (side) dimension of the cell 90 deg to the terminals. It has further been concluded that the simple, hermatically sealed cell as tested by GSFC at NAD Crane and successfully flown on all Mariner Mars missions by JPL is adequate for the mission requirements.

The battery packs will consist of a welded aluminum or milled magnesium box of appropriate size with mating top as shown in Figure 4-11. After the cell complement is placed in each box and wired, epoxy or urethane would be added to provide the necessary dampening, thereby minimizing still further fragility problems in the high g environment. Another significant advantage of the module packaging concept is ease of cell or pack replacement in the event of cell failure during testing.

It should be emphasized that no actual high g batteries have been built and tested during this study. Data from the references was collected and carefully analyzed for similar applications and, hence, deemed useful and valid. Based on both the GSFC and JPL C-SAD data, a packaging weight penalty of 30 to 50 percent (due to high g) has been used for this mission. More detailed design analysis and testing will be required. Additionally, the stray field compensation becomes more of a problem with the multiple pack design. Again, detailed analysis and actual test will be most useful. From data obtained on other battery programs, the latter is not considered a serious problem.

TABLE 4-24. CHARACTERISTICS OF SOLAR PANEL DESIGNS

Mission	Number of Cells Series X Parallel and Total	Output at 28 V at Earth, w,* With Proton Event / Without Proton Event	Output at 28 V at Venus, w With Proton Event / Without Proton Event	Panel Weight Less Substrate, kg	lb	Basic Panel Height,** cm	(in.)
Probe							
Thor/Delta	77 x 90	91	(a) 145	4.04	(8.9)	47.8	(18.8)
	6930	96	(b) 162				
Atlas/Centaur	84 x 93	95	(a) 170	5.17	(11.4)	45.7	(18.0)
	7812	100	(b) 183				
Orbiter							
Thor/Delta	81 x 106	99	(a) 179	4.99	(11.0)	58.2	(22.9)
	8586	105	(b) 202				
Atlas/Centaur	84 x 108	101	(a) 193	5.76	(12.7)	52.1	(20.5)
	9072	107	(b) 213				

*Degradation is that caused by the moderate solar event described in text.

**Panel height exceeds this value when there are cutouts; see layout drawings.

4.4 SOLAR PANEL DESIGN, ANALYSIS AND PERFORMANCE

This section describes the analysis and trades involved in selecting the solar array for the Pioneer Venus mission.

Parameters of the optimum array configurations are shown in Table 4-24 for each mission. The table shows the number of series and parallel cells, array weight, array height, and the design-value power outputs near Earth and near Venus.

The solar panel outputs are predicted by computer on the basis of the Hughes solar cell model of Brown, Hodgman, and Spreen (Reference 1). In the model the outputs of single cells and arrays can be predicted on the basis of four parameters, which are: the short-circuit current, I_{sc}; the open-circuit voltage, V_{oc}; and the current and voltage at the cell maximum power point, I_{mp}, and V_{mp}, respectively.

Hardware selections for the candidate arrays are described in Table 4-25. For reasons of cost, reliability and ease of fabrication, 2 cm x 2 cm N-on-P boron-doped silicon cells were selected for the missions. For these, a tradeoff on array weight versus cell parameters indicated that 2Ω-cm, 0.2 m (8 mil) thick cells, with 0.15 mm (6 mil) thick coverglasses are the best choice to minimize array weight for all proposed missions, i.e., for the probe and orbiter in both the Thor/Delta and Atlas/Centaur versions. However, optimum array size and layout varies according to the mission.

Design Considerations

Important solar panel design considerations are summarized in Table 4-26. The panel must be designed to produce the desired power levels shown, taking into account distance from the sun, panel temperature, and radiation damage. Further losses due to fabrication transmission and system voltage drops must be considered.

Temperature

Solar panel temperature predictions are presented in Figures 4-12 thru 4-14 as a function of time from launch. These show the increasing temperature which must be considered in the design as the distance from the sun decreases.

Magnetic Cleanliness

The use of ferromagnetic materials has been avoided entirely, thus eliminating any contribution of the solar array to residual external magnetic fields. Current loops are the only other possible source of magnetic fields within the solar panel, and their fields can be minimized at the magnetometer by careful cell layout, in which the magnetic component created by

TABLE 4-25. COMPONENTS AND MATERIALS

Solar cell	Silicon, 2 x 2 cm, N/P, 2 ohm-cm .020 cm (0.008 in) thickness
Coverslide	0211 microsheet, 0.015 cm (0.006 in) thickness, ultraviolet and AR coatings
Temperature sensor	Platinum resistance, temperature range -165 + 200°C
Diode	3 A, V_F 0.8 V at 300 ma, 25°C
Connector	25 pin, 20 AWG
Solar cell adhesive	General Electric - RTV 566
Coverslide adhesive	Dow Corning - RTV 93500
Interconnect	0.005 cm (0.002 in), chem etched copper, solder plated
Bus strip	Strip copper 0.025 cm (0.010 in) thick, 1.27 cm (0.50 in) wide, solder plated

each series group of cells is very nearly cancelled by parallel, but opposite, currents in an adjoining cell group. By this means, it is anticipated that the array contribution to magnetic background will be held to an acceptable level. For example, the net uncancelled magnetic contribution of the array should be comparable to or less than that produced by a single c ell group carrying 0.3 A along 0.61 m (2 ft) of the spacecraft axis. Assuming the magnetometer to be located at least 213 cm (84 in.) from the spin axis, the observed field from such a line current would be under 5 gamma. With careful layout, it should be possible to achieve field levels substantially lower than 5 gamma.

Radiation

The primary source of solar cell degradation in the Pioneer Venus spacecraft is high energy flux from solar proton events. Except for negligibly brief periods, the spacecraft will not see the high energy trapped particles encountered in the near-Earth orbits. An estimate for a very severe solar

TABLE 4-26. SOLAR PANEL DESIGN CONSIDERATIONS

Factor	Nominal	Remarks
Temperature	Function of distance from sun and planet	At Venus Orbiter, 73.9°C Probe, 70.0°C
Solar intensity	$1/R^2$ (R in AU)	At Venus Orbiter, 1.91 Probe, 1.88
Voltage/cell, V Current/cell, A	0.460 0.1195	(Specified at maximum power point)
Ripple	1.00	
Fabrication Loss		
Voltage Current	1.00 0.967	
Transmission loss	0.98	
Angle of incidence effect	0.9619	Deviation from cosine
Diode drop, V	0.755	
Panel harness drop, V	0.345	
Radiation		
Voltage Current	0.962 0.970 0.937 0.949	Orbiter Probe Orbiter Probe
Current Ratio: I_{mp}/I_{sc}	0.927	
Voltage Ratio: V_{mp}/V_{oc}	0.800	

Table 4-26 (continued)

Required Power		
Probe (Thor/Delta)	84 138.9	W at Earth W at 107 days and Venus
Probe (Atlas/Centaur)	170	W at Venus
Orbiter (Thor/Delta)	84 168	W at Earth W at Venus
Orbiter (Atlas/Centaur)	193	W at Venus
Spectrum of moderate solar proton event (at Earth)		
Above 10 Mev:	5 (10^9) proton/cm^2	
Above 30 Mev:	2 (10^9) proton/cm^2	
Above 100 Mev:	3 (10^8) proton/cm^2	

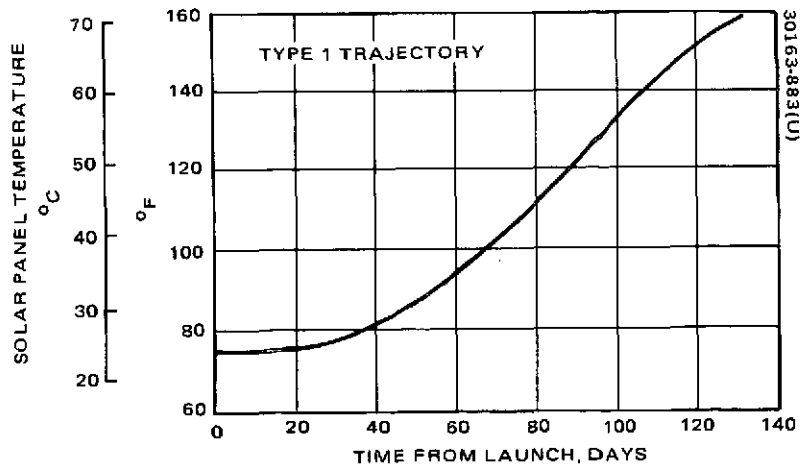

FIGURE 4-12. THOR/DELTA AND ATLAS/CENTAUR PROBE BUS SOLAR PANEL TEMPERATURE VERSUS TIME

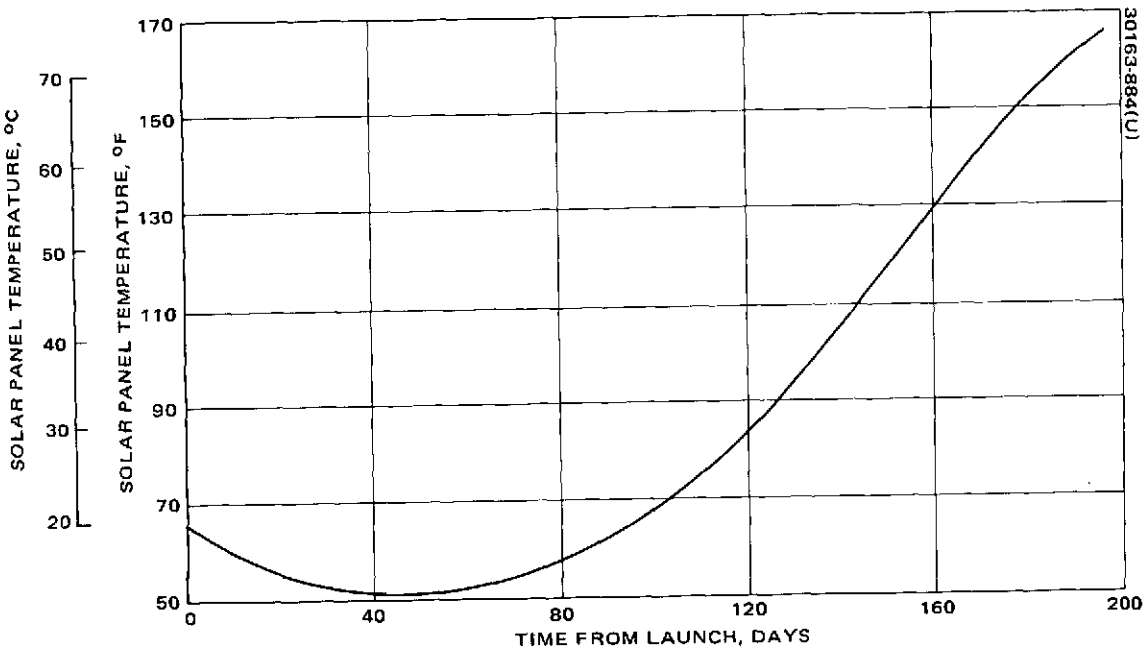

FIGURE 4-13. THOR/DELTA ORBITER SOLAR PANEL TEMPERATURE VERSUS TIME

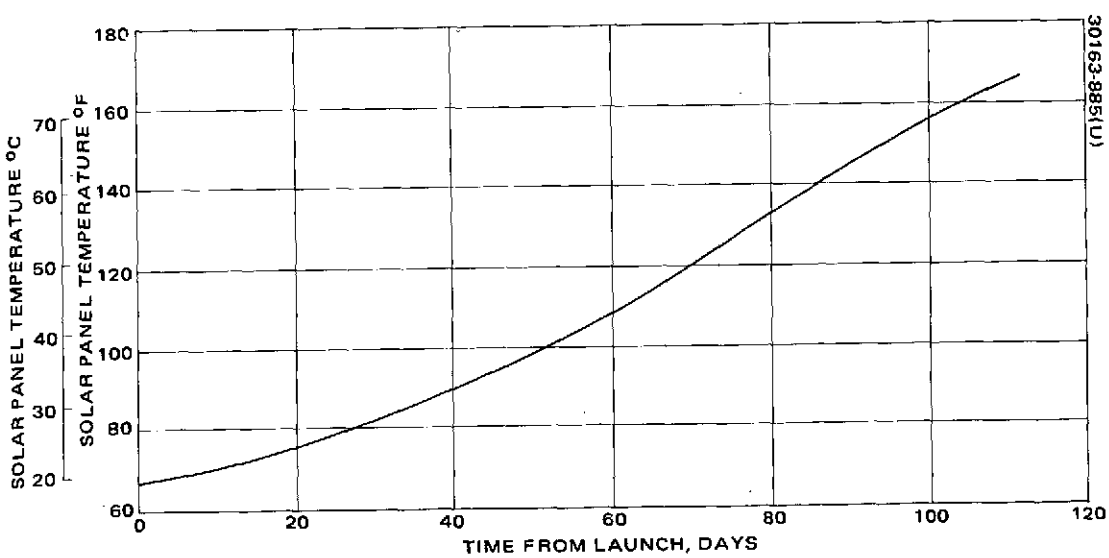

FIGURE 4-14. ATLAS/CENTAUR ORBITER SOLAR PANEL TEMPERATURE VERSUS TIME

proton event has been made in (Reference 2) and has been used in this study for comparative purposes. However, such an event is unlikely and the penalty on a lightweight solar array is so severe that it was judged impractical to design for such an event. A similar conclusion was reached by J. R. Thomas (Reference 3), in his assessment of the Mariner Venus Mercury mission radiation environment. In this study, the solar panel is designed to meet mission requirements under degradation from a moderately large solar event, which is as large as all but the few largest events of the 19th solar cycle, and which is comparable to the largest event seen in the 20th cycle. The 19th was the most severe of the observed solar cycles, and the 20th was substantially quieter. The Pioneer Venus missions will take place during the 21st cycle, which is expected to be much like the 20th. For purposes of this study, a "significant solar proton event" is one which is large enough to significantly degrade a solar panel. History indicates that only one such event is to be expected during an interval of 1 yr or less. Therefore, the moderately strong radiation assumed here provides a reasonably, high confidence, upper limit on the solar cell degradation for the Pioneer Venus missions.

Because the radiation exposure of the spacecraft may not be as great as the moderate level assumed for design purposes, the output data have been given for two cases, moderate exposure and no exposure. More detailed information is given in later paragraphs, where, for the Thor/Delta Orbiter and Probe buses, power profiles are predicted, and estimates of array performance are given for the very severe proton levels of Reference 1.

Solar Panel Circuit Design Plus Cell Selection

To minimize cost and to allow use of existing fabrication techniques, solar cell surface dimensions of 2 x 2 cm were selected for all missions. For cells of this size, existing tooling may be used for reliable fabrication of cell groups with widths of one, two or three cells, and arbitrary length. To enhance reliability and minimize assembly costs, groups that are three cells wide are presently planned for most portions of the solar panels. Since high resistance to radiation is desirable, the doping structure selected is N/P. Lithium-doped cells have been considered because they partially recover from radiation damage. However, conventional boron-doped cells have been selected for this mission because of their lower cost and more reliable quality.

Hughes is developing fabrication techniques and tooling for solar panels with 2 x 6 cm cells. These cells offer increased output per unit weight and area and are being implemented on two on-going programs. A change to 2 x 6 cm cells can be made with only minor modification of the present designs if the need arises.

The remaining important parameters of the cell optical unit are: cell thickness, cell base resistivity, and coverglass thickness. All of these

factors are related to the power output of the covered cell after exposure to radiation, and the determination of an optimum combination is chosen from a set of twelve viable design alternatives, i.e., units with 2 or 10 ohm-cm cell base resistivity, 0.021 cm (8 mil) or 0.030 cm (12 mil) cell thickness, and 0.015, 0.030, 0.051 (6, 12, or 20 mil) thick coverglass. Cell output and mass increase with cell thickness, but so does radiation damage. Increased base resistivity decreases both radiation damage and cell output. Increased coverglass thickness decreases radiation damage, but it increases weight. For this study, the optimum choice of parameters is that which minimizes array weight, substrate excluded. The choice is made on the basis of tradeoff data, which is displayed in Tables 4-27 and 4-28 for the probe and orbiter mission, respectively. The Thor/Delta versions are used for the tradeoff. To facilitate the tradeoff analysis, the arrays are sized according to criteria that are simpler than those used in the final optimum designs, which are discussed later in this section. The weights shown in the table are valid for comparison purposes, but they do not represent fully optimized array weights.

For a realistic design, the panel must be such that, at the high temperatures near Venus, the maximum power point of the output curve lies near the nominal 28 V operating point of the power subsystem. For the tradeoff, the number of series cells in the array was adjusted to put these two points as close together as possible. The number of parallel cells was then set at the minimum needed to meet mission power requirements both near Earth and near Venus. Because of its lower temperatures and lower solar intensity, the near-Earth environment actually determined this number.

Optimum Configuration

The tradeoff indicates that the 2 ohm-cm, 0.20 mm (8 mil) thick cells with 0.15 mm (6 mil) thick coverglasses are a best choice of the alternatives considered for both probe and orbiter missions. For this type of c ell, the optimum design configuration was obtained by the following steps: 1) the number of series cells was gradually reduced below that used in the tradeoff study to the point where the computer prediction of array output at Venus exceeds the requirements by the smallest possible margin; 2) if necessary, the number of series and parallel cells were adjusted further, in order to meet both Earth and Venus requirements with minimum weight; 3) finally, consideration was given to the feasibility of array layout on the spacecraft, with reasonably low ripple, and low magnetic moments. In the optimum configuration, the array parameters were changed from their weight-optimum values to the minimum degree necessary to meet these constraints on the layout. Factors used in the design of the optimum configurations have already been presented in Table 4-26. The circuit parameters of the candidate designs are given in Table 4-24.

Solar Panel Layout

The selected solar panel design for the orbiter and probe bus is cylindrical in configuration. The Thor/Delta solar array is contained on a 71 cm (28 in) long cylindrical substrate of epoxy fiberglass face sheets over

TABLE 4-27. PROBE BUS SOLAR CELL TRADEOFF

Alternate	Ohm, cm	Cell Thickness, cm (mils)	Output Parameters, V	Coverglass Thickness, cm (mils)	Number of Cells: In Series x In Parallel	Number of Cells: Total	Earth Output at 28 V, W	Mass, kg (lb)	Power at Venus, W
P-1	2	0.021 (8)	0.129, 0.575 0.1195, 0.46	0.015 (6)	83 x 87	7,221	88.6	4.20 (9.25)	157.5
P-2	2	0.021 (8)		0.030 (12)	82 x 86	7,052	89.3	5.03 (11.10)	158.3
P-3	2	0.021 (8)		0.050 (20)	81 x 84	6,804	88.3	6.07 (13.38)	156.1
P-4	2	0.030 (12)	0.136, 0.595	0.015 (6)	80 x 84	6,720	89.0	4.47 (9.86)	157.8
P-5	2	0.030 (12)	0.1269, 0.475	0.030 (12)	79 x 82	6,478	88.7	5.17 (11.39)	157.4
P-6	2	0.030 (12)		0.050 (20)	78 x 81	6,318	89.2	6.16 (13.59	157.8
P-7	10	0.021 (8)	0.129, 0.548	0.015 (6)	89 x 85	7,565	88.9	4.40 (9.69)	158.1
P-8	10	0.021 (8)		0.030 (12)	88 x 84	7,392	88.9	5.28 (11.63)	157.2
P-9	10	0.021 (8)	0.120, 0.430	0.050 (20)	87 x 83	7,221	88.4	6.43 (14.18)	155.1
P-10	10	0.030 (12)	0.1365, 0.555 0.1272, 0.445	0.015 (6)	86 x 82	7,052	89.1	4.70 (10.36)	158.1
P-11	10	0.030 (12)		0.030 (12)	85 x 80	6,800	88.4	5.43 (11.97	156.6
P-12	10	0.030 (12)		0.050 (20)	84 x 79	6,638	88.3	6.47 (14.27)	155.8

TABLE 4-28. ORBITER BUS SOLAR CELL TRADEOFF

Alternate	Ohm, cm	Cell Thickness cm (mils)	Output Parameters, V	Coverglass Thickness, cm (mils)	Number of Cells: In Series / In Parallel	Number of Cells: Total	Earth Output at 28 V, W	Mass, kg (lb)	Power at Venus, W
O-1	2	0.021 (8)	0.129, 0.575 0.1195, 0.460	0.015 (6)	85 x 106	9,010	98.8	5.23 (11.54)	191.6
O-2	2	0.021 (8)		0.030 (12)	84 x 104	8,736	99.0	6.23 (13.74)	192.1
O-3	2	0.021 (8)		0.050 (20)	83 x 103	8,549	99.7	7.61 (16.77)	193.1
O-4	2	0.030 (12)	0.136, 0.595 0.1269, 0.475	0.015 (6)	82 x 103	8,446	99.5	5.62 (12.40)	192.6
O-5	2	0.030 (12)		0.030 (12)	81 x 100	8,100	99.1	6.46 (14.25)	192.4
O-6	2	(12)		0.050 (20)	80 x 98	7,840	99.1	7.64 (16.85)	192.3
O-7	10	0.021 (8)	0.129, 0.548 0.120, 0.430	0.015 (6)	91 x 103	9,373	99.0	5.45 (12.01)	192.0
O-8	10	0.021 (8)		0.030 (12)	90 x 102	9,180	99.4	6.55 (14.44)	192.1
O-9	10	0.021 (8)		0.050 (20)	90 x 101	9,090	99.3	6.09 (17.84)	193.0
O-10	10	0.030 (12)	0.1365, 0.555 0.1272, 0.445	0.015 (6)	88 x 100	8,800	99.5	5.86 (12.92)	192.5
O-11	10	0.030 (12)		0.030 (12)	87 x 98	8,526	99.5	6.80 (15.00)	192.6
O-12	10	0.030 (12)		0.050 (20)	86 x 96	8,256	98.9	8.05 (17.74)	190.7

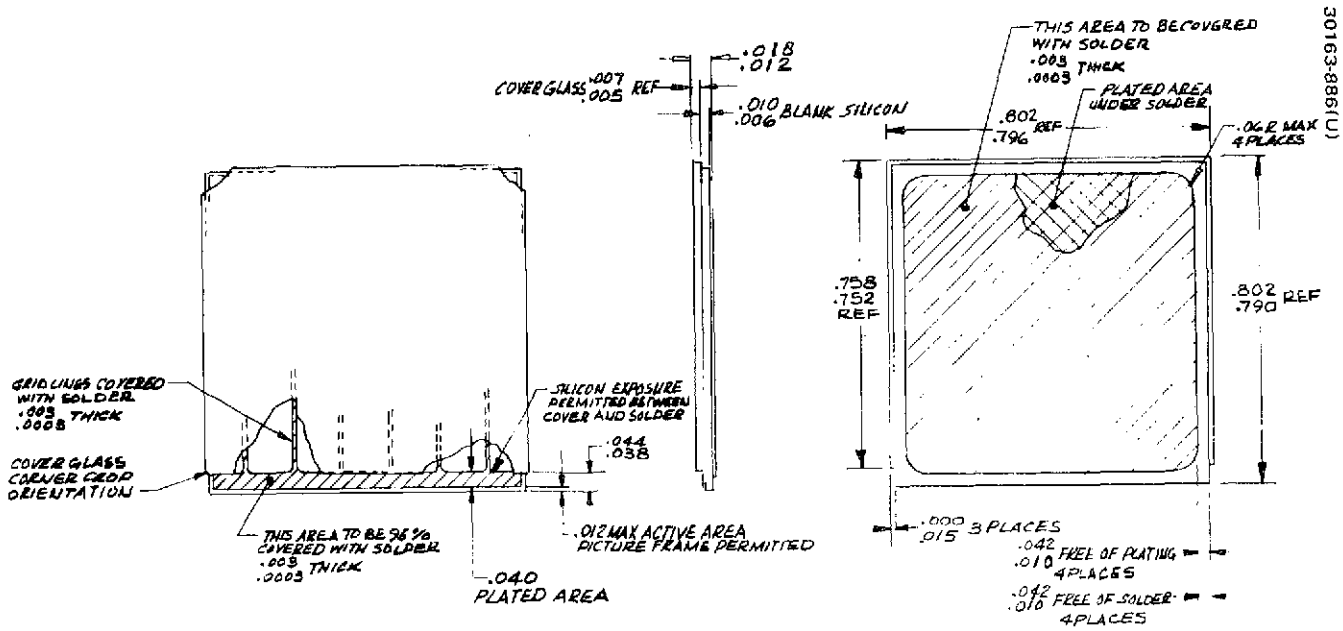

Notes -- Unless otherwise specified

1. Cell cover adhesive to be RTV 93500

2. Cell cover adhesive shall be cured at or above 65°C for 30 minutes min.

3. Cell cover adhesive shall not extend more than .005 beyond edge of cell cover

4. The average weight per lot of the assembled solar cells (including cover) shall not exceed 0.475 grams per cell

5. Solder application shall be by dip process with additional thickness control processing.

6. Cell solder weight as determined by a 200 cell sampel lot of production cells weighed before and after solder application shall be as follows:

   28 milligrams minimum per cell on the sample
   32 milligrams average, minimum for the sample
   60 milligrams average, maximum for the sample

7. 54.97 milliwatt minimum average power per lot

8. No combination of grid gaps shall exceed three percent of the total grid length

FIGURE 4-15. SOLAR CELL ASSEMBLY

aluminum honeycomb, 213 cm (84 in) in diameter. The Atlas/Centaur array is contained on a similarly constructed cylinder 254 cm (100 in) in diameter and 84 cm (33 in) long. The panel cutouts (for spinup and radial jets, sun sensor, etc.) have been minimized and many of those required have been located above the equipment shelf reducing panel penetrations.

Solar Array Construction and Component Selection

Solar panel temperature predictions (see Figures 4-12 through 4-14) indicate that present Hughes solar panel construction and processes have adequate thermal design margins; therefore, solar panel fabrication processes and techniques developed on previous Hughes satellite programs will be used to fabricate the Pioneer Venus solar panels. The use of a cylindrical aluminum honeycomb with fiberglass facesheets panel structure (substrate) is consistent with many previously flown Hughes spacecraft. The major components and materials required in the fabrication of the solar panels are shown in Table 4-25.

Solar Cell Assembly

The solar cell assembly selected for the Pioneer Venus solar panels is the type used on the Hughes FRUSA (Flexible Rolled Up Solar Array) program -- shallow diffused, N/P, 2 ohm-cm, fully soldered, and 0.0203 cm (0.008 in.) thick. The solar cell assembly is shown in Figure 4-15 and is summarized in Table 4-29. The solar cell assembly has the following significant features:

1) All titanium-silver contact areas will be solder coated to prevent degradation from humidity and radiation.

2) The Dow-Corning microsheet coverslide with antireflectant and ultraviolet coatings, will cover all active solar cell areas.

3) Dow RTV 93500 coverslide adhesive will be used.

4) Plating and solder coverage of contacts will be closely controlled and inspected.

5) Tolerances on solar cells, coverslides, and assembly have been tightened from previous industry standard designs.

6) The 0.015 cm (6 mil) coverslide thickness yields the lowest weight panel for given power.

The power output of the solar cells with coverglass applied under air mass zero spectral conditions, and solar radiation intensity of 135.3 mW/cm^2 shall meet the following requirements:

Temperature	Test Condition Voltage	Power
25 ± 2°C	0.460 ± 0.002	54.97 mW average

TABLE 4-29. SOLAR CELL ASSEMBLY

Solar cell	
Type	Silicon N/P
Size	2 x 2 cm
Thickness	0.020 cm (0.008 in.)
Base resistivity	2 ohm-cm
Contacts	Silver-titanium solder coated
Coverslide	
Material	Microsheet 0211
Thickness	0.015 cm (0.006 in.)
Coatings	Antireflective selective ultraviolet
Coverslide adhesive	RTV 93500
Power output	54.97 mw minimum average, 25°C, one sun
Weight	0.475 grams maximum

The selected solar cell configuration is identical, except for tightened tolerances, to cells currently in high volume production. The selection is therefore considered to be conservative in that the manufacturers have demonstrated the ability to fabricate and deliver similar solar cells.

Panel Construction Details

A typical cross section representative of the panel is shown in Figure 4-16. The solar cells are bonded to the substrate in cell groups consisting of three cells in parallel by the required number of cells in series with GE adhesive RTV 566. Redundant isolation diodes are utilized with each series/parallel cell group, and redundant wiring is used between all cell groups and the power bus. The exposed interconnect and wiring areas of the solar panel will be covered with an adhesive insulating material to prevent the array from showing a positive ground to the plasma, thus preventing the spacecraft chassis from developing a large negative voltage from absorbed electrons. This improves conditions for a number of experiments.

Solder-dipped solar cells with silver titanium contacts will be used on the solar panels. The solder thickness limits on the cells will be weight controlled. This has enabled a more reproducible automated array interconnection process which produces uniform fillets to the mesh, which are adequate for mechanical and electrical contact and are reliably inspectable, but which utilize a minimum of solder. No solder will be added in the process, i.e., only the existing solder on the cell and interconnect is reflowed. Wicking will only occur at the mating surface between the mesh and the cell contact, and there it will only be in the form of small fillets. Wicking will not occur beyond the cell contact area. The automated induction soldering array assembling process has produced a highly uniform and reproducible product at Hughes using these improved cells. Very little manual rework will be required. When rework is employed, no solder will be added, i.e., only existing solder will be reflowed or the cell will be replaced. By this means it is possible to eliminate solder sticking into the mesh during hand rework. Solder wicking will not be permitted by the inspection criteria and, as a final precaution, will be watched for in the 100 percent microscopic inspection of the assembled cell groups.

The interconnect design is composed of preformed, chemically etched, 0.05 mm (2 mil) copper mesh with solder plating. The solder will be controlled from 0.007 mm (0.3 mil) to 0.01 mm (7 mil) thick during the electroplating process. The configuration provides reliable redundant connections to the cell and is compatible with handling and electrical conduction requirements. The 0.005 cm (2 mil) thickness of the copper foil was chosen based on successful use of this thickness on the Intelsat IV, FRUSA, and advanced military programs. The 0.005 cm (2 mil) foil will permit a more thermally durable contact to the silicon than is achieved with thicker interconnects.

The solar cells will be segregated into discrete power ranges and will be soldered into series-parallel cell groups using the Hughes automatic

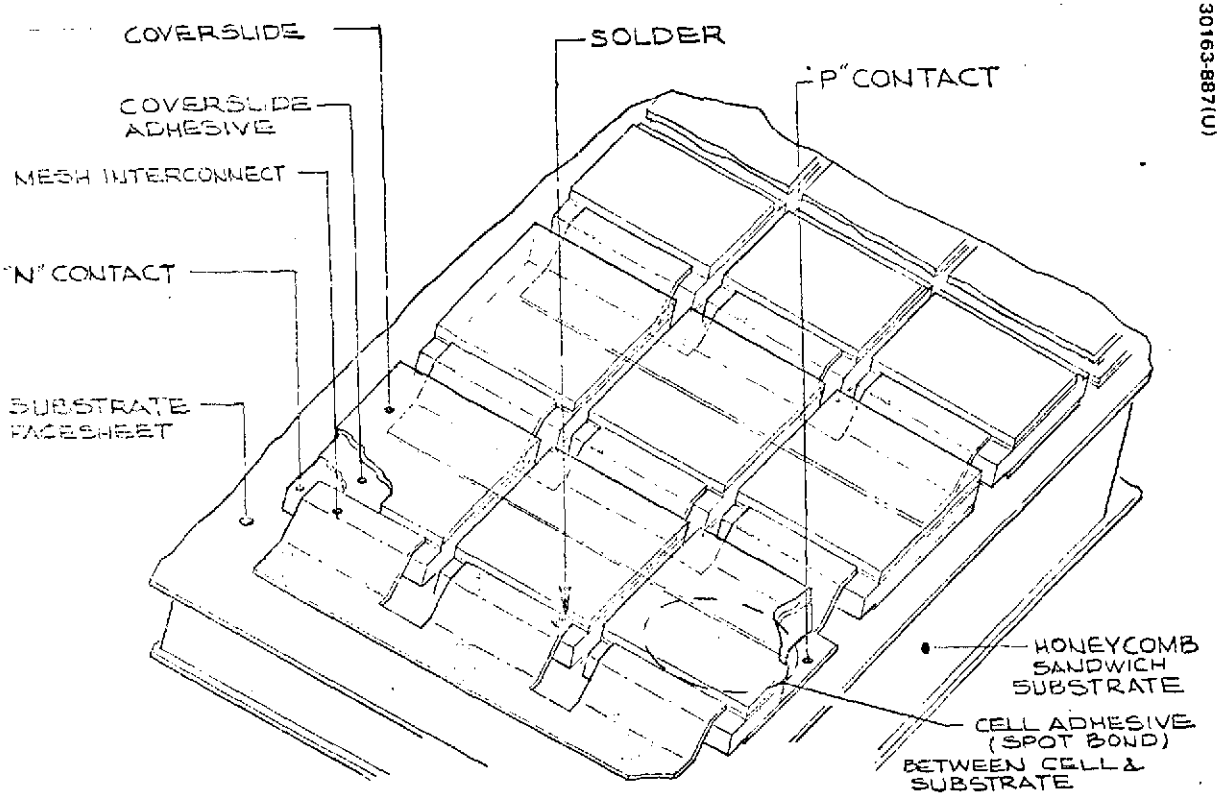

FIGURE 4-16. TYPICAL SOLAR CELL PANEL ASSEMBLY

soldering machine. After assembly, each cell group will be cleaned, electrically tested and inspected prior to delivery to project stores for subsequent bonding. Prior to the bonding operation, the substrate and bonding surface of solar cells will be cleaned and primed. The adhesive RTV 566 will be applied to the prepared cell surfaces on a weight per cell basis using an automatic application process and process controls previously developed at Hughes on other programs. A vacuum bonding fixture, containing the completed cell groups, will be properly oriented on the panel sector being bonded and a controlled pressure and temperature cure cycle initiated. Elevated temperature curing of the adhesive will be achieved through the use of electric blankets.

All solar panel fabrication processes will be performed in environmentally controlled clean rooms having limited personnel access. When fabrication is completed, the solar panels are transported to the spacecraft assembly area where the panels will again be cleaned.

Performance Predictions

For the Thor/Delta versions of the probe and orbiter, Earth to Venus power profiles are shown in Table 4-30. Two curves are given for each case, representing output without radiation exposure, and with exposure to the moderate proton event, respectively. Most probably, the array output will resemble that of the higher, no exposure, curve during the early phases of the missions, and performance will be in-between curves during the latter phases. However, since the exact size and occurrance of solar events cannot be predicted, power outputs anywhere between the two curves must be regarded as possible. Current/voltage characteristics at Earth and at Venus are shown for the Thor/Delta solar array candidates in Figure 4-17 for no radiation and moderate radiation exposure. All outputs predicted in this study assumes that the spacecraft axis is oriented normal to the incident solar rays.

In the unlikely event of a solar proton event as severe as that of Reference 2, the candidate panel outputs would fall substantially below the requirements for a completely successful mission. However, some power would still be available. For the severe flare, the current degradation factor for the candidate cells would be 0.83 for the probe bus and 0.88 for the orbiter. Different values have been used for the probe since the solar proton radiation intensity it experiences is adjusted to a sun-spacecraft distance of 0.858 AU, midway through the mission. For the orbiter, it is adjusted to 0.724 AU, the distance at Venus. For both cases, the available power output at Venus would be about 30 percent below requirements. On the other hand, a solar panel designed to meet requirements after such an event would be correspondingly heavier. Because of this heavy penalty, and the low probability of such a severe event, such a design was not deemed optimum in this study.

Alternate Orbiter Design

Near periapsis, the orbiter solar panel temperatures may rise far above the normal near Venus value of 73.9 deg C. This is due to the high

TABLE 4-30. THOR DELTA SOLAR ARRAY POWER PROFILES

Days	R(AU)	T, °C	Solar Panel Output (28 V) Power, W	
			No Solar Flares	Moderate Solar Flares
Probe bus 77 series x 90 parallel				
0	0.986	23.9	96	91
20	0.982	24.4	97	92
40	0.956	27.8	103	98
60	0.915	33.9	112	106
100	0.803	55.6	144	133
107	0.779	58.9	156	140
133	0.729	70.9	162	145
Orbiter 81 series x 106 parallel				
2	1.022	19.4	105	99
50	1.074	10.6	95	89
120	0.944	31.1	124	116
140	0.875	43.3	146	136
160	0.802	56.1	173	159
191	0.724	73.9	202	179

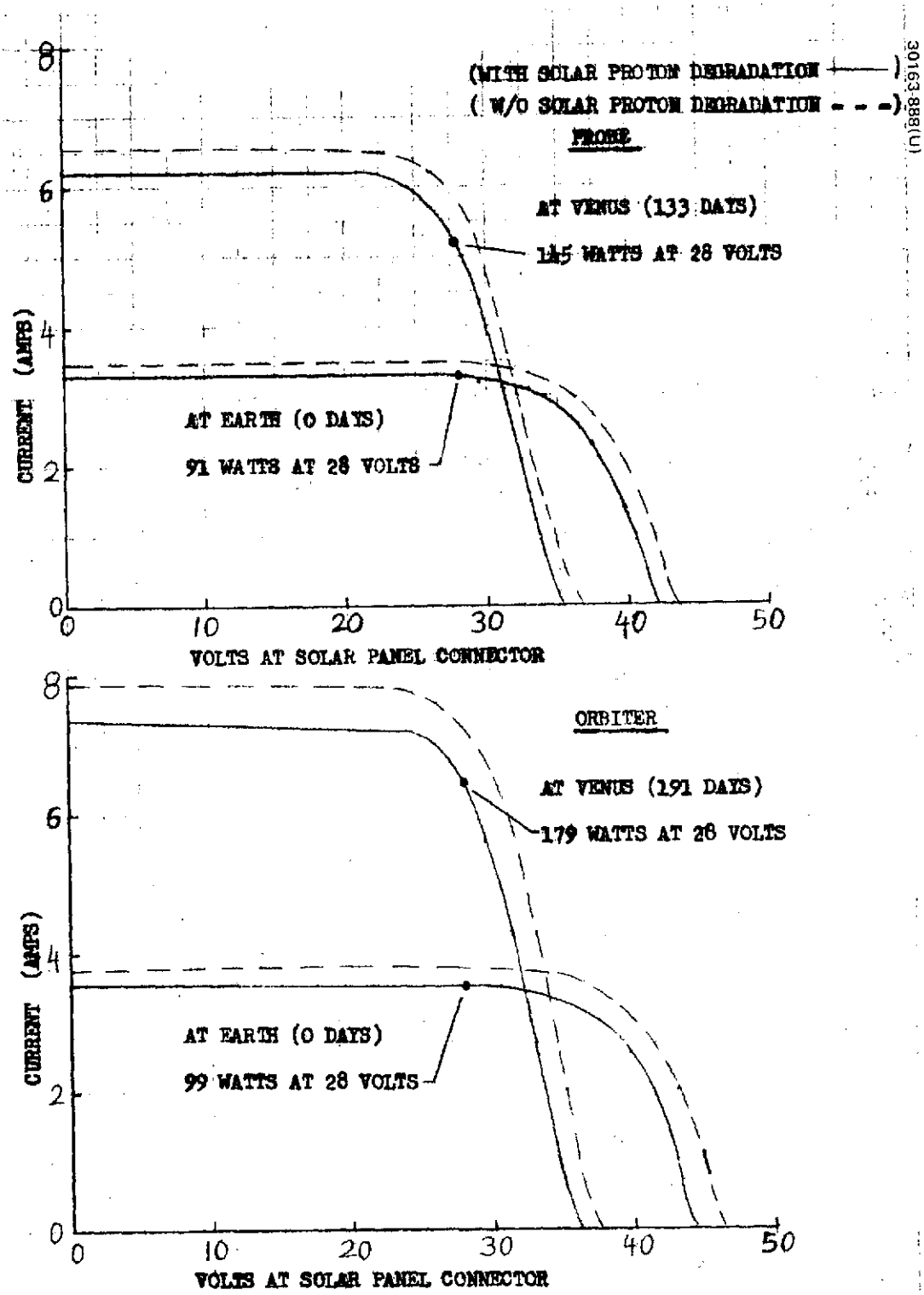

FIGURE 4-17. THOR/DELTA OUTPUT CHARACTERISTICS

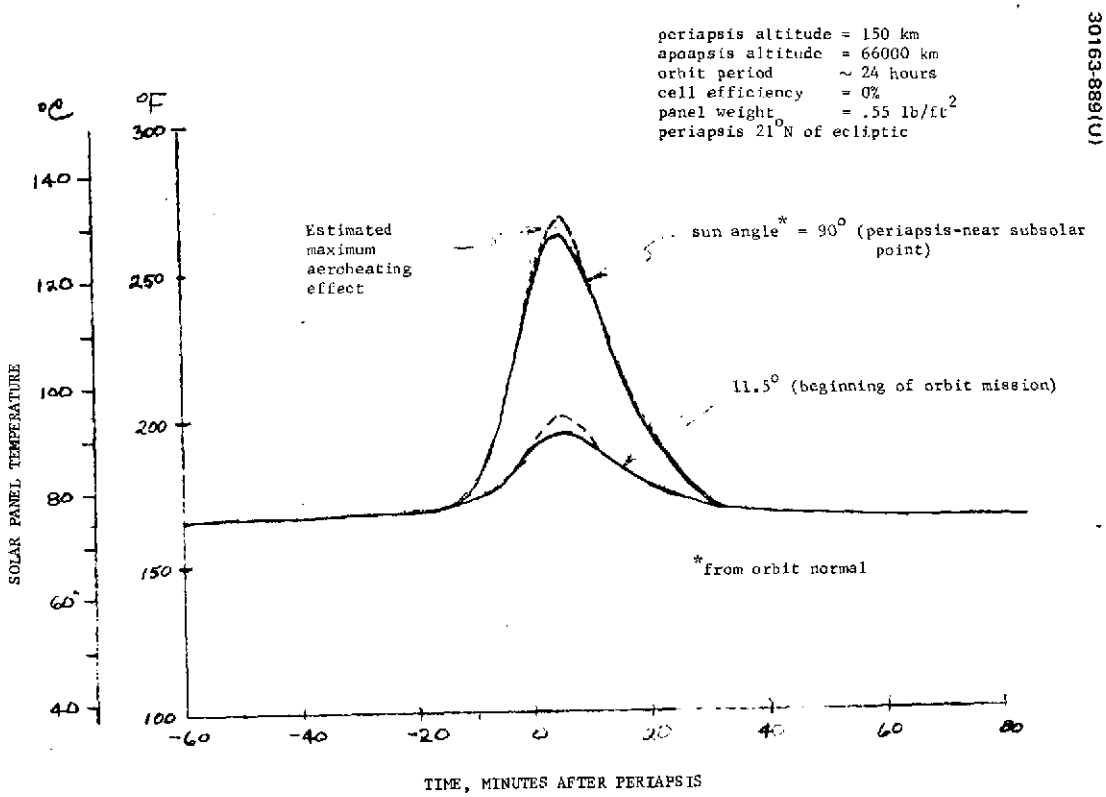

FIGURE 4-18. ORBITER SOLAR PANEL RESPONSE TO PERIAPSIS HEATING

Venus Albedo, and to aerodynamic heating at altitudes near 150 km for the orbital geometry which occurs late in the mission. The temperatures near periapsis are shown in Figure 4-18 for two cases. The lower curve applies to a 150 km periapsis after orbit insertion, when the plane of orbit is 78.5 deg away from the sun vector. The lower curve represents a worst case for the first 122 days after insertion. The higher curve represents the worst case for the entire mission; it occurs at about 178 days, when the sun vector lies in the plane of the orbit.

The candidate orbiter solar panel has not been designed to deliver full power above 74 deg C, as shown in the solid line output versus temperature curve of Figure 4-19. Consequently, some battery power must be supplied near periapsis to meet full load demands. The output predictions for the panel at periapsis indicate that the use of supplemental battery power is a workable arrangement. For comparative purposes, however, an alternative array configuration, which delivers significant power at periapsis, has also been considered. The alternative configuration has been chosen to have approximately the same weight and total number of cells as the candidate design, but the numbers of series and parallel cells are higher and lower, respectively. This increases power near periapsis, but decreases power near Earth. Of the equivalent-weight alternatives, only one meets the re requirements on cell layout while providing reasonable alternative near-Earth power outputs. That configuration has 95 cells in series x 90 cells in parallel, and it has the output versus temperature curve shown in dashed lines in Figure 4-19. Although it has advantages at high temperatures, the alternate configuration delivers only 84 watts (at 28 V) near Earth, and this is likely to prove too restrictive for mission needs. At periapsis, high temperatures of up to 125 deg C will drive the panel open-circuit voltage close to 28 V, and panel output will vary with temperature from its full value to zero. Orbiter candidate solar panel output, for the two 150 km periapses, have been plotted as a function of time in Figure 4-20. These predictions include the effects of radiation degradation. The complete current voltage characteristics at 5 min after periapsis (corresponding to the highest temperatures) are shown in Figure 4-21. They indicate that substantially more power is available at voltages below the nominal 28 V operating point.

For the alternate (95 series x 90 parallel) configuration, the periapsis outputs would be higher than those for the design candidate. Although this alternative does not appear to be a practical one, the outputs have been calculated for comparative purposes and are listed below:

Orbiter Alternate 95 x 90 Configuration Output

With radiation degradation

Near earth: 0.957 suns, 19.4°C power at 28 V = 84 W

Near venus: 1.91 suns, 73.9°C power at 28 V = 183 W

5 min after 150 km periapsis, 21 deg above ecliptic plane

At orbit insertion, orbit 78.5 deg from sun vector — power at 28 V = 185 W

Worst case, orbit 0 deg from sun vector — power at 28 V = 80 W

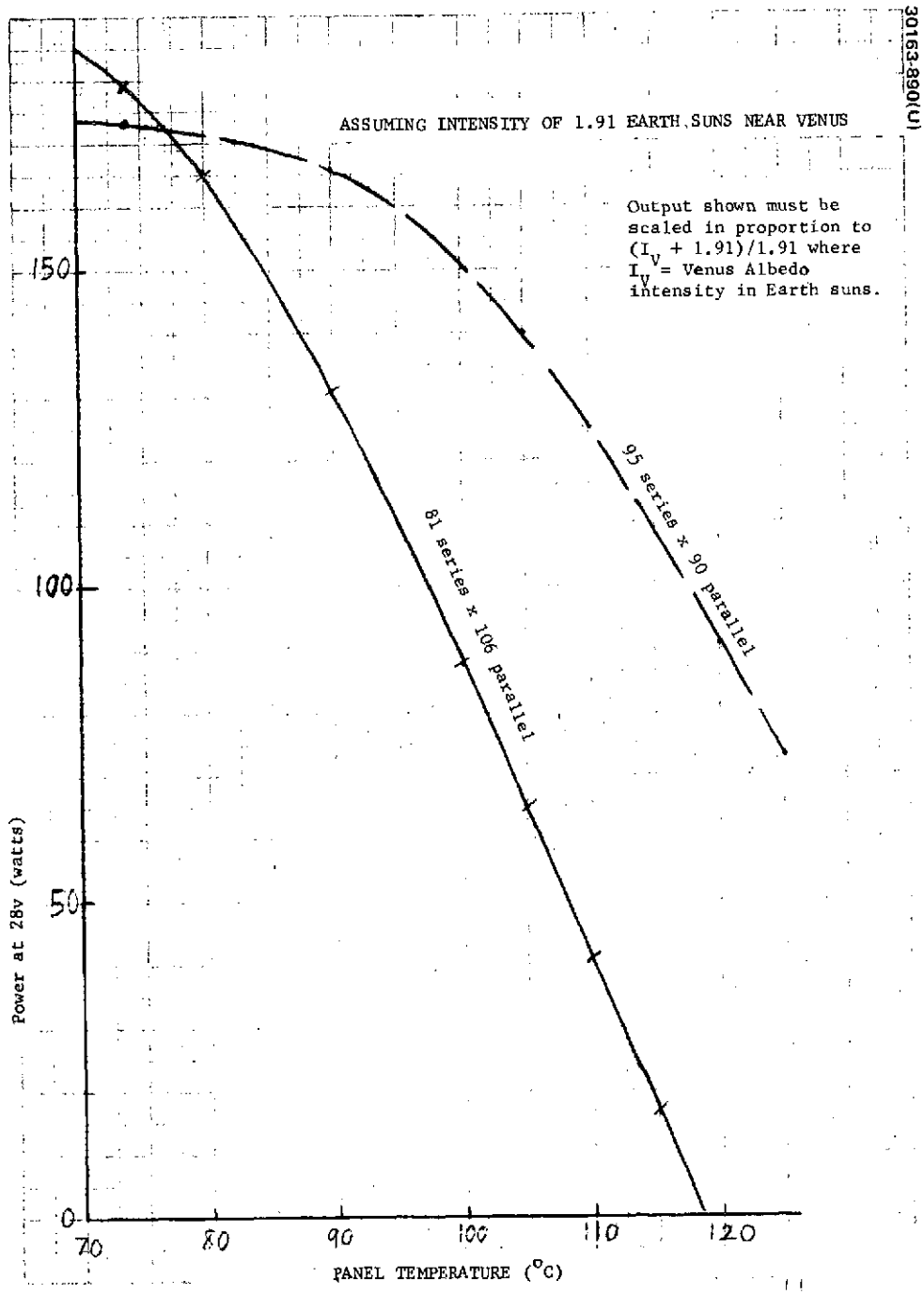

FIGURE 4-19. SOLAR ARRAY OUTPUT VERSUS TEMPERATURE

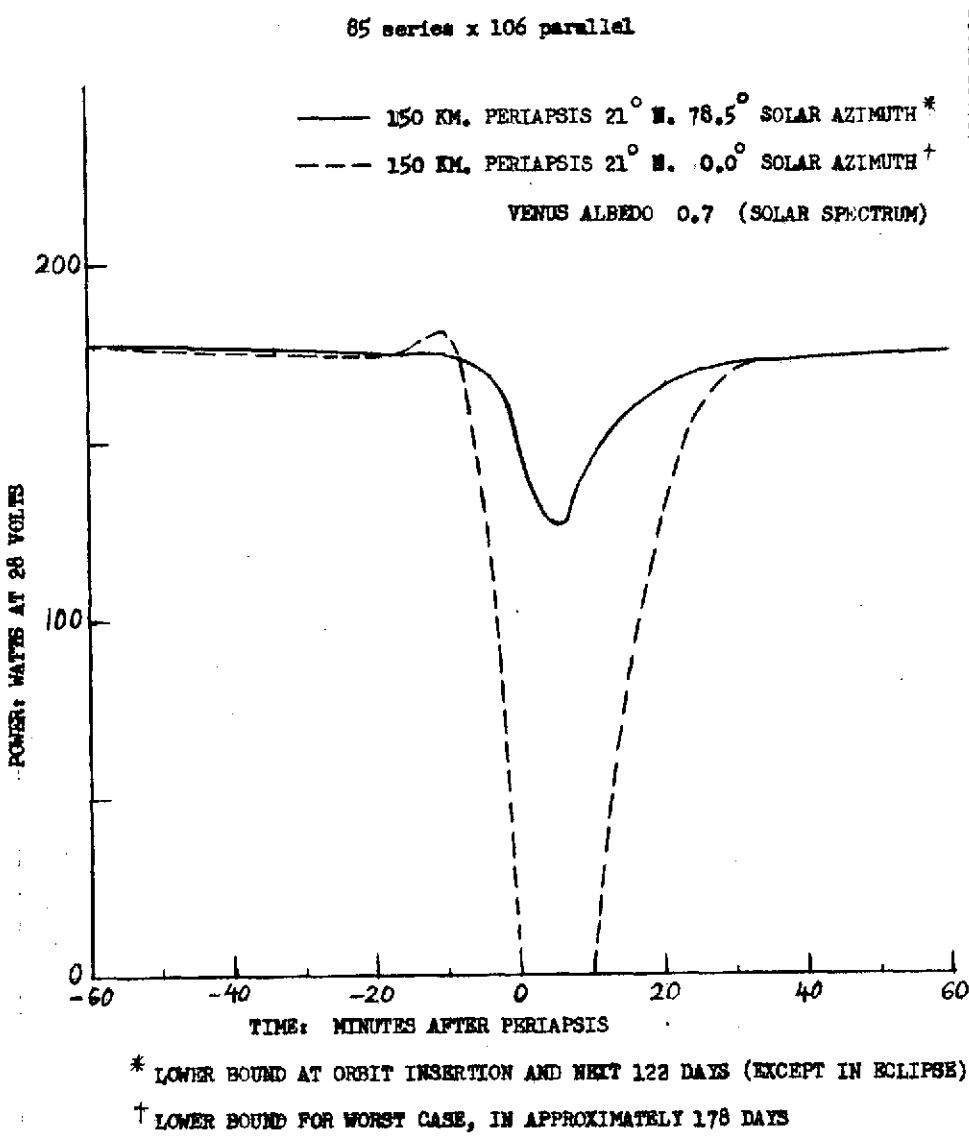

FIGURE 4-20. ORBITER SOLAR PANEL OUTPUT NEAR PERIAPSIS FOR THOR/DELTA CANDIDATE ARRAY

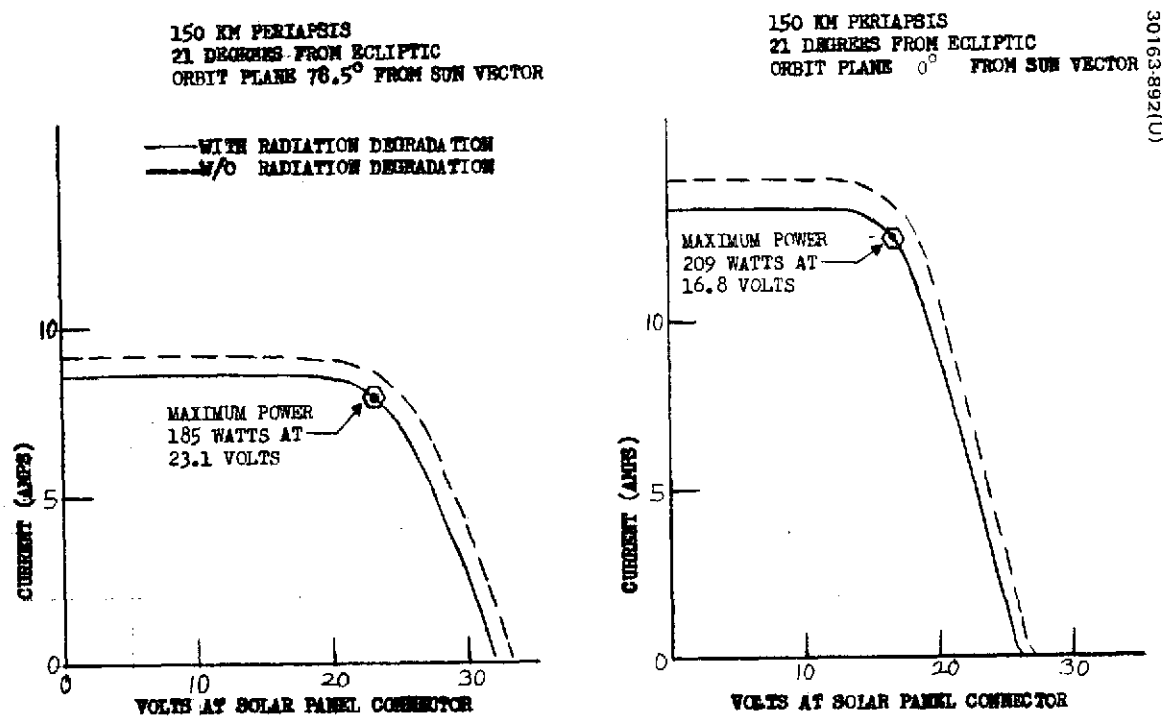

FIGURE 4-21. THOR/DELTA CANDIDATE ORBITER SOLAR PANEL OUTPUT AT PERIAPSIS +5 MIN

4.5 POWER ELECTRONICS DESIGN

This section discusses the electronics design of the power subsystem as it existed at the midterm review. The designs presented herein for the Thor/Delta and Atlas/Centaur are based on existing hardware in most instances. The Atlas/Centaur baseline relies heavily on OSO-I derived equipment. A new design for the probe bus battery charger is used for the large and small probe silver-zinc batteries. Power switching for the experiments is incorporated in a newly designed power interface unit on the probe bus and probes. Redundancy in some of the units on the Atlas/Centaur spacecraft has resulted in a slightly heavier power subsystem when compared with the Thor/Delta design. Dual batteries with individual charge/discharge controllers have been incorporated into the Atlas/Centaur design.

The Thor/Delta design does not have unit redundancy and requires more development engineering to achieve the same reliability and low weight required of the subsystem. A single battery and associated boost-add-on discharge regulator is used on the Thor/Delta spacecraft desigh. The boost regulator is derived from an existing design, although some redesign is required to achieve low weight and higher efficiency. The requirements of the high g environment of the large and small probes are satisfied by proper packaging design. This study did not investigate the packaging techniques in detail, but a cursory review of present schemes and techniques shows no major problems exist.

The following sections give a functional description of each power electronics unit comprising the power subsystems for the Thor/Delta and Atlas/Centaur. The physical design of each unit will employ the standard guidelines utilized on previous Hughes spacecraft with deviations from standard practice where necessary to assure a reliable design. All components will be packaged in aluminum chassis with the higher heat dissipative components (power transistors, diodes, etc.) mounted directly on the housing to provide a low thermal impedance to the mounting surface. Lower power dissipating components will be mounted on printed circuit boards with a heat aonducting epoxy to provide the required thermal path for conduction to the housing and mating surface. All soldering will be performed to NASA standards. Relays and other vibration sensitive elements will be mounted with the least sensitive axis in the plane of high vibration or g loading. After testing, the components will be encapsulated with a lightweight polyurethane foam to ensure mechanical integrity during exposure to the high vibration environment during launch and Venus entry.

Bus Voltage Limiter

The bus limiter design is common to both Thor/Delta and Atlas/Centaur. It limits the maximum voltage on the unregulated bus during any transient period such as emergence from solar eclipse or when the spacecraft load is light. A set of three and four limiters for the probe and orbiter buses,

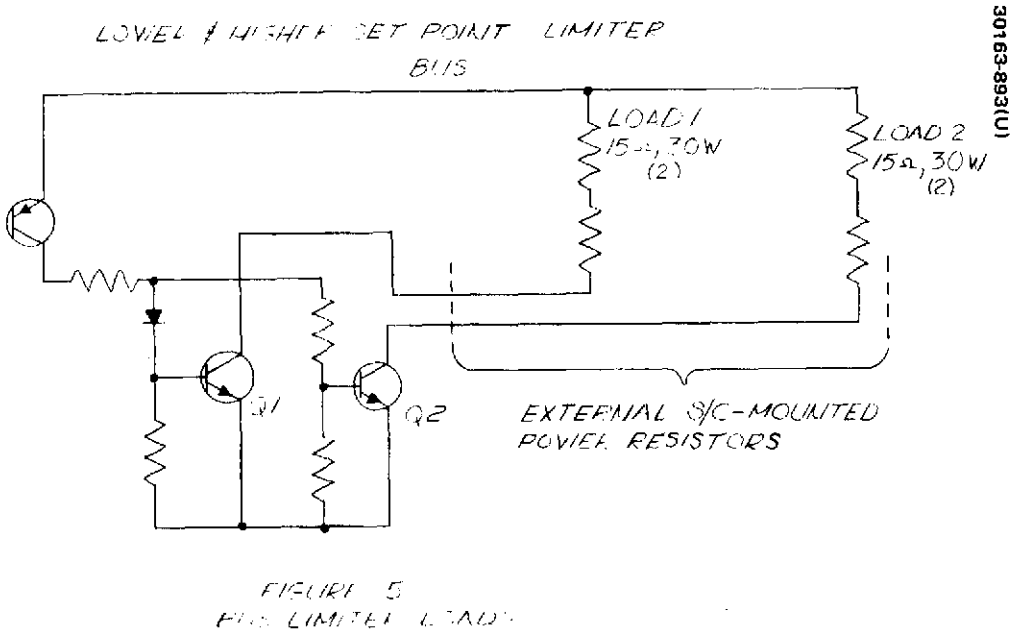

FIGURE 5
BUS LIMITER LOADS

FIGURE 4-22. BUS LIMITER LOADS

respectively, are located in each spacecraft and each limiter has remotely located power resistors. The power resistors are distributed in the spacecraft to optimize the thermal design. The bus limiters present only standby losses while the bus is less than 32.6 V and present maximum loading at 33.0 V. Each limiter and its load resistors dissipate 66 W minimum at 33 V. Maximum power dissipation in the electronics portion of each limiter assembly is 11.8 W.

The three limiters for the probe bus and four limiters on the orbiter are divided into two groups with setpoints of each group being separated by approximately 200 mV (32.7 + 0.1 and 32.9 + 0.1 Vdc) to prevent overlap. The lower setpoint limiters are designed to operate early in the life of the mission. The remaining (higher setpoint) limiter(s) will not operate or turn on unless several of the loads are turned off.

Two sets of load resistors are included with each limiter to facilitate heat dissipation as shown in Figure 4-22. Both sets of limiters are designed to operate within 200 mV of the 400 mV range illustrated in Figure 4-23. Two power resistors are included in the design with staggered turnon. Transistors Q1 and Q2 have offset drive currents to prevent both transistors from operating at peak power level simultaneously. Controlled staggering decreases the dissipation internal to the bus limiter by approximately 50 percent. This effect is depicted in Figure 4-24. The performance and operating characteristics of the limiters are given in Table 4-31.

Each limiter consists of a magnetic latching relay, voltage sensing amplifier, with a reference, driver, and power transistors which shunt current through resistors to ground.

The bus limiter requires an additional command input (enable backup) which is used to assure that at least two of four limiters are on at all times. R1, CR3, and CR4 provide the added inputs. Limiters are commanded on in pairs. When one is commanded off its mate is commanded on and vice versa. The implementation of this is shown in Figure 4-25.

Nickel-Cadmium Battery Charger

The battery charger shown in Figure 4-26 is used to charge the nickel-cadmium battery on both the Thor/Delta and Atlas/Centaur spacecraft. Battery charging is accomplished by a scheme that provides an unlimited charge current until the bus voltage reaches a temperature-biased preset battery voltage value, then the charge current tapers to a trickle current. A brief summary of the charge controller characteristics is presented in Table 4-32. This includes functions, power requirements and physical parameters. Some of the important aspects of the charge controller in relation to battery charge currents and other load currents such as the spacecraft load current and bus limiter currents are discussed below.

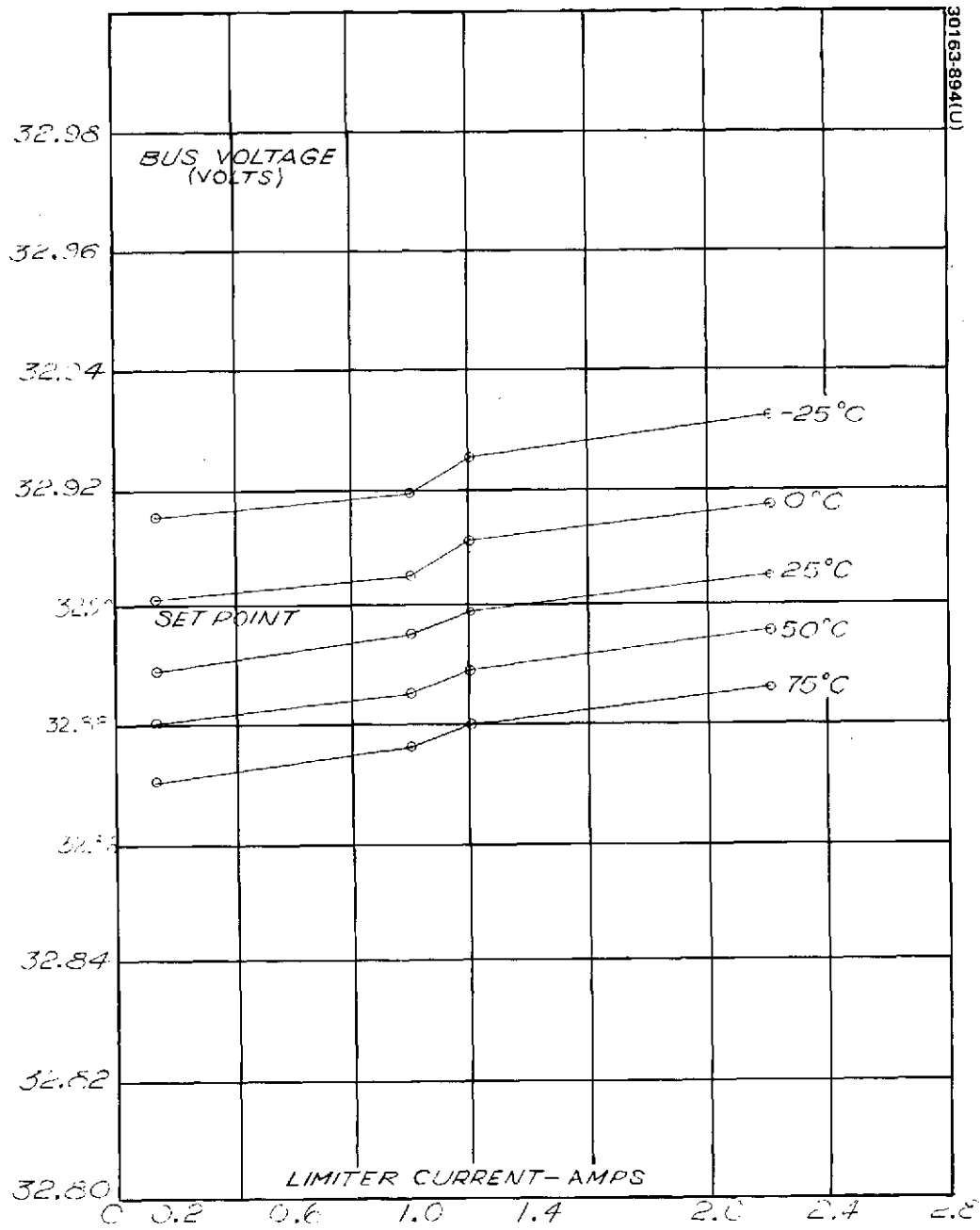

FIGURE 4-23. BUS LIMITER OPERATING RANGE OF UPPER LEVEL

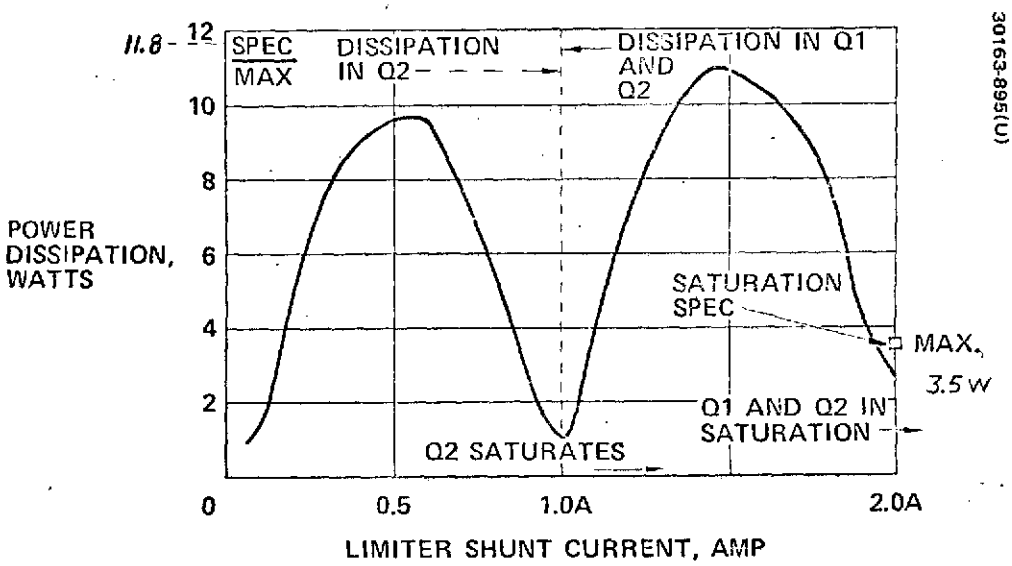

FIGURE 4-24. BUS LIMITER INTERNAL POWER DISSIPATION

TABLE 4-31. SUMMARY OF BUS LIMITER CHARACTERISTICS

Number of limiters required:	Three units for the probe bus Four units for the orbiter bus
Voltage limit range:	32.6 to 33.0 V
Set points:	32.7 and 32.9 V
Power dissipation per limiter:	
Standby:	0.3 W at 23.0 to 32.0 V input
Saturation:	3.5 W at bus 33 V
Limiting:	66.0 W minimum at 33 V bus, including load resistor dissipation (two 1.0 A loads per limiter)
Command capability	
Turn ON/OFF:	Relay contacts
Telemetry:	Relay status Transistor voltage (derive load currents)
Limiter size:	
Volumetric	Height: 5.33 cm (2.10 in.) Width: 6.35 cm (2.50 in.) Length: 9.53 cm (3.75 in.)
Load resistors:	Four each 15 and 30 W; 0.56 x 0.62 x 1.91 exclusive of terminals and mounting tables and 0.24 kg (0.53 pound) per set
Mass (total):	0.39 kg (0.85 pound) per limiter plus 0.63 kg (1.38 pound) total per limiter, 0.24 kg (0.53 pound) resistors

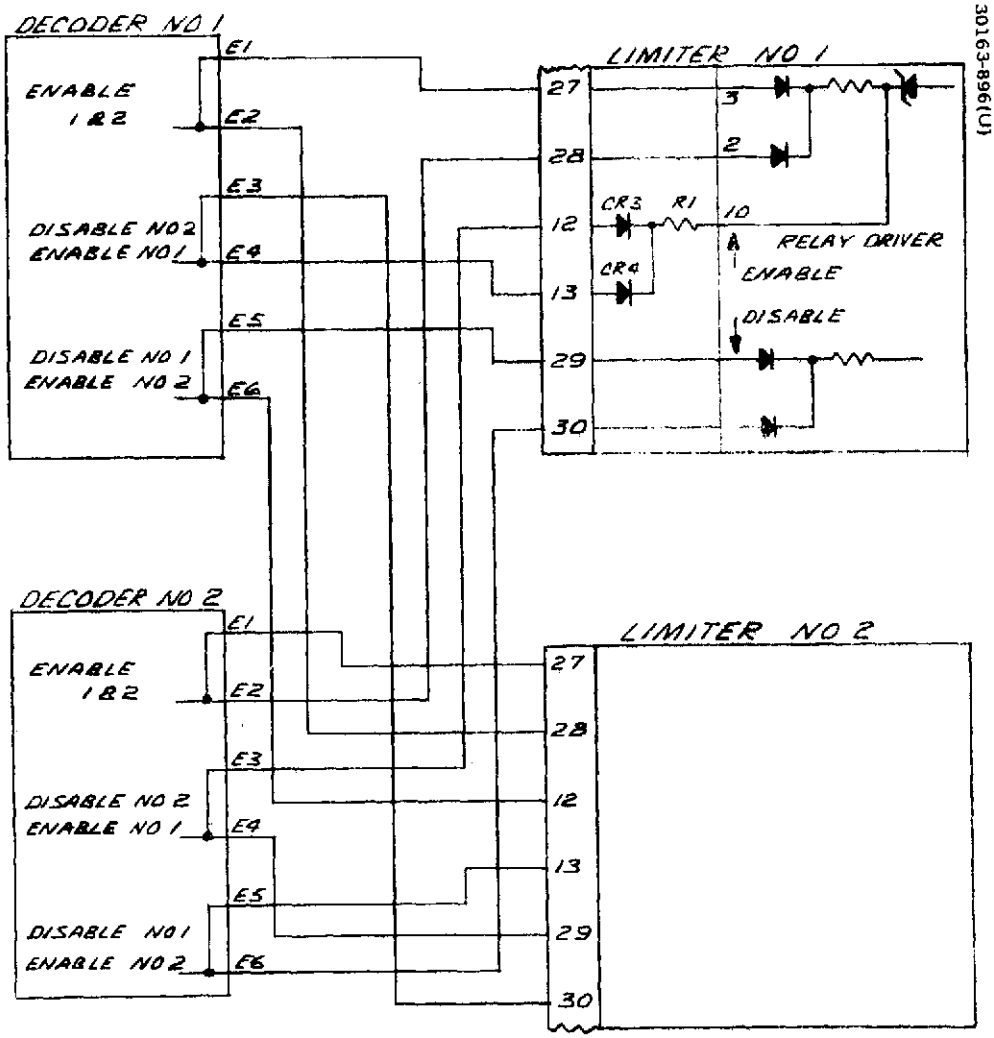

FIGURE 4-25. BUS LIMITER COMMAND INTERFACE CONNECTIONS

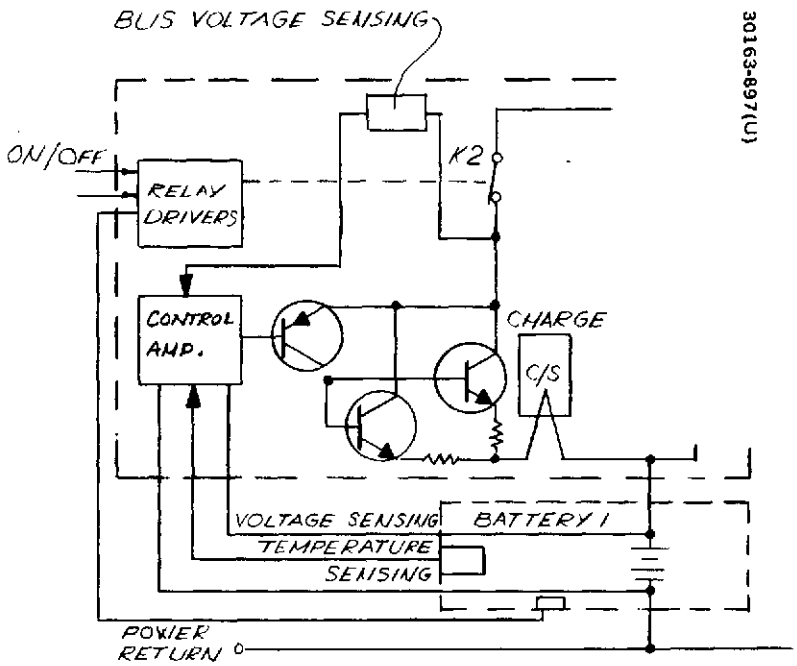

FIGURE 4-26. BATTERY CHARGER

TABLE 4-32. ORBITER BATTERY CHARGER CHARACTERISTICS

Charge control:

Maximum charge current:	8.0 A capacity
Power dissipation:	Shunt: 3 W Series: 75.0 W at 3 A

Command requirements:

- Battery charge enable (over temperature override)
- Battery charge disable

Charge control:

- Automatic charge termination
- Overtemp termination

Command control:

- Charge control level selection
- Charge enable/disable

Telemetry:

- Relay status (5)
- Charge current
- Battery voltage

Size:

Height:	6.35 cm (2.5 in.)
Width:	11.68 cm (4.6 in.)
Length:	15.75 cm (6.2 in.)

Mass:

1.2 kg (2.7 pound) $\pm$ 0.3 kg (0.06 pound)

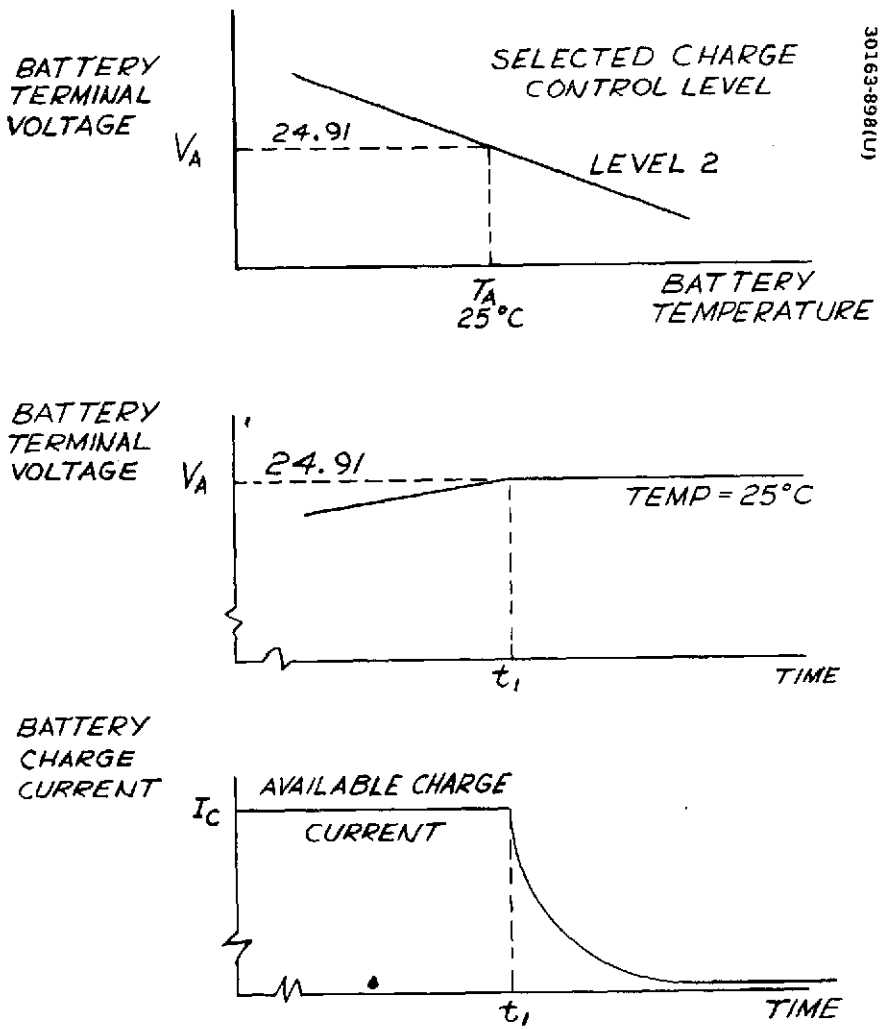

FIGURE 4-27. SELECTED CHARGE CONTROL LEVEL

In order to utilize all of the available current, the charge control circuit will have an "uncontrolled" charge mode which can be initiated upon exiting eclipse and can exist until the battery voltage rises to a predetermined level (i.e., bus voltage is greater than 27.27 V) (See Figure 4-27). When this occurs, battery charging will be changed to a constant voltage mode, with the charge current tapering off to a trickle charge rate at this voltage. Eight charge control constant voltage mode levels may be selected by command. The eight charge levels are preselected by command actuated relays. Three double pole relays are utilized to provide $2^3 = 8$ charge control levels. One pole is dedicated to level selection and the other to provide a telemetry status signal indicating relay position.

Silver-Zinc Battery Charger

The charger proposed for the silver-zinc batteries on the Thor/Delta and Atlas/Centaur limit at 0.4 ± 0.1 A at a regulated voltage of 1.93 ± 0.01 V/cell. The charge current begins to taper to a trickle once the battery terminal voltage reaches the regulated potential to a final level of 2 to 10 A. As shown in the functional block diagram of Figure 4-28 the charger assembly contains five identical charging circuits with current sensor and a large and small probe checkout bus implemented with relays. Each probe can be sequentially selected for either battery charging or powered for checkout. All selectable functions are ground commanded via the on-board command generator.

Battery Discharge Regulator

The battery discharge regulator utilized on the Thor/Delta spacecraft is of the boost-add-on type. The regulator functions to condition the battery terminal voltage to an acceptable level for application to using subsystems under all conditions of load variations. The design selected for use is electrically identical to the battery controller presently being used on a classified program. Minor design changes will be performed to facilitate accommodation of the lower power levels required. The thermal design of the regulator will allow high power dissipation with a minimum weight penalty. A summary description of the regulator performance characteristics and operational modes is given in Table 4-33. A block diagram of the regulator is shown in Figure 4-29.

Current Sensor

The current sensor used on the Thor/Delta and Atlas/Centaur employs a transductor with a full scale sensitivity of 18 At. The characteristics of the current sensor are given in Table 4-34. The transductor current sensor circuit described here is also used in the battery charge and discharge regulator to sense control and charge current and to provide charge and discharge current telemetry signals. Current sensors are also used to monitor the solar panel current, experiment currents, and bus limiter currents.

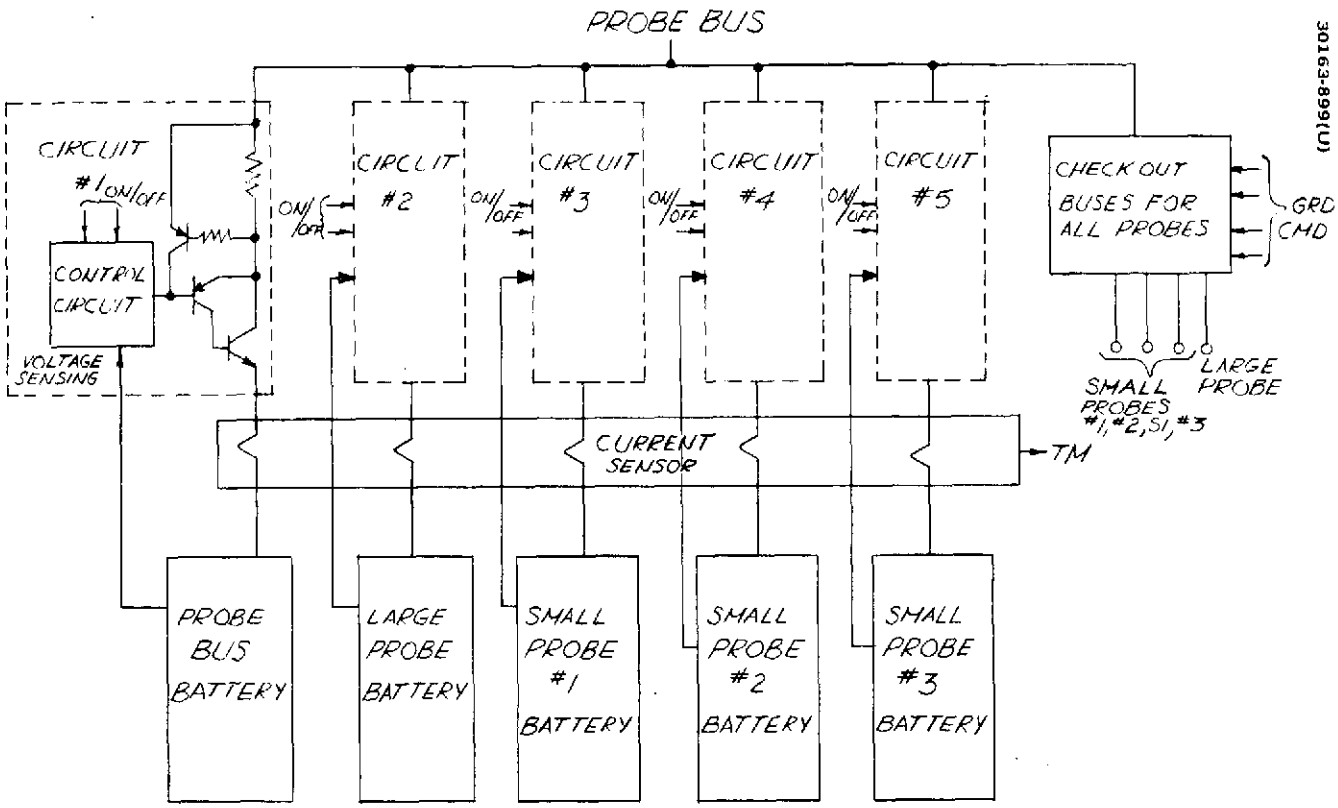

FIGURE 4-28. BATTERY CHARGER FUNCTIONAL BLOCK DIAGRAM

TABLE 4-33 DISCHARGE REGULATOR PERFORMANCE CHARACTERISTICS

Input Voltage (battery voltage)	14.3 to 24.3 V
Output voltage (bus)	26.5 to 27.85 V Full load to no load
Power - Nominal Maximum	175 W 222 W
Unit size	7.6 x 12.7 x 20.3 (m (3.0 x 5.0 x 8.0)
Unit mass	2.7 kg (6.0 lb)
Efficiency	85 percent at full load
Command interface Requirement	Regulator inhibit ON Regulator inhibit OFF

TABLE 4-34. CURRENT SENSOR CHARACTERISTICS

Maximum power dissipation: 0.4 W - 23.0 to 33.0 V

Telemetry requirements: Input current range - 0 to 15 amps

	Height	Width	Length
Size:	4.67 cm (1.84 in.)	3.66 cm (1.44 in.)	6.58 cm (2.59 in.)
Mounting surface:		15.7 cm^2 (2.44 $in.^2$)	16.7 cm^2 (2.59 $in.^2$)
Mass:		0.14 kg (0.30 lb)	

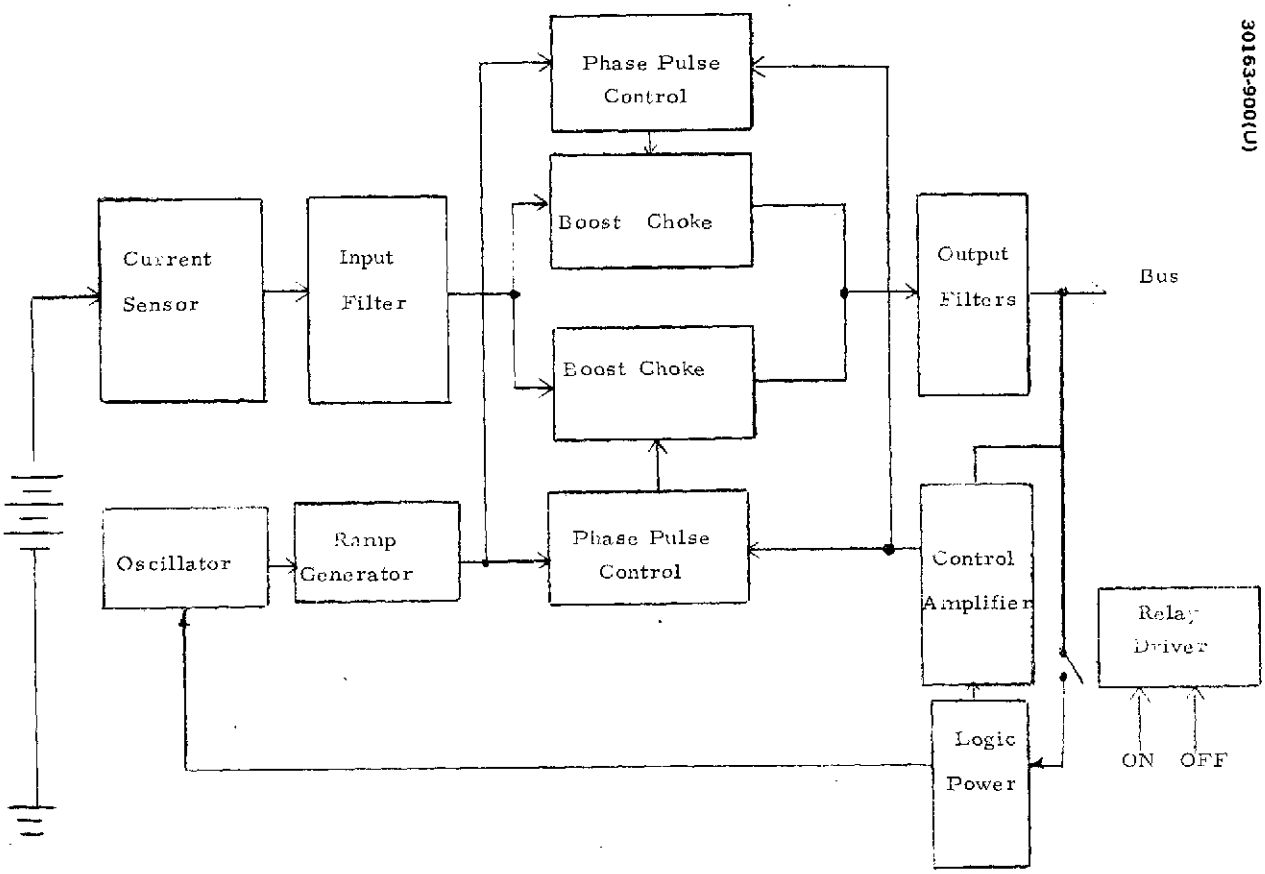

30163-900(U)

FIGURE 4-29. THOR/DELTA BATTERY DISCHARGE REGULATOR BLOCK DIAGRAM

The basic sensor is a magnetic transductor consisting of two saturable cores with a common sense winding linking both cores. When one core is saturated on one-half cycle, the other core is unsaturated, such that following unsaturated transformer theory, $N_pI_p = N_sI_s$, or $I_p = N_sI_s/Np$, and $E_o = N_sRI_s/N_g$ for R_L 100, providing that (NI) exciting is $N_s I_s$, which is true for a small nickel iron core. Referring to Figure 4-30, RL is the telemetry load resistance and R is the terminating resistance (R8 and R9 in parallel). The transducer excitation is provided by a small two transistor square wave inverter. The inverter circuit chosen is a Royer saturable magnetic design containing one transformer with only one secondary winding to excite the transducer.

The transductor can monitor current in either the positive supply line or in the negative return of the solar panel. The sense wires are threaded through an access port in the current sensor and the magnetic sensor within. There is no loss of accuracy due to common mode voltages which can contribute to inaccuracies when op amp circuits must be used, and the power (voltage) drop is less because a shunt resistor is not required. The output of the transductor has the additional advantages of lower complexity, higher reliability and its unsusceptibility to latch up. The output error is less than 2 percent (of full scale).

Fuses are used in the current sensor for failure protection. The redundant fuse uses a 51 ohm series resistor to ensure that the primary fuse passes the majority of the current. The fuse resistance at rated current is approximately six ohms, maximum. Redundant series capacitors provide EMI filtering between the input line and the chassis.

Overload Control Unit

In the orbiter bus on both the Thor/Delta and Atlas/Centaur, an overload control unit is under consideration to protect the power bus when an experiment or spacecraft load fails.

A block diagram of an overload control unit is shown in Figure 4-31. Relay K_1 can select a redundant overload control circuit, and relays K_2 through K_7 provide the capability to switch power to six outputs. The ability to turn the unit ON and OFF by command is provided.

The overload control operates in a saturated mode for any input voltage (23 to 33 V) as long as the output current is less than the limit current, 3.0 ±0.8 A. Overload control is designed to limit current 3.0 ±0.8 A and interrupt power when the output falls due to current limiting. A voltage comparator compares the input output voltages. When the output voltage falls five volts below the input voltage due to current limiting, a transistor switch is turned OFF. To reapply power, an ON command must be received by the overload control. To prevent simultaneous application of power to all outputs, the individual relays K_2 through K_7 may be opened prior to restoring bus power.

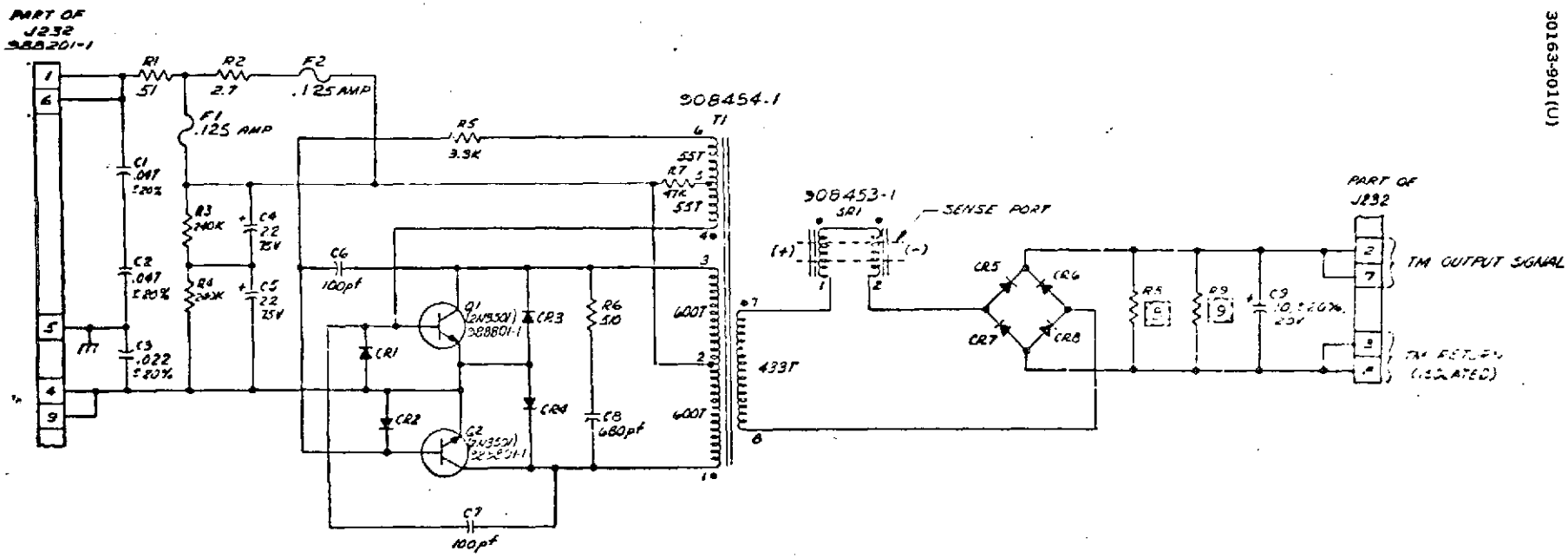

FIGURE 4-30. CURRENT SENSOR SCHEMATIC DIAGRAM

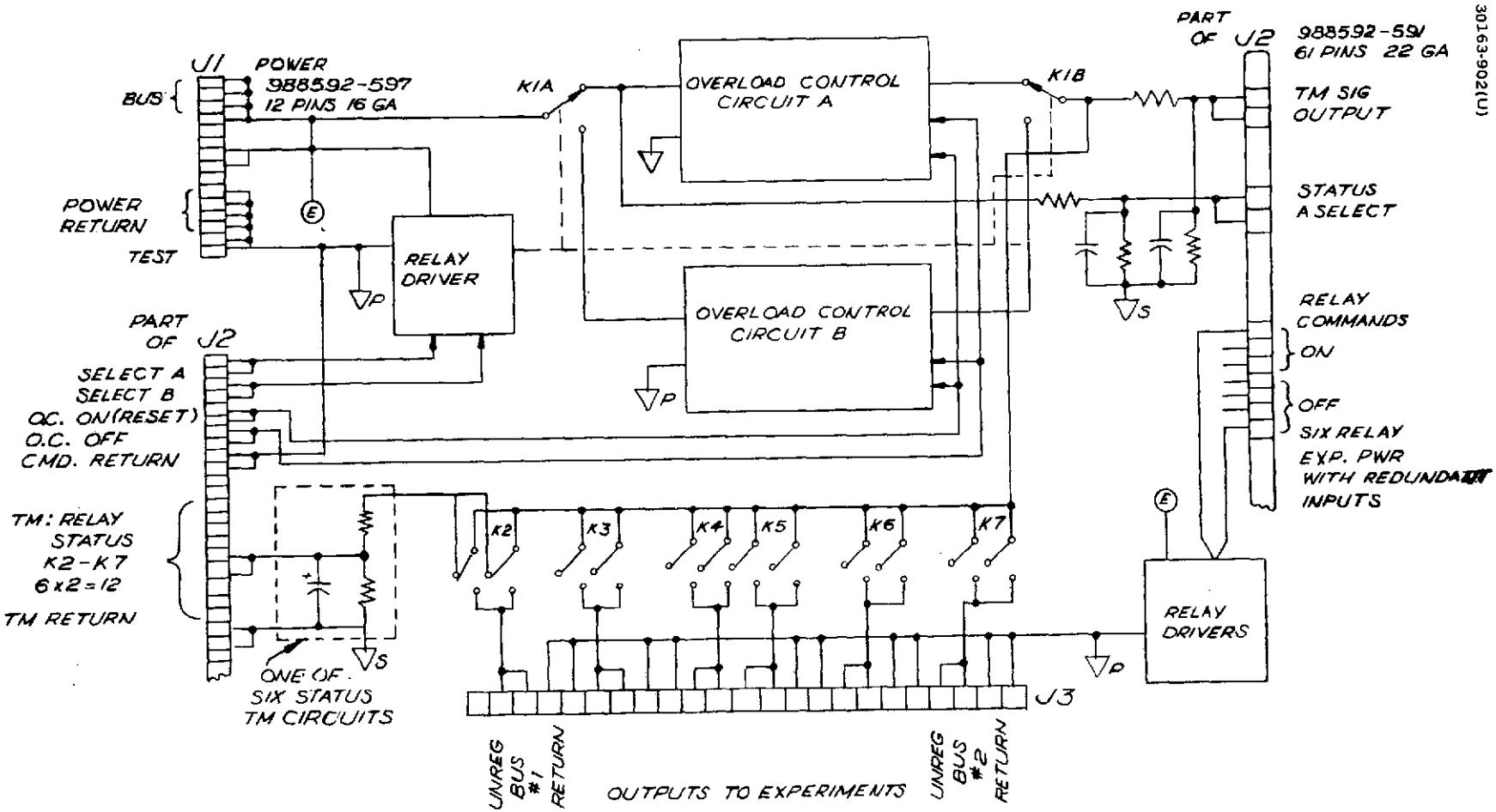

FIGURE 4-31. OVERLOAD CONTROL UNIT

Power Interface Unit

There are two types of power interface units, presently planned for use on the large probe, small probe and probe bus. The power interface unit 1 will contain five small relays and three large relays, and their associated command circuits.

The power interface 2 will contain two large relays, three small relays, and their associated command circuits (see Table 4-35).

The switches are controlled by ground station commands. They are each driven by individual command circuits. Each switch is protected by redundant fuses (see Figures 4-32 through 4-35).

Heater Control

The heater control, which is energized by ground command, provides ON and OFF control of power for spacecraft heaters.

Each heater control unit contains two separate circuits for control of two separate heaters. Input bus power for each circuit is redundantly fused, and each circuit contains its own command buffer/relay driver. Each heater carries a maximum of 240 mA at 33.0 V. Table 4-36 summarizes the unit characteristics.

The heater control is used to control the spacecraft heater system. The function of the control is to connect and disconnect power to the spacecraft heaters by ground command.

The commands are received by a command buffer and relay driver composed of Q1-Q4 in Figure 4-36. Q3 and Q4 turn the relay on. Q1 and Q2 turn the relay off. The relays are the magnetic latching type; hence relay coil power is supplied for only the duration of the command pulse.

The input commands may have a variation in amplitude between 4 and 15 V and still be accepted by the command buffer. Fifteen volt pulses of up to 100 Msec will not cause the command to be executed. The low pass filter of R12, R11, and C6 allows the short pulses to be ignored. VR2 and the gating diodes CR13 and CR14 give a noise immunity level capability in excess of 3 V. When a proper (ON) command is given, Q4 will be turned ON and draw base current from Q3 through R7. R9 and C4 provide a noise immunity level for Q3. As Q3 turns ON, coil power is delivered through CR8 to one of the coils in the magnetic latching relay, K1. CR9 and CR10 suppress the voltage spike from the relay coil inductance at the end of the command pulse. C5 and R10 form a command pulse stretching network to assure relay transfer. The relay contacts are connected in series to satisfy the maximum voltage requirement. The redundant fuses are provided for short protection. The circuit is similar to the previously qualified Telesat heater control.

TABLE 4-35. POWER INTERFACE UNIT PERFORMANCE CHARACTERISTICS

Relay (Hughes P/N 908325), rating 10 A at 28 V	
Relay (Hughes P/N 908305), rating 0.5 A at 28 V	
Unit size:	Power interface unit 1 (large probe), 3.8 x 10.2 x 15.2 cm (1.5 x 4.0 x 6.0 in.)
	Power interface unit 2 (small probe), 3.8 x 10.2 x 10.2 cm (1.5 x 4.0 x 4.0 in.)
Unit mass:	Power interface unit 1, 1.1 kg (2.5 lb)
	Power interface unit 2, 0.7 kg (1.5 lb)
Power dissipation, W:	Power interface unit 1, 2.5 with 200 W load
	Power interface unit 2, 0.2 with 53 W load
Overload protection - redundant fuses	
Command Characteristics:	Logic 0, 12 V at 3 ma, 4 ms ± 20 percent
	Logic 1, 12 V at 3 ma, 4 ms ± 20 percent
	DC rejection, ± 4 Vdc
	AC rejection, ± 50 μsec, +26 V pulse referenced to 0 Vdc

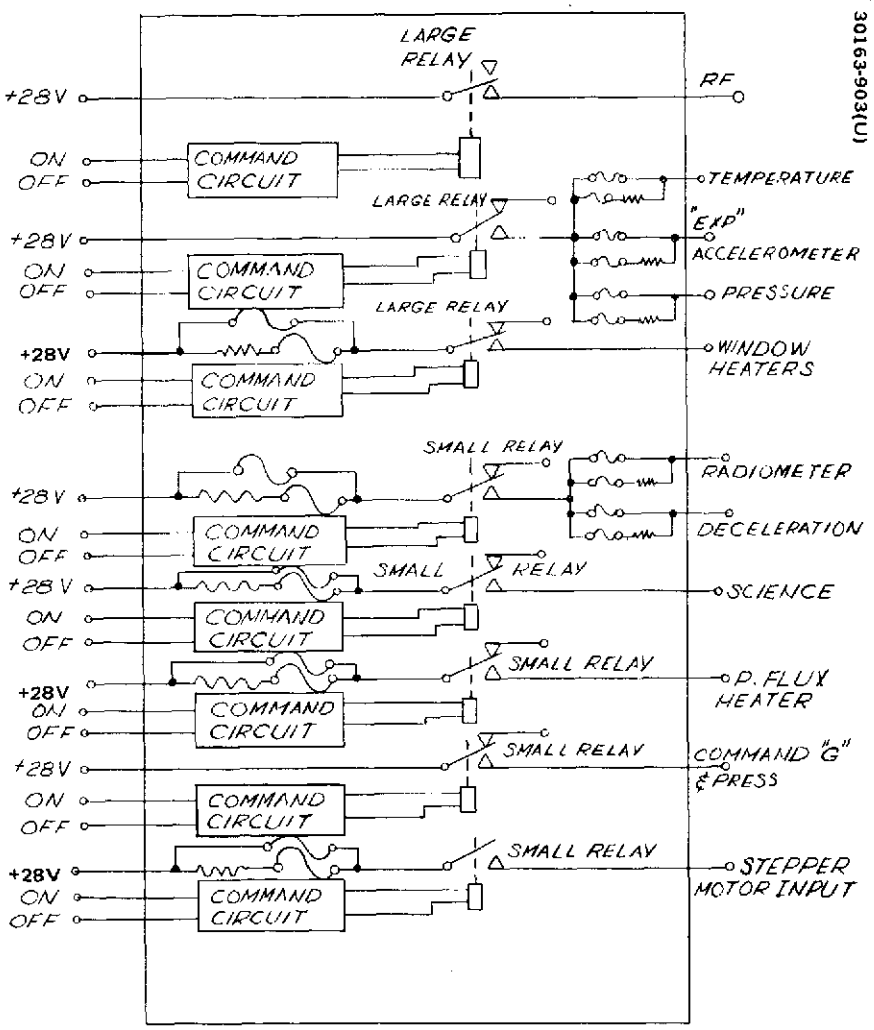

FIGURE 4-32. LARGE PROBE POWER INTERFACE UNIT 1

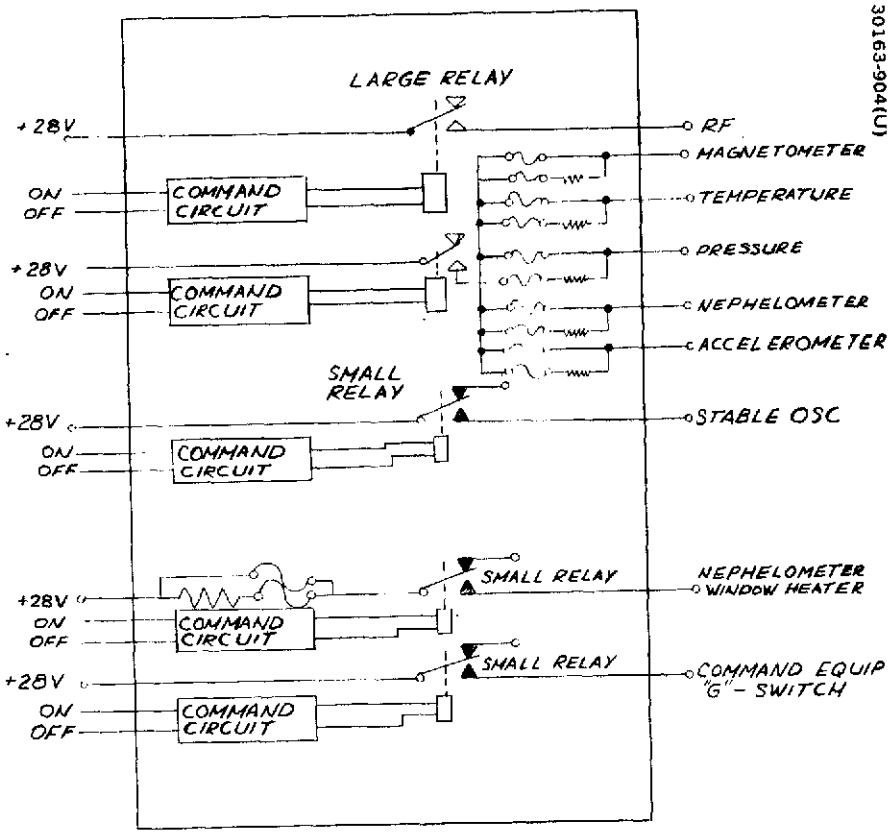

FIGURE 4-33. SMALL PROBE POWER INTERFACE UNIT 2

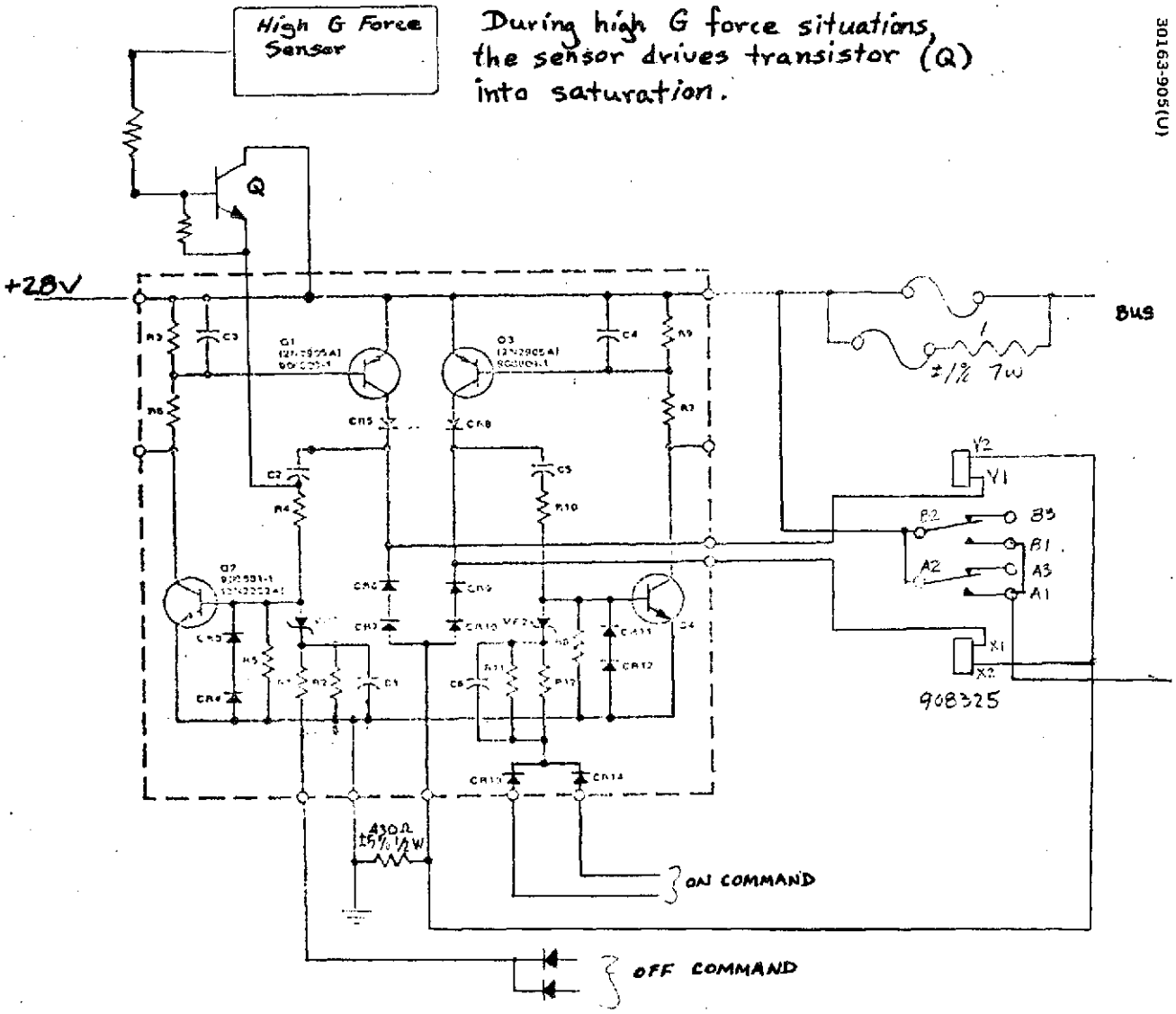

FIGURE 4-34. LARGE PROBE RELAY AND COMMAND CIRCUITRY

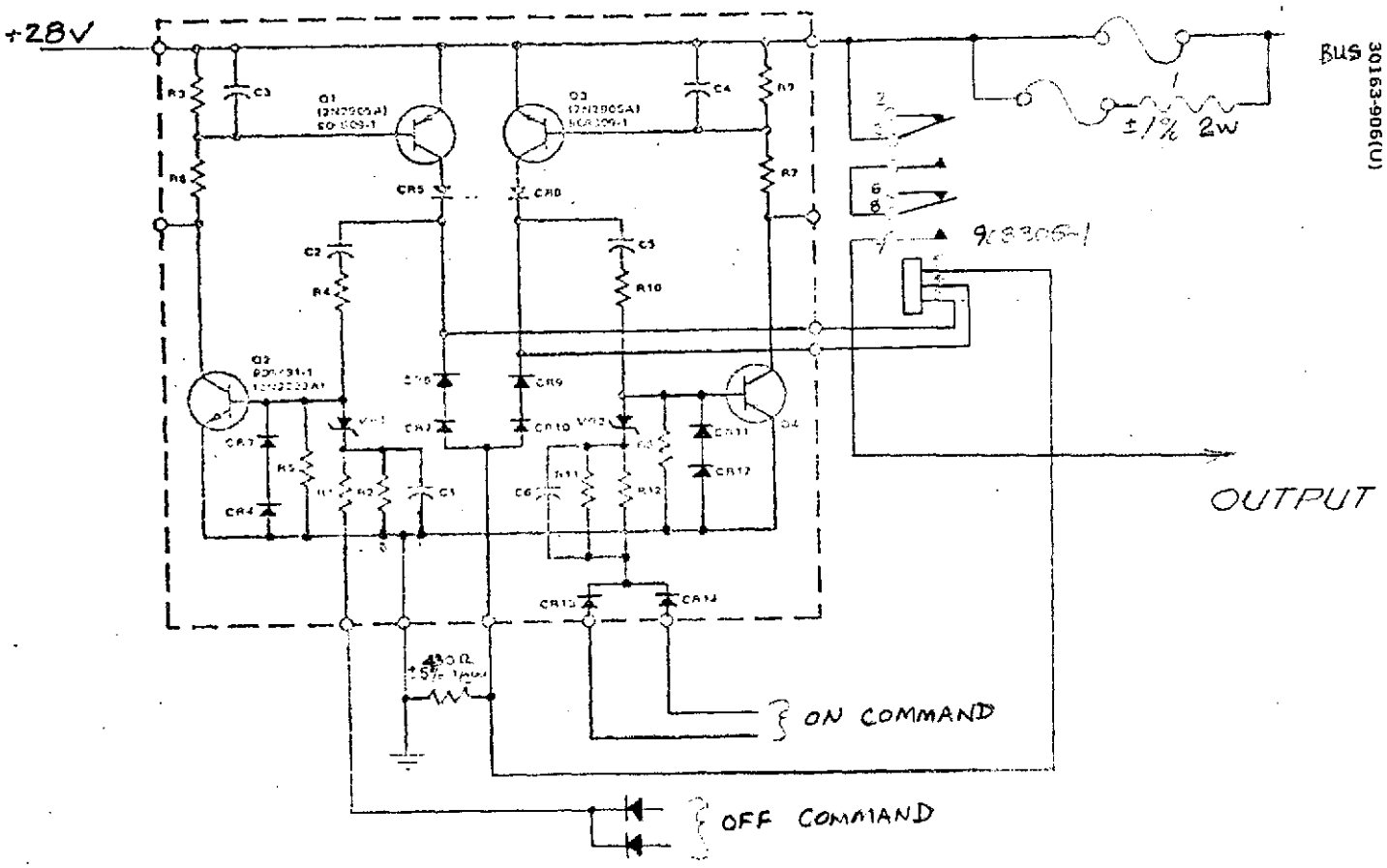

FIGURE 4-35. SMALL PROBE RELAY AND COMMAND CIRCUITRY

TABLE 4-36. SUMMARY OF THE HEATER CONTROL CHARACTERISTICS

Input	
Voltage	22 to 33 V
Current	
Standby	500 A maximum
Load	240 mA maximum
Command requirements	
Heater A ON	
Heater A OFF	
Heater B ON	
Heater B OFF	
Unit mass	0.23kg (0.5 lb)
Unit size	3.25 x 6.50 x 7.47 Cm (1.28 x 2.56 x 2.94 in)

Discharge Control - Atlas/Centaur

In the orbiter and probe bus designs on the Atlas/Centaur each battery will discharge through a set of redundant diodes instead of a boost regulator. Redundant discharge diodes are connected in series with commandable relay switches to allow each battery to discharge into the bus when the bus voltage is approximately 1 V lower than battery voltage. Figure 4-37 shows a detail connection. In normal operation, CR1 and CR2 provide the primary discharge path via K1. Discharge diodes CR3 and CR2 are back up diodes. Relay K1 is only transferred when the backup discharge diodes are required because of a failure of one of the primary diodes (open or short), to prevent the discharge of one battery into another, or to reconnect a battery to the bus when the diodes open. The relay is energized by a ground command.

Undervoltage Switch - Atlas/Centaur

An undervoltage switch is added to both orbiter and probe bus designs on the Atlas/Centaur. The function of the undervoltage switch s to provide isolation between the power system bus and the spacecraft oad bus in the event of a bus voltage failure. If the failure resulted in abnormally high currents, or the batteries undergo an extreme depth of discharge, the switch senses the resulting low bus voltage and opens the power system bus and the spacecraft load bus. Telemetry signals are provided for essential bus voltage and reset status. This unit is presently used on the HS 331 program and is being qualified for flight hardware.

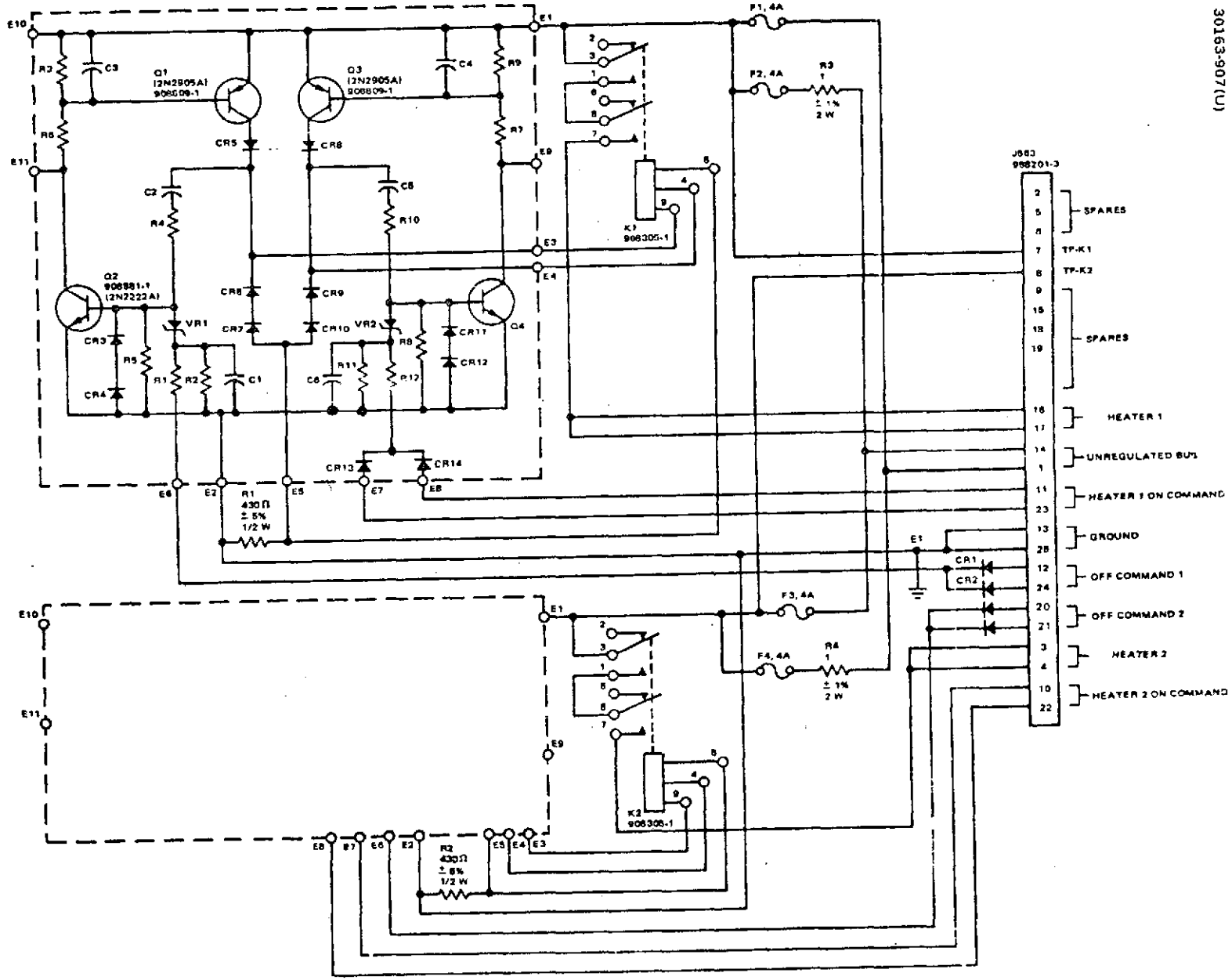

FIGURE 4-36. HEATER CONTROL UNIT SCHEMATIC DIAGRAM

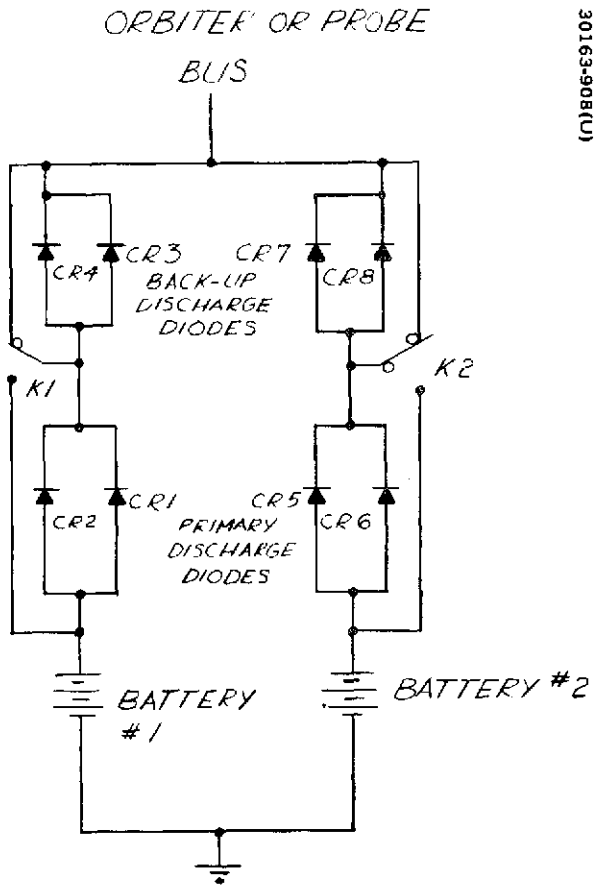

FIGURE 4-37. ATLAS/CENTAUR BATTERY DISCHARGE SCHEMATIC DIAGRAM

REFERENCES

1. W. D. Brown, G. W. Hodgman, and A. T. Spreen, "Computer Simulation of Solar Array Performance," Sixth Photovoltaic Specialists Conf., Cocoa Beach, Florida, March 28-30, 1967.

2. NASA technical Memorandum TM X-64627 "Space and Planetary Environment Criteria Guidelines for Use in Space Vehicle Development," Marshall Space Flight Center, Ala. 1971 revised.

3. J. R. Thomas, "Mariner Venus Mercury 1973 Mission Solar Proton Environment: Fluence and Dose," JPL Quarterly Technical Review, Vol. 2, Dec. 1972.

5. THOR/DELTA BASELINE

The Thor/Delta baseline power subsystem design for the probe bus and orbiter is shown in Figures 5-1 and 5-2, respectively. Differences exist in the two systems only in the type of battery, number of bus limiters, inclusion of a probe (large and small) battery charger on the probe bus, and implementation of the power interface units.

The subsystem utilizes a boost-add-on battery discharge system with a regulator that maintains the bus voltage at 27 ± 1 V dc during periods of insufficient solar panel power. The probe bus utilizes a 13 cell silver-zinc battery. The orbiter bus, on the other hand, utilizes an 18 cell nickel-cadmium battery to meet the longer cycle-life requirements of the orbiter mission.

The battery charger for the orbiter will replenish battery energy utilized during launch, trajectory correction maneuvers, and eclipse modes of operation. The charger utilizes a voltage controlled charge with turn-on set for approximately 26.5 V dc. Charge current is controlled until one of eight selectable voltage levels is reached, at which time the current tapers to a trickle level.

The probe bus battery charger utilized to charge the silver-zinc battery employs a current limit with a regulated upper voltage level. The charger provides a current limit at 0.4 amps maximum at a regulated voltage of 1.93 ± 0.01 V/cell. The charge current tapers after the regulated voltage is reached (i.e., output of the regulator equals the battery terminal voltage) to a trickle level of 2-10 mamp. The probe bus also contains a charger for the large probe and small probe that is identical in design to the main bus charger. Provisions have also been made to supply checkout power to each probe selectively upon command from the probe bus.

The orbiter array has been sized to provide 179 W (EOL) while the probe bus has a 145 W capability. The array has been laid out to minimize stray fields that might interfere with magnetometer measurements. Table 5-1 includes a summary of the panel parameters.

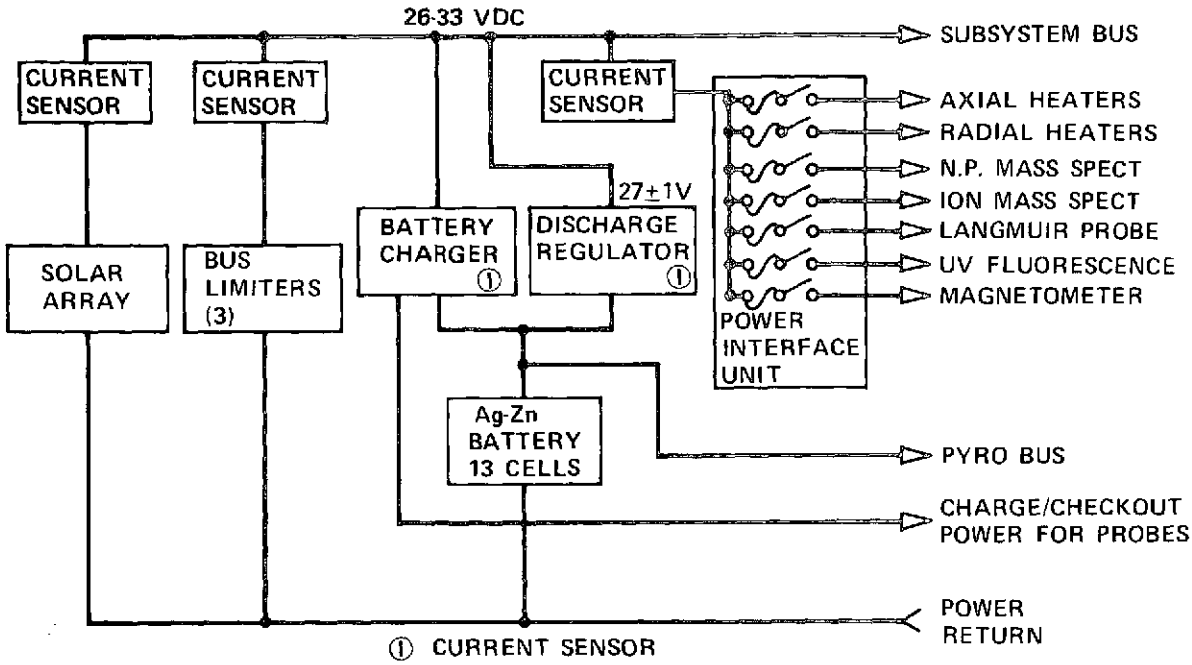

FIGURE 5-1. THOR/DELTA PROBE BUS POWER SUBSYSTEM

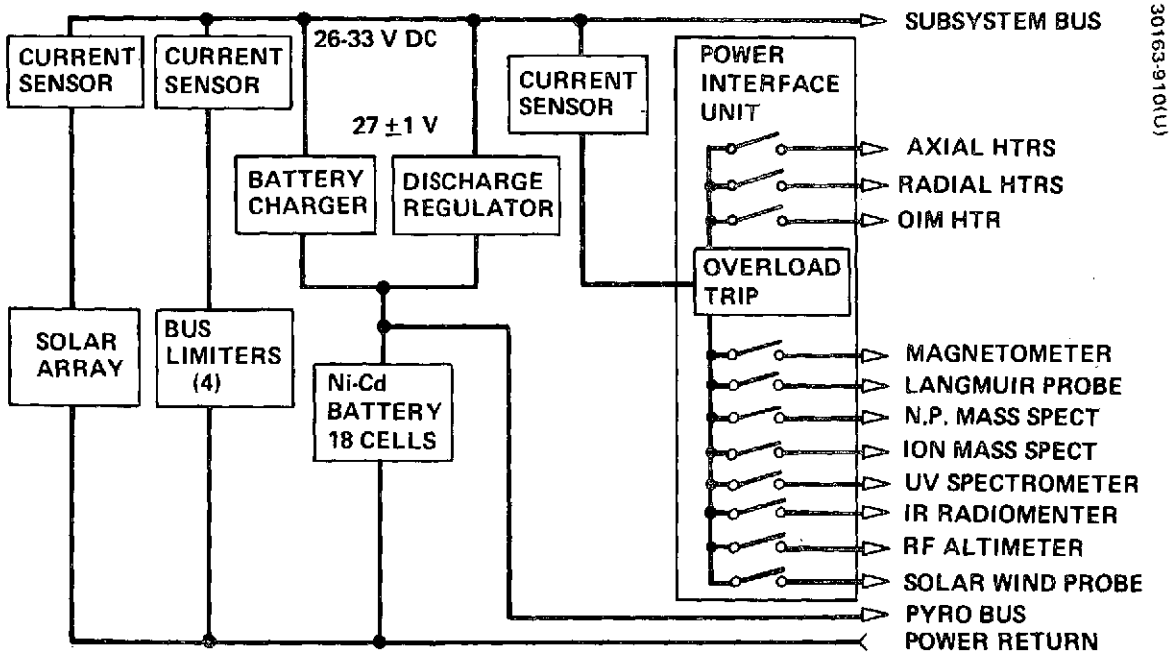

FIGURE 5-2. THOR/DELTA ORBITER BUS POWER SUBSYSTEM

TABLE 5-1. THOR/DELTA SOLAR PANEL CHARACTERISTICS

Solar Cell	
Cell type	2 x 2 cm N/P, 2 ohm-cm 0.20 mm (8 mil) thick
Coverglass	0.15 mm (6 mil) thick, 0211 microsheet
Cell output at 25°C at 1 sun	119.5 ma at 460 mV
Cell adhesive	GE RTV 511/577
Coverglass adhesive	Dow-Corning RTV 63489
Interconnect	0.05 mm (2 mil) chem-etched copper, solder plated

Solar Panel Item	Orbiter	Probe
Total cells	8586	6930
Series X parallel	81 x 106	77 x 90
Power at 28 V		
Earth without rad	105	96
Earth with rad	99	91
Venus without rad	202	162
Venus with rad	179	145
Panel length, cm (in.)	57.2 (22.5)	46.7 (18.4)
Panel weight, kg (lb) (less substrate)	4.99 (11.0)	4.04 (8.9)

Bus limiters have been included in the design to limit the array output voltage to approximately 33 V dc. Four and three limiters are utilized on the orbiter and probe bus, respectively. The limiters are grouped and set points are staggered and the power resistors strategically located throughout the spacecraft for thermal balance. The lower end of the bus voltage range (26 V dc) is determined by the battery and discharge controller. Each limiter is ground commandable.

The probe bus utilizes a power interface unit implemented with relays and redundant fuses for power switching. Power is switched individually to heaters and each experiment subsystem. The orbiter bus utilizes overload control units with a centrally contained overload trip circuit within the unit for bus protection and for experiment protection.

6. ATLAS/CENTAUR BASELINE DESIGN

The final selection of the elements comprising the power subsystem was based on the results of several design and tradeoff studies. All elements of the subsystem were evaluated based on the requirements of the mission and were selected to minimize development costs of the subsystem. As indicated earlier in the section on regulated versus unregulated bus, such factors as the spacecraft configuration, load power required and adaptability to new load requirements strongly influenced such choices as the solar array configuration, an unregulated primary bus, and diode isolated batteries.

The orbiter spacecraft has the difficult dual requirement of low magnetic fields to ensure optimum magnetometer performance and a long battery cycle life. The design choice of relatively low cost nickel-cadmium batteries (over silver-zinc or silver-cadmium) led to considering mu-metal shielding to achieve the required low remnant magnetic fields and/or physically locating the batteries as far as possible from the magnetometer.

The solar panel designs were selected after careful consideration of the anticipated thermal environment. It was concluded that present Hughes fabricating techniques would meet all requirements of both missions. Further, a design could be implemented which would minimize the solar array's contribution to the magnetic fields.

In all cases, an attempt has been made to utilize existing hardware designs where possible. The Atlas/Centaur design has been implemented utilizing a maximum of OSO designed hardware. One exception is the power switching units. The orbiter bus utilizes the OSO overload control units with minor modifications to accommodate the increased load power. The probe bus has a newly designed power interface unit that redundantly fuses each load individually to preclude one failed or faulted load from removing power from all experiments during the critical planet entry phase.

6.1 ORBITER AND PROBE BUS FUNCTIONAL DESCRIPTION

The Atlas/Centaur orbiter and probe bus power subsystems have been designed with maximum commonality and compatibility between the orbiter and probe bus. With the exception of the power interface unit on the probe bus,

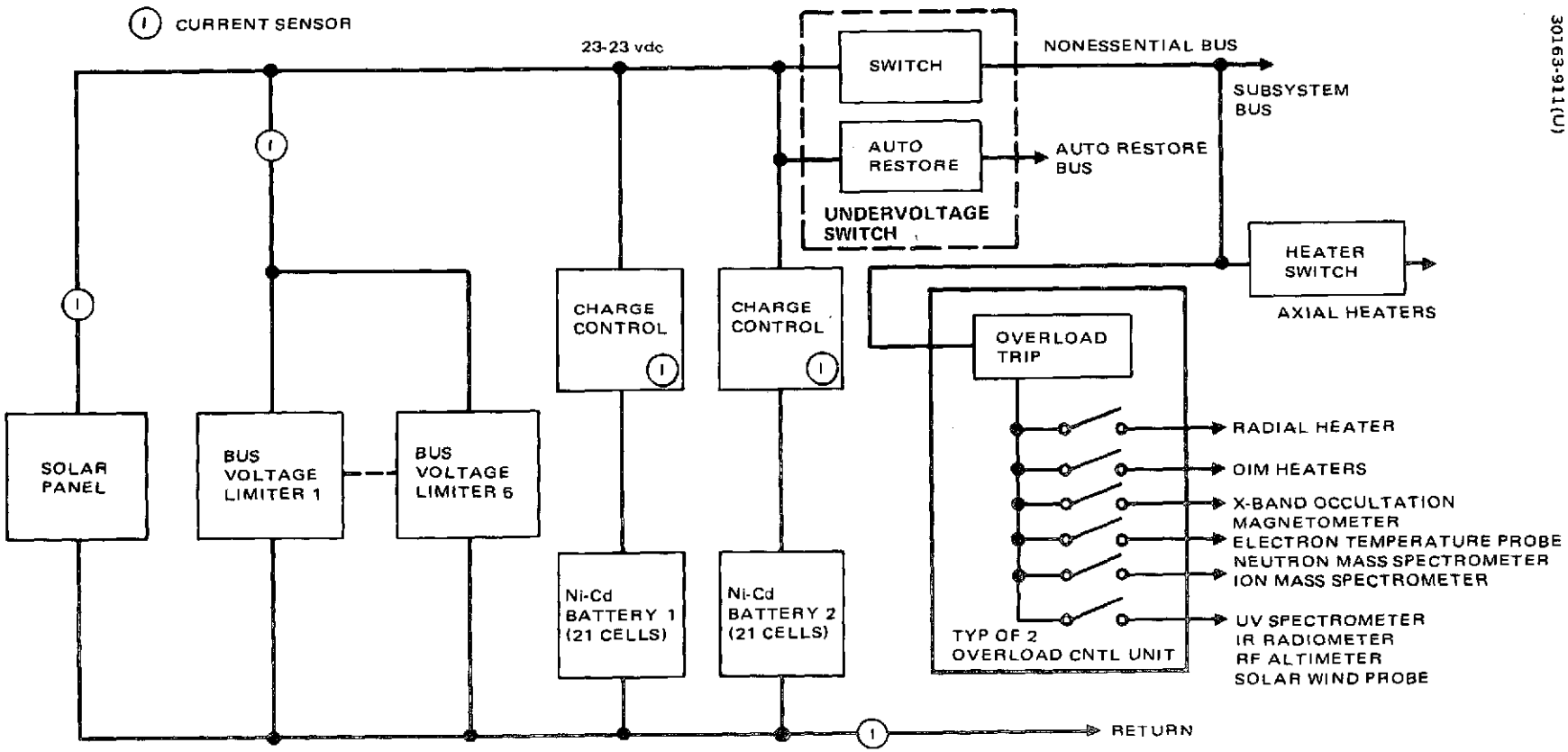

FIGURE 6-1. ATLAS/CENTAUR ORBITER POWER SUBSYSTEM

30163-911(U)

the power electronics units are derived from the OSO spacecraft. A brief description of each element comprising the power subsystem follows. Block diagrams of the orbiter and probe bus are shown in Figures 6-1 and 6-2. The power electronics units for the orbiter and probe bus condition and control the power developed by the solar array and batteries for the utilizing subsystems. Tables 6-1 and 6-2 list the elements that comprise the orbiter and probe spacecraft.

Solar Array

The orbiter and probe bus solar arrays have been sized to supply required spacecraft power at end of life (EOL) with adequate margin to guard against solar radiation damage. As indicated in the solar array design and analysis section, the design is such that the contribution of magnetic fields is minimized. As a direct result of the above study, the array design is implemented with 2 x 2 cm N/P silicon cells with 2 ohm-cm base resistivity and 0.20 mm (8 mils) thickness. The cover slides are to be 0.15 mm (6 mils) thick utilizing both ultraviolet and antireflective coatings.

Batteries

Both the orbiter and probe bus will utilize identical battery designs. Nickel-cadmium cells have been selected to meet the cycle life requirements of the orbiter spacecraft. A 21 cell design consisting of three 7 cell packs per battery will be used. Each system will require two batteries per spacecraft. The battery system will include appropriate thermal sensors for control purposes. The design includes thermal sensors to preclude overheating during battery charging. Maximum depth of discharge (DOD) on the orbiter is approximately 70 percent during apoapsis eclipse; 10 to 25 percent DOD occurs during periapsis passes. The short eclipses will result in a DOD of approximately 40 percent with all required loads activated. Maximum DOD for the probe bus battery is expected to be 57 percent.

Bus Voltage Limiters

Excess solar array power will be dissipated in the bus voltage limiters. Six and five OSO type limiters (each with a 66 W capability) shall be utilized on the orbiter and probe bus, respectively. Each shall have its set point (bus voltage level for turnon) adjusted to a value that minimizes potential thermal problems. The voltage input range shall be 23 to 33 Vdc with the limiting voltage or clamp level set for 32.6 to 33.0 Vdc. Maximum power dissipation for each limiter when not on shall be 0.3 W over the operating voltage range. Each limiter is commandable and has sufficient telemetry outputs to facilitate status determination.

Redundancy is provided in terms of excess power dissipation available in the limiters. With a single failed limiter, the remaining limiters each have the capability of dissipating 66 W. With normal spacecraft loads maximum excess power should never exceed 50 W.

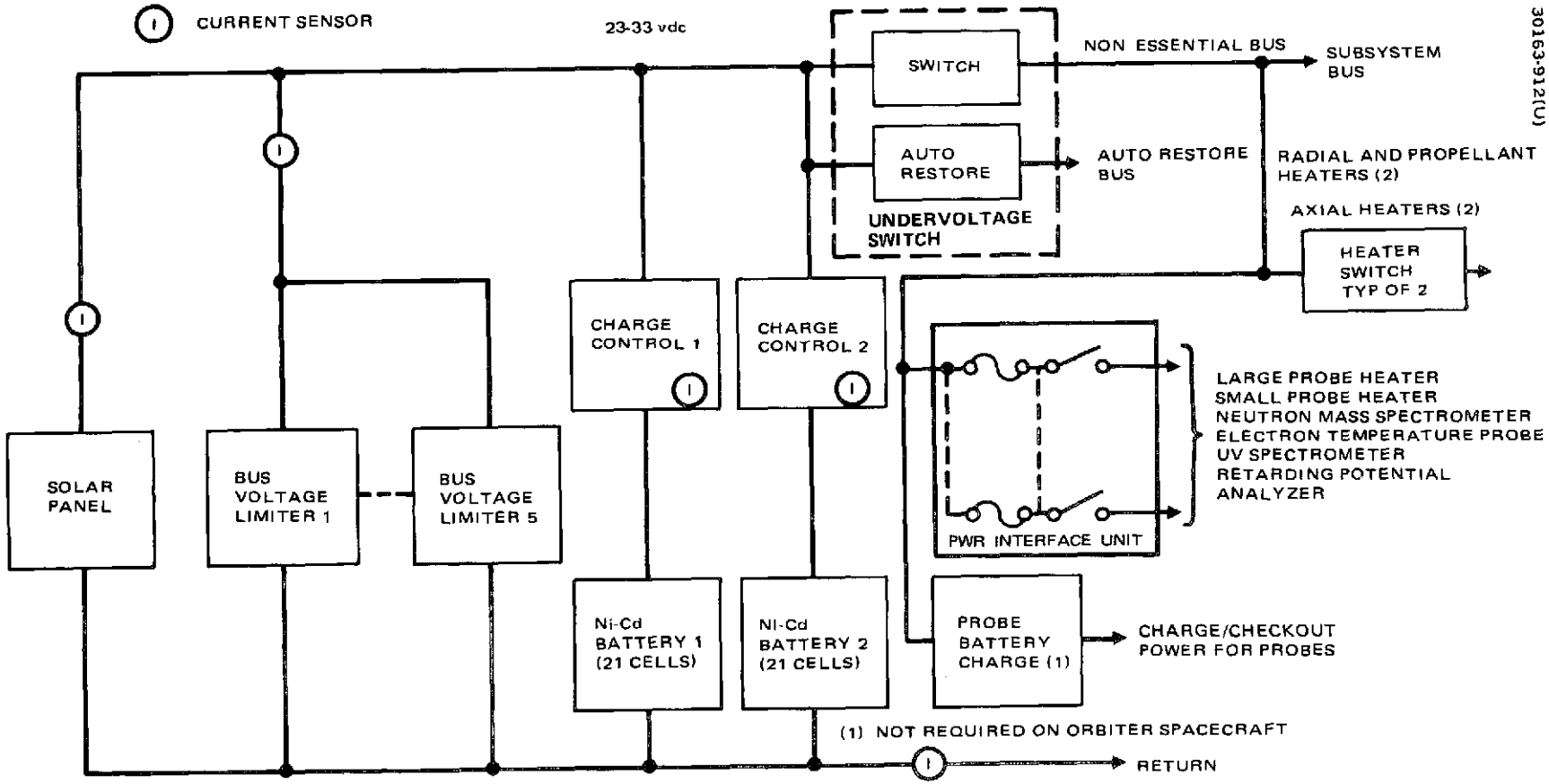

FIGURE 6-2. ATLAS/CENTAUR PROBE SPACECRAFT POWER SUBSYSTEM

TABLE 6-1. ATLAS/CENTAUR ORBITER BUS POWER SUBSYSTEM EQUIPMENT

Item	Unit Size cm (in.)	Total Mass Weight kg (lb)	Quantity per Spacecraft
Charge/discharger controllers	7.9 x 16.0 x 18.0 (3.1 x 6.3 x 7.1)	3.4 (7.4)	2
Bus limiters	5.3 x 8.9 x 10.9 (2.1 x 3.5 x 4.3)	3.8 (8.3)	6
Undervoltage switch	6.6 x 10.7 x 10.7 (2.6 x 4.2 x 4.2)	0.8 (1.7)	1
Current sensors	5.3 x 6.1 x 6.4 (2.1 x 2.4 x 2.5)	0.5 (1.1)	3
Heater switch unit	3.3 x 5.1 x 7.6 (1.3 x 2.0 x 3.0)	0.2 (0.5)	1
Overload control	7.6 x 10.7 x 18.0 (3.0 x 4.2 x 7.1)	2.7 (6.0)	2
Electrical Total		11.3 (25.0)	
Battery	-	11.2 (24.6)	
Solar array height (less substrate)	79.5 (31.3)	8.8 (19.5)	
Subsystem Total		31.3 (69.1)	

TABLE 6-2. ATLAS/CENTAUR PROBE BUS POWER SUBSYSTEM EQUIPMENT SUMMARY

Item	Unit Size cm (in.)	Total Mass Weight kg (lb)	Quantity per Spacecraft
Charge/discharge controller	7.9 x 16.0 x 18.0 (3.1 x 6.3 x 7.1)	3.4 (7.4)	2
Bus limiters	5.3 x 8.9 x 10.9 (2.1 x 3.5 x 4.3)	3.1 (6.9)	5
Undervoltage switch	6.6 x 10.7 x 10.7 (2.6 x 4.2 x 4.2)	0.8 (1.7)	1
Current sensors	5.3 x 6.1 x 6.4 (2.1 x 2.4 x 2.5)	0.5 (1.1)	3
Power interface unit	3.8 x 10.2 x 10.2 (1.5 x 4.0 x 4.0)	0.7 (1.5)	1
Heater switch	3.3 x 5.1 x 7.6 (1.3 x 2.0 x 3.0)	0.5 (1.0)	2
Probe battery charger	6.4 x 14.0 x 17.8 (2.5 x 5.5 x 7.0)	1.8 (4.0)	1
Electrical Total		10.7 (23.6)	
Battery	-	11.2 (24.6)	2
Solar array height (less substrate)	67.1 (26.4)	7.6 (16.7)	1
Subsystem Total		29.4 (64.9)	

Battery Charge/Discharge Controller

The battery charge controller will replenish battery energy utilized during launch, trajectory correction maneuvers, and eclipse modes of operation. One unit is provided for each battery. Charge current will be uncontrolled until one of eight selectable voltage levels is reached, at which time the current will taper to a trickle level. Charge termination will be automatic upon reaching preset charge/overcharge status unless terminated prematurely by battery over temperature sensors. Manual charge termination may be executed by ground command.

The probe bus will also contain four chargers for silver-zinc batteries on the large and small probes and checkout capability. The silver-zinc chargers will provide a current limited at 0.4 A maximum at a regulated voltage of 1.93 ±0.01 V/cell. The charge coltage shall taper (after the regulated voltage is reached) to a level of 2 to 10 mA. Separate chargers will be used for each probe (one large and three small) with provisions for applying checkout power sequentially.

Undervoltage Switch

To protect the battery against inadvertent bus faults that could result in discharging the battery to abnormally low levels, an undervoltage switch has been incorporated into the design. The undervoltage switch will provide isolation between the essential and nonessential buses in the event of a load or bus failure.

Heater Switch

A heater switch unit supplements the power switching capability of the overload control units and power interface units of the orbiter and probe buses, respectively. This unit is comprised of commandable relays and fuses for bus protection. Primary bus power is switched to the heaters upon command.

Power Interface Unit

Major power switching on the probe bus is accomplished within the power interface unit. Redundant fuses are utilized along with magnetically latching relays in the design implementation. A complete description along with schematic diagrams is included in subsection 4.6.

Current Sensors

Current sensors are utilized within the power subsystem for status determination. The sensor employs a transductor with a full scale sensitivity of 18 A turns. Excitation is provided by a Royer Saturable magnetic oscillator with one winding used to excite the transducer. Current can be monitored in either the positive or negative side of the power line with negligible loss. The full scale accuracy of the device is ±2 percent.

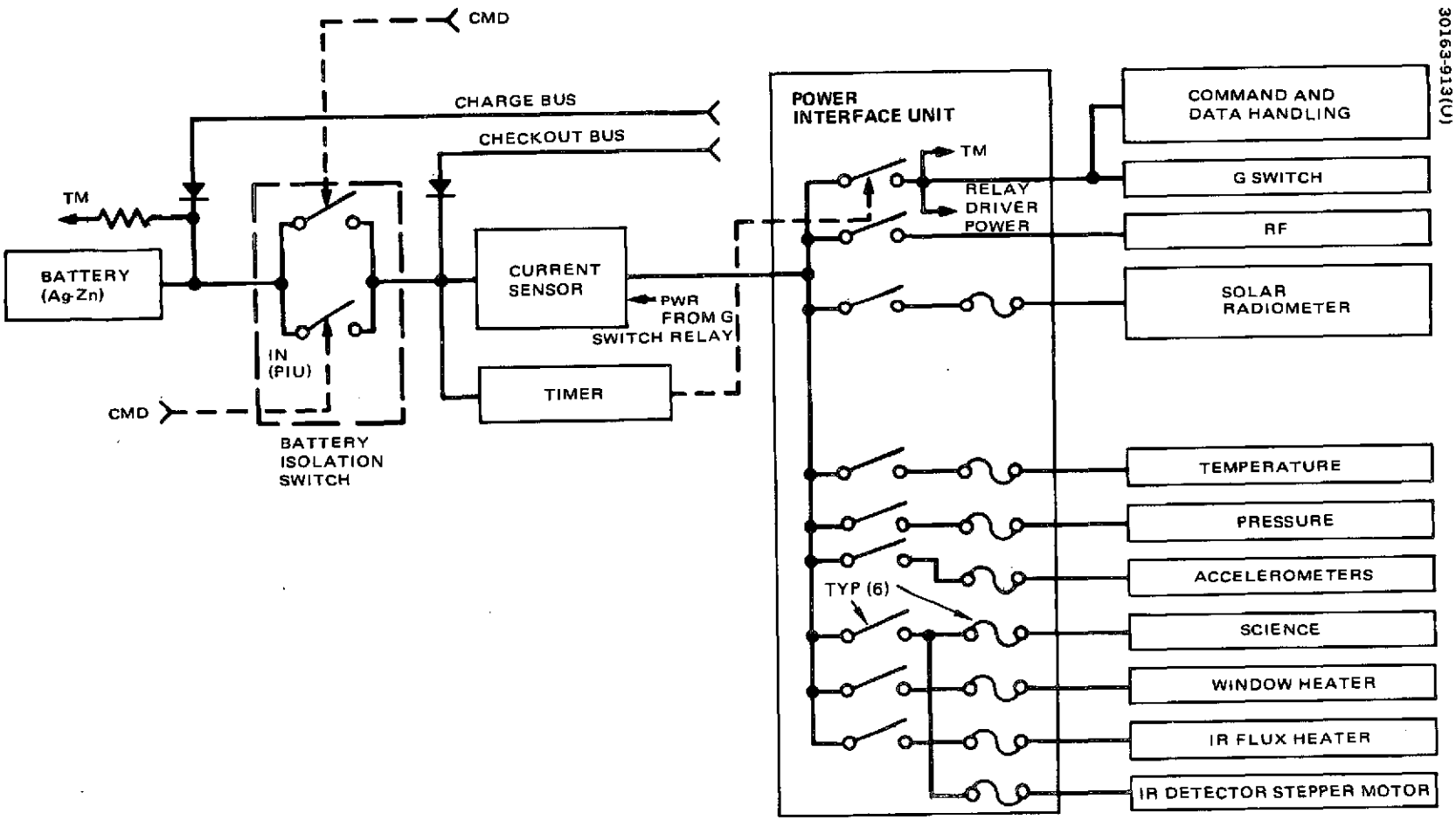

FIGURE 6-3. LARGE PROBE POWER SUBSYSTEM

6.2 LARGE AND SMALL PROBES FUNCTIONAL DESCRIPTION

Power Electronics

The large and small probes have identical unregulated power subsystem designs supplying 24 to 33 V with differences existing only in power handling capability and the number of switches provided to distribute power to load subsystems. Primary power in each case is provided by an 18 cell silver-zinc battery sized to assure all energy needs of the probes. A maximum DOD of 80 percent is allowed over the entire mission life of the probes. Special packaging and development considerations have been explored to ensure that the high "g" environment to be encountered during planet entry can be accommodated.

The battery is connected to the load switches through a redundant isolation relay that is activated prior to separation from the probe bus. The voltage input range to the isolation switch and loads will be 25.2 to 29.7 Vdc with an average discharge voltage of 26.5 Vdc.

A current sensor has been included in the design for status determination. Voltage telemetry outputs, e.g., the battery terminal voltage, will also be available to aid in status determination. Each probe will have included in its design a battery charge bus and a power checkout bus. Battery charging and probe checkout will be accomplished as available power permits.

Power switching on board the probes is accomplished with the power interface units. Fusing has been incorporated in all switches except critical loads, e.g., RF, command and data handling, G-switch, and the stable oscillator.

A block diagram of the large and small probe is shown in Figures 6-3 and 6-4, respectively. The physical characteristics of elements comprising the large and small probe power subsystems are shown in Table 6-3.

Probe Batteries

The small and large probes are each powered by a single silver-zinc battery consisting of 18 cells each. The average design discharge voltage of each cell is 1.47 Vdc, resulting in an average battery terminal voltage of 26.5 Vdc. The nominal discharge voltage range will be from 25 to 29.7 Vdc, assuming a per cell voltage of 1.4 to 1.65 Vdc.

The reliability of the probe power subsystem is derived from a highly reliable battery through the selection of appropriate separator materials and sufficient plate current density to ensure reliable operation. Reliability further depends on the operating temperature range of the battery. Adequate precautions will be taken to ensure that no battery operation occurs beyond specified temperature limits.

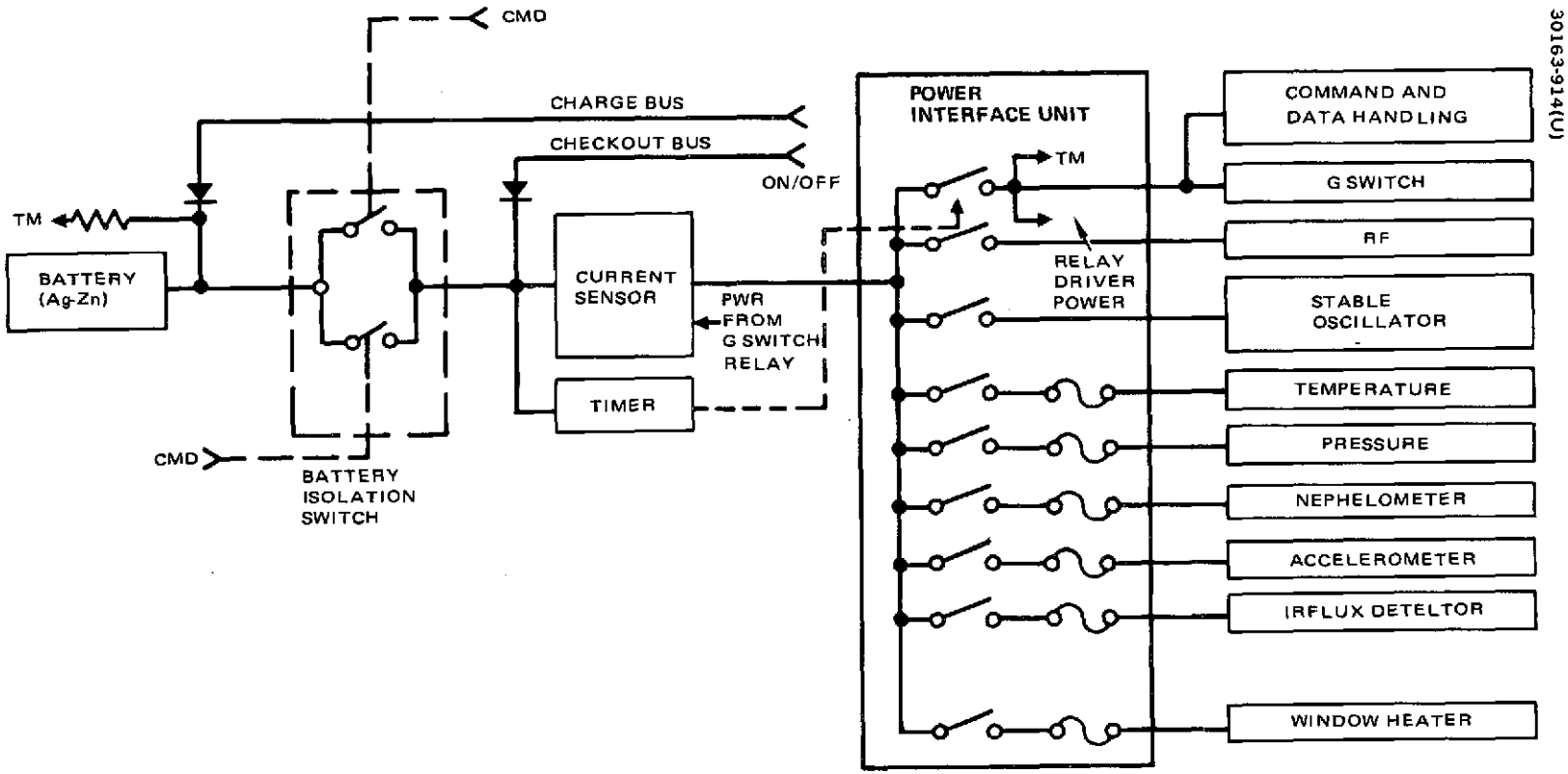

FIGURE 6-4. SMALL PROBE POWER SUBSYSTEM

TABLE 6-3. ATLAS/CENTAUR PROBES POWER SUBSYSTEM EQUIPMENT SUMMARY

Item	Quantity per Spacecraft	Unit Power Dissipation, W	Total Mass Weight kg (lb)
Large Probe			
Battery (Ag-Zn)	1	-	10.5 (23.2)
Power interface unit	1	0.20	2.2 (4.9)
Current sensor	1	0.37	0.16 (0.35)
Total			12.90 (28.45)
Small Probe			
Battery (Ag-Zn)	1	-	3.6 (8.0)
Power interface unit	1	1.0	1.4 (3.0)
Current sensor	1	0.37	0.16 (0.35)
Total			5.15 (11.35)